NTNU

Norwegian University of
Science and Technology

# Digital Twin Solution for Structural Health Monitoring of Stadia Structures

Monitoring of Vibrations Caused by Dynamic Crowd Loads at *Lerkendal Stadion*

**Henrik Løfaldli**

Master of Science in Engineering and ICT
Submission date: June 2018
Supervisor: Terje Rølvåg, MTP
Co-supervisor: Bjørn Haugen, MTP

Norwegian University of Science and Technology
Department of Mechanical and Industrial Engineering

# Preface

This work is a Master's thesis in Industrial ICT at NTNU as part of the study program for Engineering and ICT. It has been carried out in the spring semester of 2018, and a preliminary specialisation project was carried out in the fall of 2017. The project is carried out in co-operation with the company *Fedem Technology AS* as one of the initial plans for their new endeavours into digital twins and the industrial internet of things. The project supervisor, *Terje Rølvåg*, was the one to propose *Lerkendal* as one of the cases to be investigated and has provided guidance and attendance during the entire project period. *Bjørn Haugen*, as the co-supervisor, has also been available for advice and counselling when needed. The people from *Fedem Technology* has provided all equipment used as well as custom software for the system. *RBK* has provided access to all matches during the entire project period so the measurements could be taken throughout the year. A special thanks to *Per Haugnes*, as the Operations Manager at the stadium, and the crew at the VIP-section that has provided help and services when necessary. The assumed background for readers of this report is someone who has a general understanding of the field of structural dynamics, signal processing, the finite element method, and modal analysis.

Trondheim, June 11, 2018

Henrik Løfaldli

*Engineering is the art of modeling materials we do not wholly understand, into shapes we cannot precisely analyze so as to withstand forces we cannot properly assess, in such a way that the public has no reason to suspect the extent of our ignorance.*

*by Dr. A.R. Dyke, 1946*

# Abstract

The combination of increased computational power, sophisticated sensors, and telecommunications enable monitoring by utilising the digital twin concept. A digital twin is a virtual representation of a physical asset, that runs a simulation based on real data that is affecting the said asset. Digital twins have many potential uses, one of which is structural health monitoring. This work concerns the exploration and development of a system for structural health monitoring for stadia structures. The dynamic load of a crowd on a structure is complex and hard to model correctly. The vibrations caused by such a load causes concern among attendants and officials alike. Such concerns could be validated or invalidated by the use of a monitoring system. The digital twin concept utilises a simulation based on data from recorded events and gives free reign for the solver to generate loads to recreate the recorded behaviour with a digital twin. The monitoring system has three main components which are the edge, the core, and the consumption. The edge captures behaviour, whereas the core recreates the behaviour on the the digital twin, and the consumption visualizes the recreated events for an end user of the system. All components of the system has successfully been investigated and is capable of providing an event based monitoring system from recorded events. The system has not been automated and developed into a closed-loop, however, all parts are mature for further development into a more complete product by streamlining and automating the process.

# Sammendrag

Kombinasjonen av økt databehandlingskraft, sofistikerte sensorer og telekommunikasjon muliggjør strukturhelseovervåking ved å benytte digital-tvilling-konseptet. En digital tvilling er en virtuell representasjon av en fysisk gjenstand, som utfører en simulering basert på reelle data som påvirker nevnte gjenstand. Digitale tvillinger har mange potensielle bruksområder, hvorav en er strukturhelseovervåking. Det følgende arbeidet ser nærmere utforskning og utvikling av et system for strukturhelseovervåking for stadionstrukturer. Den dynamiske belastningen til en folkemengde på en struktur er kompleks og vanskelig å modellere riktig. Vibrasjonene forårsaket av en slik belastning medfører bekymring blant både publikum og ansatte. Slike bekymringer kan bli validert eller avkreftes ved bruk av et overvåkingssystem. Digital-tvilling-konseptet vil benytte en simulering basert på data fra målte hendelser og gir simuleringsløseren spillerom til å generere lasten for å gjenskape den registrerte oppførelsen på en digital tvilling. Overvåkingssystemet har tre hovedkomponenter som er "the Edge", "the Core", og "the Consumption". "The Edge" fanger oppførselen, mens "the Core" gjengir oppførselen på den digitale tvillingen, og "the Consumption" visualiserer de gjengitte hendelsene for en sluttbruker av systemet. Alle komponenter i systemet har blitt undersøkt og er i stand til å levere et hendelsebasert overvåkingssystem fra registrerte kamper. Systemet har ikke blitt automatisert og utviklet til en lukket sløyfe, men alle deler er modne for videre utvikling i et mer komplett produkt ved å strømlinjeforme og automatisere prosessen.

# Abbreviations

**API** - Application programming interface
**AVT** - Ambient vibration testing
**BPM** - Beats per minute
**CAD** - Computer aided design
**CSV** - Comma separated values
**FEDEM** - Finite element dynamics of elastic mechanisms
**FEM** - Finite element model
**FFT** - Fast Fourier transform
**FVT** - Forced vibration testing
**I/O** - Input/Output
**ISO** - International Organization for Standardization
**RMS** - Root mean square
**RBE** - Rigid body element
**RBK** - Rosenborg ballklub
**VDV** - Vibration dose value
**YAML** - YAML ain't markup language

# Contents

# Chapter 1

# Introduction

## 1.1 Background and Motivation

In the late summer of 2017 *Trondheim*'s pride *RBK* qualified for the *Europa League* in football after beating the previous year's runner-up *Ajax FC* in the decisive match at *Lerkendal*. An excited crowd attended the stadium and filled the grandstands to their maximum capacity. *RBK* has an official supporter group known as *Kjernen*, that is situated at the upper level of one of the grandstands. This supporter group is known for their passionate and never-ending singing, chanting, and jumping as their team fights on the green field beneath them. One of the songs in their repertoire is set to the melody of the themes song for the Swedish TV-series about *Pippi Långstrump*, where the crowd join together and jump to the beat of the song, which is provided by a drummer situated at the middle of the group. The match against *Ajax* was season high for crowd excitement and as such the periodic load of the supporters caused vibrations in the grandstand, that was perceivable for the entire stadium, and especially for the very important personnel paying for seats in the VIP section situated directly underneath the vibrating cantilever. These vibrations propagate through the ground below the pitch and make lamps and windows shake in the student housings located across the road from the stadium. This song occurs once every half of the matches played at *Lerkendal* and cause varying levels of vibrations at every match.

*Fedem Technology AS* and Professor *Terje Rølvåg* proposed a project concerning this load case and its effect on the grandstand as a case suitable for a new solution for monitoring structural health by utilising the digital twin concept. After a meeting with officials from *RBK*, the project was initiated, and a heavy burden

of free attendance at the VIP-section for all matches through the fall and spring was graciously accepted as a necessary sacrifice in the name of science. *Fedem Technology AS* provided hardware for monitoring and guidance for parts of the monitoring solution. The project will be one of the first instances of trying to implement a structural monitoring system and will provide insight into challenges, opportunities and ideas for future endeavours for monitoring the structural health of physical assets.

## 1.2 Problem Description

The task is to explore and develop a new solution for monitoring the structural health of a grandstand utilising the concept of a digital twin. This solution includes making a digital representation of the grandstand, capturing the behaviour of the physical grandstand, connecting the physical and digital twin, and providing a visualisation of the digital recreation of the physical asset's state and behaviour. Further, the behaviour of the grandstand when excited by dynamic crowd loads will be analysed, as there is a specific load case of interest that has caused concern among crowd and management alike.

## 1.3 Project Scope

### 1.3.1 Objectives

The initial objective is to set up a hardware solution for structural monitoring, i.e. capturing the behaviour of the grandstand. Furthermore, the data connection between the physical and virtual twins must be established. Following this, the physical behaviour needs to be recreated virtually in the digital twin. In addition, an application for visualising the recreated behaviour shall be established. Lastly, the data from the matches will be analysed as to better understand the response and load case that that causes concern.

### 1.3.2 Limitations

The system is to be explored, meaning that all steps of the solution have been identified and that the system is able to produce results that are adequate for an initial version of a structural monitoring system. The system will not be an automated closed loop able to perform a structural monitoring service. Nevertheless,

the components necessary for such an automated system to be developed shall be presented and explored. The analysis of the structural behaviour during the crowd induced loads is not to be used as a certification to prove acceptable vibration levels during occupancy, yet they could be used in a future assessment of the safety concerns from both attendees and management at the stadium. The final solution and the processes explored does not represent the exact recreation of the behaviour, nor does the signal processing recreate the exact signals for motion. The signal does, however, provide a usable signal for a proof of concept of an emerging technology. The virtual representation is a result of a preliminary study leading up to this master's thesis and will not receive notable tuning nor modification.

## 1.4 Thesis Structure

The thesis begins with a theory and background part in chapter 2 and chapter 3 that covers some of the areas that require definitions and clarifications, as well as an overview of the field of crowd loads on stadia structures. Chapter 4 presents the proposed system and its components and is intended to give an overview of a general system for structural health monitoring. The pre-emptive work of creating the digital twin and simulations using the model is covered in chapter 5 and chapter 6. Chapter 7 and chapter 8 covers the capturing and processing of the vibrations, where the hardware and methods used are presented. A presentation and analysis of the events that have been processed during the project are covered in chapter 9 and chapter 10. The digital twin solver is presented and tested in chapter 11, whereas the web visualiser is presented in chapter 12. The final two chapters cover the discussion, further work, and conclusion in chapter 13 and chapter 14.

# Chapter 2

# Theory

## 2.1 Digital Twin

The term Digital Twin is used in many different contexts, and the definition varies depending on what physical asset it represents. Grieves and Vickers [26] proposes the following definition for Digital Twins, as one of the few publications on the field:

> The Digital Twin (DT) is a set of virtual information constructs that fully describes a potential or actual physical manufactured product from the micro atomic level to the macro geometrical level. At its optimum, any information that could be obtained from inspecting a physical manufactured product can be obtained from its Digital Twin.

Fedem also has a definition on their website [22] where a descriptions of their applications for the digital twin solution is presented as:

> A solution to monitor and analyse in real-time the behaviour of structures and mechanical systems under the influence of complex and dynamic loads. The solution is based on a digital representation of a unique real asset that applies structural finite element models in combination with sensor feeds and classical (Newtonian) physics to replicate the physical state of the asset at any point in time. This information can be used in applications built for a wide range of purposes.

Seeing as this project concerns developing a solution based on the Fedem-description, the latter definition of the concept will be the one referenced in the thesis.

### 2.1.1 Components and Concept Description

Fedem also has an explanation of the components of the system which are:

**Edge capabilities,** for observing key aspects of the real asset's state and behaviour. This typically implies sensors with corresponding edge processing capabilities for data quality enhancements, such as calibration, filtering, and time synchronisation.

**The core runtime,** , using the input stream from the edge to render a (near) real-time digital reflection of the asset's state.

**The consumption layer** that subscribes to selected data streams from the Digital Twin for various applications. This can be specific end-user applications for monitoring and control, and it can be legacy applications for maintenance and asset management or the data stream from the twin might feed into data analytics and machine learning stacks for pattern recognition and decision support.

Their concept description presents the system based on observations and stimulations. Observations are made by physical sensors on the asset, and actuator motion is decided by measurement data and applied to the virtual model.

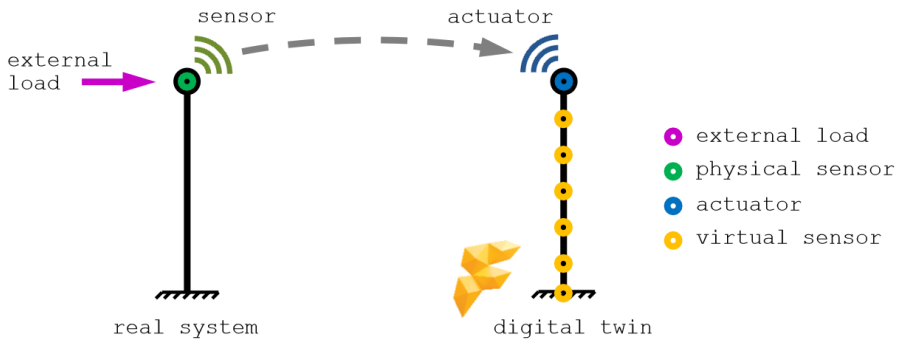


Figure 2.1: The general Digital Twin concept used in SAP Leonardo. From Fedem Technology AS [22]

### 2.1.2 Usefulness

The usefulness of digital twins are their ability to bridge the gap between the analogue and digital world, as it translates real observations into something understandable

for machines [22]. Fedem Technology further presents the following list of useful applications for the technology:

- Remaining life assessment of the structure
- Inspection/maintenance planning based on actual load history
- Relationship between loads and power production for control system policies
- Early damage detection for pre-emptive maintenance and shut-down prevention
- Hindsight to foresight – access to (aggregated) time series for design feedback
- Virtual inspection support
- Predict consequences of (adverse) future operating conditions
- Multi-asset orchestration/control and synchronisation
- Inspection/monitoring process support (cost reduction)
- Visualization and inspection of stresses at inaccessible/hidden locations

## 2.2 Accelerometer

An accelerometer is a sensor that measures vibrations of an object on which it is mounted. The acceleration measured is *proper acceleration*, i.e. accelerations in relation to a resting reference frame, as defined in [45]. The basic construction of an accelerometer is described on page 271 in [42]. It consists of a mass loaded spring that acts upon a piezoelectric crystal. The force acting upon the crystal is proportional to the acceleration caused by vibrations. An accelerometer is usually able to measure acceleration along three axes.

## 2.3 Signal Analysis

### 2.3.1 Nyquist-Shannon Sampling Theorem

The theorem concerns the ability to recreate an analogue signal as a digital signal consisting of discrete samples. The theorem states that if a signal contains no frequencies higher than $B$Hz it is satisfactory to use a sampling rate of $f_s$Hz such that $B < f_s/2$ [47].

### 2.3.2 Fourier Analysis

Fourier analysis provides some useful features for model analysis and testing.

#### Fourier Series

This series describes an infinite series that represent periodic functions in terms of cosines and sinuses accordingly. This is found on page 474 in [34]. The series is on the form

$$f(x) = a_0 + \sum_{n=1}^{\infty}(a_n \cos nx + b_n \sin nx), \tag{2.1}$$

where $f(x)$ is a periodic function and $a_0$, $a_n$, and $b_n$ are constants.

#### Discrete Fourier Series

A discrete version of the series is a function that is defined only at $N$ discrete points $(t_k, f(t_k))$ and is represented by a series that is finite on the form

$$f(t_k) = \frac{1}{2}a_0 + \sum_{n=1}^{\frac{N}{2}\text{ or }\frac{(N-1)}{2}} \left(a_n \cos\frac{2\pi nk}{N} + b_n \sin\frac{2\pi nk}{N}\right). \tag{2.2}$$

The discrete form is most commonly used when analysing digital signals.

#### FFT

Computations of the discrete Fourier series is usually done by using the Fast Fourier Transform which is described by Cochran et al. [15] as follows:

> The fast Fourier transform is a computational tool which facilitates signal analysis such as power spectrum analysis and filter simulation by means of digital computers. It is a method for efficiently computing the discrete Fourier transform of a series of data samples (referred to as a time series).

The FFT applied to the signals in this thesis is from the `numpy.fft` package, which provides the necessary tools for both calculating and plotting the signal on this form [49].

### 2.3.3 Cumulative Numerical Integration

A cumulative integration provides a summation of the integrated function to produce a new function on the same domain. This is used to convert the time series of an acceleration signal into a velocity signal, and further into a position signal. The Integration applied to the signal in this thesis is the `cumtrapz` function from the `numpy.integrate` package [50]. This function performs a cumulative integration using the trapezoid rule.

### 2.3.4 Butterworth Filter

A filter for signal processing is used for removing unwanted frequency components from the signal. A low pass filter is a filter that allows only frequencies lower than a given cut-off to pass whereas a high pass filter allows only frequencies higher than a cut off to pass. The Butterworth filter was designed to have an as flat as possible frequency response in the passband, i.e. not affecting the frequencies that are intended to pass through. The order of the filter determines how steep the transition-band is, between the passband and the stopband. Increasing the order also increases the latency of the signal. The filter design in this thesis is uses the `butter, lfilter`, and `freqz` functions from the `scipy.signal` package [51].

## 2.4 Modal Analysis

Modal analysis is defined by Fu and He [23] as

> the process of determining the inherent dynamic characteristics of a system in forms of natural frequencies, damping factors and mode shapes, and using them to formulate a mathematical model for its dynamic behaviour. The formulated mathematical model is referred to as the modal model of the system, and the information for the characteristics are known as its modal data.

A mode consists of the three properties: natural frequency or eigenfrequency, a displacement pattern or eigenvector, and a dampening factor.

### 2.4.1 Eigenfrequency

Eigenfrequency is the frequency or the frequencies of a systems oscillations when the system has been acted upon and then left to its own accord. For a mechanical

system, the eigenfrequencies are determined by the mass of the system bodies that oscillates and the forces pulling it toward its equilibrium state. If a system is acted upon by a periodic force with a frequency equal to the eigenfrequency a resonance between the force and the system will occur [44].

### 2.4.2 Resonance

Resonance describes that a system that has the ability to oscillate will absorb energy and cause oscillations of great amplitude when excited by a periodic force of the same amplitude as the systems eigenfrequency [41]. Figure 2.2 shows a plot that shows the transmissibility of an excitation based on the ratio between the excitation frequency and the eigenfrequency.

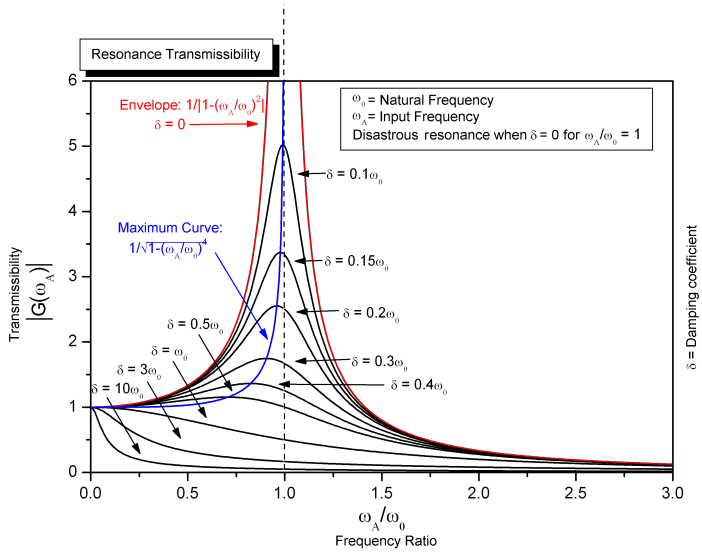


Figure 2.2: Transmissibilty versus frequency ratio, and the effect of the dampening ratio on the resonance of a simple harmonic oscillator. From Wikimedia Commons

### 2.4.3 Impulse Response

The impulse response is the reaction of a system as it is acted upon by an impulse-shaped excitation. The impulse might be mechanical in the form of a hammer strike, acoustic in the form of a bang, or electrical in the form of a voltage pulse [31]. The impulse response may provide information about the properties of a system, such as the systems eigenmodes.

# Chapter 3

# Previous Analyses and Literature

This chapter presents relevant literature for the monitoring of *Lerkendal*. The first reports are from the contractor company which were responsible for the construction of the stadium and a follow-up investigation of the earliest reported concerns of the cantilever vibrations. The article following the reports is a literature review that has compiled a coherent document for the theory and methods used in modeling crowd induced excitation on stadia structures. The final sections describe systems and methods for structural health monitoring of stadia that have been researched and presents the state-of-the-art on the field.

## 3.1 The Reinertsen Reports

Reports from previous investigations of the vibrations in the grandstand are presented as well as an evaluation of the relevance of the report and their results. The reports are found in Appendix C

### 3.1.1 Reinertsen report 2001

The original report from the construction of the grandstand was performed by *Reinertsen AS*. The report contains analyses of the seating elements, and of six different beams of *tribune D*. A minimum requirement is for eigenfrequencies to be above 6 Hz, and preferably above 7 Hz. The seating elements were analysed in SOLVIA, whereas the beams were analysed in StaadPro. An additional mass of

2.5 kN/m(per meter of seating) was added to represent the seats and other fixed inventory. The eigenfrequencies are shown in Table 3.1. Material data is found in the appendices of the report and are presented in Table 3.2:

| **Element** | **Eigenfrequency** [Hz] |
|---|---|
| Seating element | 9.00 |
| Main tribune beam | 6.96 |
| Main tribune beam w/grove | 7.06 |
| VIP beam | 6.96 |
| Lower tribune, beam 1 | 7.95 |
| Lower tribune, beam 2 | 7.25 |
| Lower tribune, beam 3 | 6.23 |

Table 3.1: Eigenfrequencies of grandstand elements as reported by Reinertsen

| | | |
|---|---|---|
| Young's modulus | $E$ | 32GPa |
| Poisson's ratio | $\nu$ | 0.17 |
| Density | $\rho$ | 2400kg/m$^3$ |

Table 3.2: Material data from original finite element analysis

**Evaluation**

The report considers the grandstand component-wise and not the entire structure as a system, which does not necessarily give any indication of the eigenfrequency in the mode of a jumping crowd on the upper tier. The material data may be used in tuning of a virtual representation of the grandstand. *Reinertsen's* report considers elements from *Tribune C*, whereas this project is concerned with *Tribune D*. These grandstands have an identical design of the upper level, and as such the analysis performed are representative of the element of *Tribune D*.

### 3.1.2 Reinertsen report 2009

The second report presents the results after RBK requested a new inspection after the supporter group *Kjernen* was moved from the lower tier of *Tribune C* to the upper tier of *Tribune D*. The displacement investigated was the vibrations of the seating elements and girders on the upper tier. The report concluded that the displacement of the upper-level cantilever is too small to pose any significant risk, meaning that the stresses in the girders are not close to causing any destructive development. Consequently, no actions were deemed necessary, although a few

measures were proposed as plausible remedial actions. One is to move the supporter group somewhere else, and the other is strutting the cantilever to a lower tier of the grandstand. Vibrations were measured in areas prone to vibrations, i.e. at the tip of the cantilever and the back rows of the seating. Vibrations were initiated by 15 men jumping rhythmically during the first survey, which caused a peak displacement of 0.9mm, whereas the peak velocity was measured at 46mm/s. The largest displacement during a match was 2mm at the tip, between two girders. The highest oscillatory velocity was around 17mm/s.

An analysis of a 2D beam model resulted in an eigenfrequency of 4.7 Hz for the first mode, while the rest had frequencies above 14 Hz. The 3D analysis of the grandstand is modelled using beams with real cross-sections. An additional load of 1,5kN/m, represents two individuals of mass 75kg. The modal analysis was performed in the STAADpro software. The lowest mode of interest was mode 12 with an eigenfrequency of 3.8Hz, which has a horizontal movement. The report says that the modes with a vertical movement of the tip of the cantilever all are above 5Hz.

**Evaluation**

This report uses a 3D analysis of the entire construction rather than the frequency of separate parts, which gives a more precise set of results than the first report. The measurements during matches are used for comparison of results from simulations. There is no information about where these peak values were measured, which is an uncertainty when comparing these with the results measured during the work in this project. The fact that 15 people rhythmically jumping caused the most significant readings implies that the rhythmical component is essential to the motion of the cantilever.

## 3.2 Vibration Serviceability of Stadia Structures Subjected to Dynamic Crowd Loads: a Literature Review [32]

The review by Jones et al. has proved itself to be a document of great value. The article covers all relevant topics and research necessary to understand the complexity of modeling and investigating the load case on the grandstand. This section will be a re-telling of the most important aspects covered in the article, in an attempt to identify the methods used today as counterparts to the digital twin method. Most concepts are relevant albeit not directly applicable in the digital twin solution. The complexity of the current models as presented in the article is a good indicator of the potency of the digital twin method. The article identifies three key issues which are:

**Source:** the quantification of dynamic crowd loading. The dynamic load of a rhythmically tuned crowd jumping will cause a load significantly higher than an equivalent static load. The response of the structure in these load cases may cause annoyance or panic among the occupants causing or observing the structure.

**Path:** the modeling of the stiffness, mass and dampening of the structure, including the effects of human occupants. The behaviour of a stadia structure is greatly affected by the occupants of the structure as the human body both act as an actuator that initiates motions and applies energy, as well as functioning as a dampener by absorbing energy from the system.

**Reciever:** the acceptability of dynamic structural responses. Several ways to quantify motion may be used to analyse load cases based on limits for comfort and panic.

The article is published in 2011 and has an update follow-up review article from 2017 which is presented in the next section of this chapter. The following subsections are titled in accordance with the sections of the parent article.

### 3.2.1 Problem Overview

The article presents several cases where crowd induced dynamics has caused problems that have required remedial work. The load applied from a crowd has been cited by Moreland [39] to increase by up to 50 % when jumping. The problematic

grandstands are most often those which include seating at the front of a cantilever design, which is prone to vibrate.

### Cases

The vibrations have been shown to create palpable vibrations until 400 meters away during a concert in Göteborg, Sweden [9]. Maracanã in Brazil experienced cracks in concrete members caused by the crowd as reported by Batista and Magluta [6]. Several other stadia in the UK required attention by the management:

- Cardiff Millennium Stadium, where props had to be installed ad-hoc and just before a major concert [25].
- Anfield in Liverpool, where three additional steel columns were required to stiffen the structure [46].
- Old Trafford in Manchester, where strict stewarding was used to reduce crowd dynamic excitation [38].
- Highbury Stadium in London, where tuned mass dampers were installed to mitigate the vibrations.

### Remedial Actions

A possible remedial action for cantilever stands experiencing vibrations are stiffening the construction by adding additional struts or columns; although stiffening might reduce motion the stresses might increase by attempting to contain the energy induced by a crowd, it will, however, decrease the visual effect. Another action is to add tuned mass dampeners, as a passive component, to remove energy from the structure. An active alternative is to utilise systems that counteract the motion, several of which are presented by Nyawako and Reynolds [43] and Ebrahimpour and Sack [17]. Other simpler actions are to either move the crowd away from the rows at the front of the cantilever or to actively manage the behaviour of the crowd, such as banning certain songs.

### Standards

Three standards are presented that accounts for the effects of the dynamic load from a crowd at stadia, the ISO guidance [28], a Canadian guidance [11], and the UK recommendations [29], each with their take on acceptable limits of vibration in

stadia constructions. The norwegian standard, Norsk Standard [40], does not cover this area.

### 3.2.2 Dynamic Crowd Loads

The loads applied to a grandstand are complex and unpredictable as the behaviour of a crowd has random behaviour from individuals. This section attempts to describe models for these loads as a generalisation of this behaviour. The two most relevant for the *Lerkendal* case is, however, the jumping load, and the bouncing/bobbing/jouncing load, where the difference between them is whether or not the humans leave the ground when acting. Jumping is an exhausting activity, and a crowd will not be able to maintain the motion over longer periods. Ginty et al. [24] presented frequency ranges for several types of groups can maintain a rhythm and found 1.8-2.3 Hz to be the range for larger crowds at concerts.

**Jumping Load** is the one capable of producing the most significant human load and may reach magnitudes several times higher than the static weight of a jumper. The load may be visualised as one half-period with force application when landing and launching oneself, and the other half period without contact with the ground, as shown in Figure 3.1.

**Bobbing/bouncing/jouncing** is similar to jumping but without actually leaving the ground. The activity is more comfortable to perform over longer periods of time and has a lower energy requirement than jumping. This activity is capable of reaching a force magnitude in the lower values of what is observed when jumping. Agu and Kasperski [4] notes that the greatest energy in the force signal occurs at twice the rate of the actual activity rate. A force history for bouncing is shown in Figure 3.2

#### Dynamic Versus Static

Several authors have investigated the load on a plan by jumping or bouncing, and a comparison is presented by Jones et al. for comparing the works of several authors in Table 3.3. The table shows that a jumping human can generate several times the load of a static human, although the results are dependent on several factors.

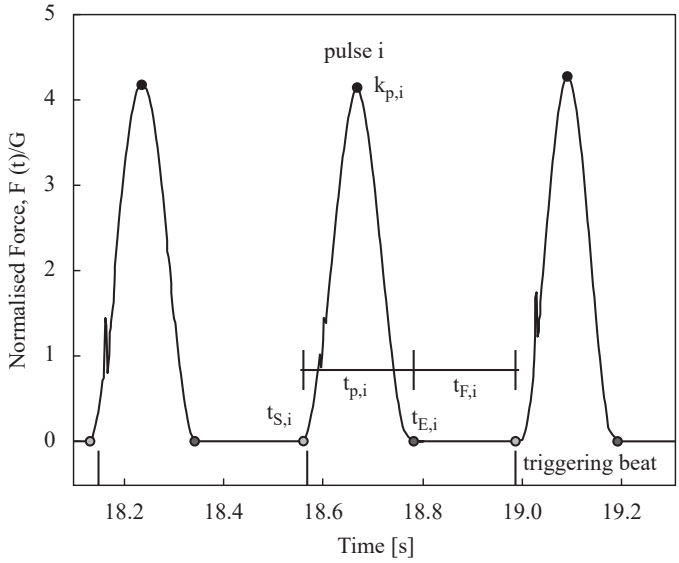


Figure 3.1: Normalised force history for a single person jumping at constant frequency. From Jones et al. [32]

| Author | Average immobile person | Tuan and Saul [54] | Ebrahimpour and Sack [17] | Moreland [39] | Tilden [53] |
|---|---|---|---|---|---|
| Action | Static | Rythmic jumping | Periodic jumping | Jumping | 'Jouncing' |
| Participants | 1 | 1 | 1 | 90 | N/A |
| Frequency | N/A | 2.2 Hz | 3 Hz | N/A | N/A |
| Load observed | 0.75 kN/person | 4.50 kN/m$^2$ | 2.85 kN/person | 1.13 kN/person | 2.04 kN/person |
| Plan load kN/m$^2$ | 2.15 | 4.50 | 8.14 | 3.23 | 5.83 |

Table 3.3: Observed equivalent static load. From Jones et al. [32]

### Half-sine Pulses

The description of loads as half-sine pulses is from Bachmann and Ammann [5] who uses a series of pulses with a given contact ration, and amplitude. The equation used to describe a fitted curve to the motion is

$$f(t) = \begin{cases} k_p G sin\left(\pi t/t_p\right), & 0 \leq t \leq t_p \\ 0, & t_p \leq t \leq T_p \end{cases}, \tag{3.1}$$

where $G$ is the static weight of a person $k_p = F_{max}/G$ is the impact factor and $F_{max}$ is the peak dynamic load. $t_p$ is the contact duration and $T_p$ is the jumping period, and $\alpha = t_p/T_p$ is the contact ratio. Bachmann and Ammann [5] observed that by assuming conservation of momentum the relation between the impact factor and the contact ratio, as the weight of the person times the activity period must equal the impulse giving

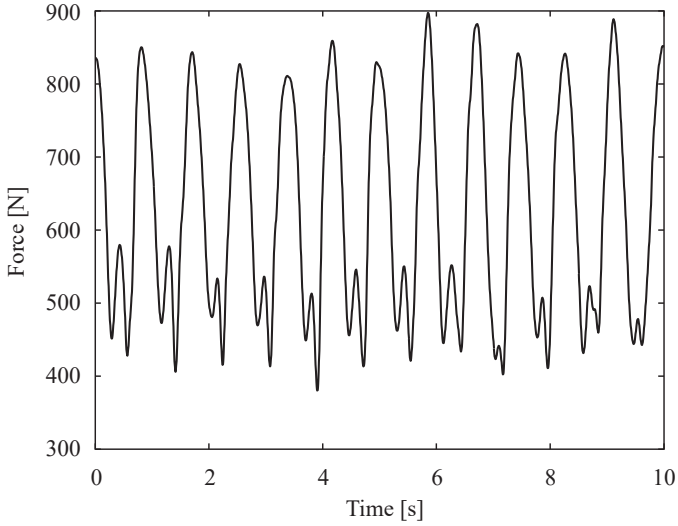


Figure 3.2: Example measured force history for jouncing. From [32]

$$\int_0^{t_p} k_p G sin(\pi t/t_p) \mathrm{d}t = GT_p, \tag{3.2}$$

giving the relationship

$$k_p = \pi/2\alpha. \tag{3.3}$$

**Fourier Series**

When wanting to apply the load as a steady state signal the use of the Fourier series to describe the load is often more precise. The typical plot of a Fourier transformed signal is shown in Figure 3.3(b). Figure 3.3(b) also shows the distinct peaks at the integer multiples of the applied frequency of the signal, further showing the excitation from harmonic frequencies meaning that low-frequency activities may induce responses from higher frequencies. The difference between Figure 3.3(b) and Figure 3.3(d) is that the signal is perfectly periodic in Figure 3.3(c), whereas Figure 3.3(a) is an more realistic signal which causes bleeding into other frequencies. Figure 3.3(e) and Figure 3.3(f) show the same signal generated by a Fourier series.

Fourier series used to represent periodic human load may be simplified to the equation

$$F(t) = G\left[1.0 + \sum_{n=1}^{\infty} r_n \sin\left(\frac{2n\pi}{T_p} + \phi_n\right)\right], \tag{3.4}$$

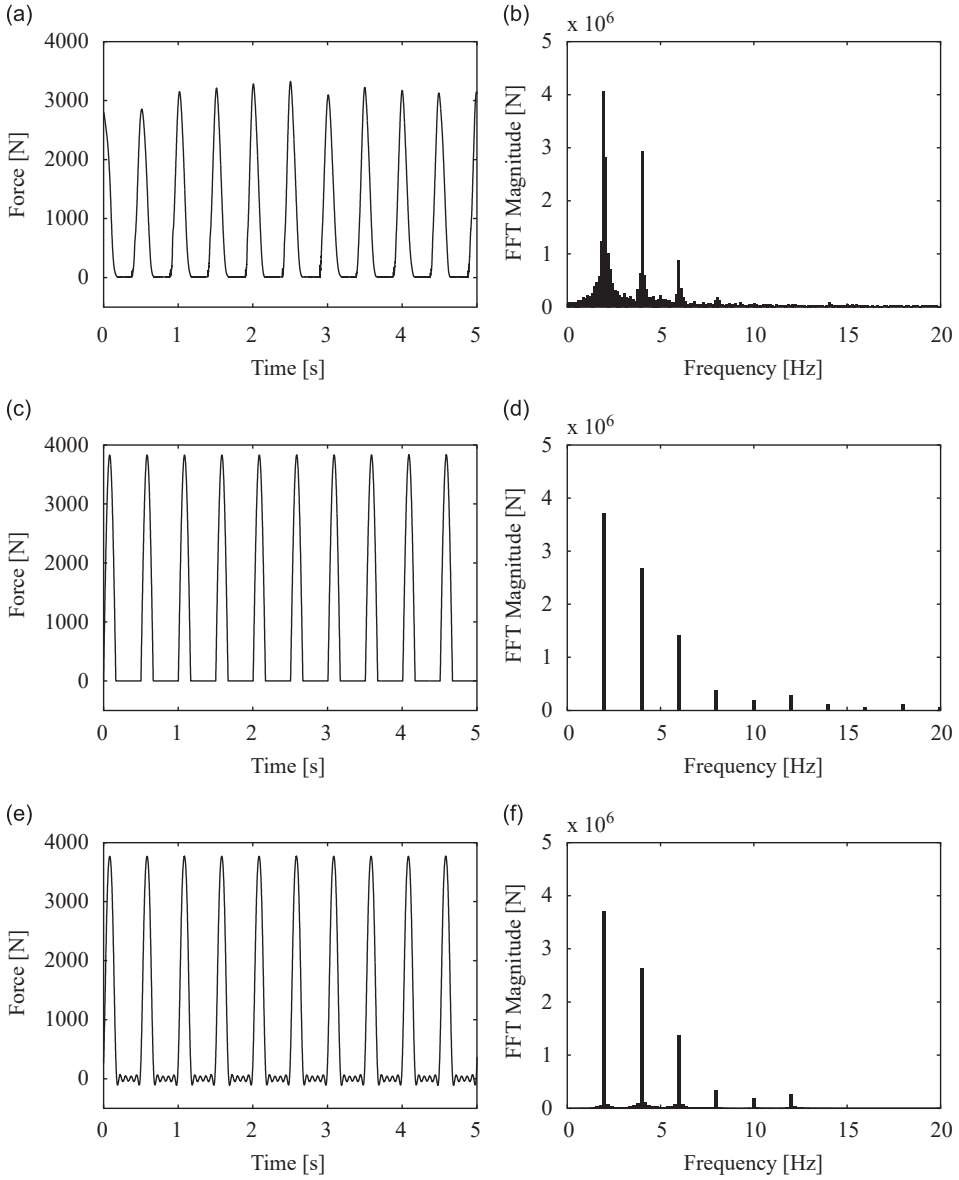


Figure 3.3: **(a)** A measured force history for jumping, **(b)** the frequency domain representation of (a), **(c)** a synthetic force history approximation using half sine pulses, **(d)** the frequency domain representation of (c), **(e)** a synthetic force history using a six term Fourier series using coefficients from Ellis et al. [18], **(f)** the frequency domain representation of (e). Figure from [32]

where $F(t)$ is the force at time $t$, $G$ is the *weight* of the jumper, $n$ is the number of the harmonic multiple of the base frequency found from $1/T_p$, $r_n$ is the Fourier amplitude coefficients or dynamic load factors (DLF), and $\phi_n$ is the phase lag in radians. Ji and Wang [30] presents the following ways to determine the different parameters:

$$r_n = \sqrt{a_n^2 + b_n^2}, \tag{3.5}$$

and

$$\phi_n = \arctan(a_n/b_n), \tag{3.6}$$

where

$$a_n = \begin{cases} 0, & n\alpha = 0.5 \\ \frac{1+\cos(2n\pi\alpha)}{1-4n^2\alpha^2}, & n\alpha \neq 0.5 \end{cases}, \tag{3.7}$$

and

$$b_n = \begin{cases} \pi/2, & n\alpha = 0.5 \\ \frac{\sin(2n\pi\alpha)}{1-4n^2\alpha^2}, & n\alpha \neq 0.5 \end{cases}. \tag{3.8}$$

**Expansion Into Crowds**

As there is no way to determine a crowd's motions pre-emptively, there are difficulties with finding a model for an entire crowd. This is because there are variations in activity level amongst the crowd, some might be passive and not participate while others could have varying activity levels. The load model is an adaptation Equation 3.4 and is described by the following equation:

$$F_v(t)_N = C(N)Q\left[1.0 + \sum_{n=1}^{k} \alpha_{n,v} \sin\left(2\pi n f t + \phi_{n,v}\right)\right], \tag{3.9}$$

Where $F_v(t)$ is applied load in the vertical direction as indicated by $_v$ at time $t$ for $N$ people in a crowd, $C(N)$ is a coordination factor given in from Table 3.6, $Q$ is the weight of the crowd, $k$ is the number of included DLFs, $\alpha_n$ is the $n$ the DLF from Table 3.4 or Table 3.5, and $\phi$ is the phase lag.

The different rhythmic ability levels in the ISO Table 3.6, is based on a crowd interpersonal coordination. The level states to what degree the action is synchronised. A wholly synchronised crowd would have a Fourier load on the action frequency and its harmonics, whereas a less coordinated crowd will bleed into neighbouring frequencies which could cause resonance frequencies close to the action frequency to be activated even without the resonance frequency being one of the harmonic

| Activity | Lively concert or sports event |
|---|---|
| Weight of participants, $w_p$ [kPa] | 1.5 |
| First harmonic, $\alpha_1$ | 0.25 |
| Second harmonic, $\alpha_2$ | 0.05 |
| Third harmonic, $\alpha_3$ | 0.00 |

Table 3.4: Relevant part of the recommended loading functions for rythmic events from Canadian Commission on Building and Fire Codes [11]

| Activity | Coordinated jumping with seats |
|---|---|
| Common frequencies, $f$ [Hz] | 1.5 - 3.5 |
| First harmonic, $\alpha_1$ [a] | 2.10 - 0.15 [b] |
| Second harmonic, $\alpha_2$ [a] | 1.90 - 0.17 [b] |
| Third harmonic, $\alpha_3$ [a] | 1.25 - 0.11 [b] |

[a] As a function of $f$
[b] $\alpha_1 = 1.7, \alpha_2 = 1.0$, and $\alpha_3 = 0.4$ may be used as first approximations

Table 3.5: Relevant part of example design parameters for coordinated activities at stationary location from International Organization for Standardization [28]

frequencies. The three coordination levels are separated between people rarely attending events at the lowest level, the middle level for people who often attend events with synchronised motion, and the highest level for trained athletes.

### 3.2.3 Dynamic Structural Properties

The simplest model of a structure is as a single degree of freedom system (SDOF), with a mass $m$, a damping $c$ and a stiffness $k$, with an acceleration $\ddot{u}$, a velocity $\dot{u}$

| Source | Harmonic 1 | Harmonic 2 | Harmonic 3 |
|---|---|---|---|
| NBC Canada[11] | Included in load amplitude | | |
| ISO, high rhythmic ability [28] | 0.80 | 0.68 | 0.50 |
| ISO, medium rhythmic ability [28] | 0.67 | 0.50 | 0.40 |
| ISO, low rhythmic ability [28] | 0.50 | 0.40 | 0.30 |
| Ellis et al. [18] | $m^{-0.082}$ | $m^{-0.024}$ | $m^{-0.31}$ |
| Bachmann and Ammann [5] | 0.75 | | |

[a] As a function of $f$
[b] $\alpha_1 = 1.7, \alpha_2 = 1.0$, and $\alpha_3 = 0.4$ may be used as first approximations

Table 3.6: Crowd coordination factors

and displacement $u$ in the relationship based on the dynamic equation

$$m\ddot{u} + c\dot{u} + ku = F(t). \tag{3.10}$$

The models may further be built up of a multi-DOF system in 2D, or as a finite element model in 3D. Most finite element models have several areas of uncertainty when representing stadia such as:

- General connections
- Support conditions (including soil-structure interaction)
- Non-structural elements (facades, partitions, etc.)
- Connections between seating decks and supporting rakers
- Cracking and other damaged members
- Contribution of 'far away' elements such as roof trusses

The FEM should therefore often undergo sensitivity studies to adapt parameters and should be updated based on test data from the physical structure in action.

### Field Testing

For testing of structures, the UK working group [29] recommends dynamic testing and modal analysis of the model. The three classes of testing of stadia structures are

**Forced vibration testing** (FVT) using instrumented shaker or impact excitation. FVT is used to generate frequency response functions, which may determine mode shapes, natural frequencies, modal damping values, and modal masses.

**Ambient vibration testing** (AVT) using the response to environmental excitation. AVT is generally used to determine global modes of a structure. The excitation often comes from wind, or tremors from traffic. The analysis often has a harder time to determine results than an FVT.

**Vibration monitoring** of controlled in service excitations from human occupants. Vibration monitoring is used to determine response to actual human-excited loads or be used to monitor structure in-service.

**FE Model Updating**

Updating the model is often necessary to refine the ability of the analytical model to represent the behaviour of the physical model based on test data. There are two main stages of this process described by Brownjohn et al. [10] which are macro-updating and micro-updating. Macro-updating covers the alteration of geometry in the model or inclusion of new elements to better represent the physical model, which often is the inclusion of components that were deemed unnecessary in the initial idealised model. These may alter the eigenfrequencies of the model, although the mode shapes should be conserved.

Micro-alteration is fine-tuning of the model after the geometry has been updated. Often by changing the parameters of the material or construction such as dampening, stiffness and mass representation both in load and in the material. Stiffness and dampening are often hard to find and introduces significant uncertainty in the FE model.

### 3.2.4 Human-Structure Interaction

The human-structure interaction is the phenomenon occurring when the human and the behaviour of the structure merge and change their dynamic properties, as Ellis and Ji [20] provided an example of when plotting an autospectra of the acceleration of an empty and an occupied grandstand seen in Figure 3.4. The problem is complex because the humans acting on the structure might vary their behaviour between applying or draining energy from the excitation. The behaviour might change for a single person and between the members of a crowd during the duration of the excitation period. When the acceleration reaches high amplitudes, around 1g, the crowd tend to start riding the motion of the structure rather than acting against it to remain in balance.

The two main method for modeling these problems are

1. Reducing and increasing damping values in an attempt to indirectly represent the phenomenon

2. Direct modeling of occupants as additional degrees of freedom in the structure, with varying levels of detail

The first method is used by the Canadian recommendations [11], while the second has been applied by the UK recommendations [29].

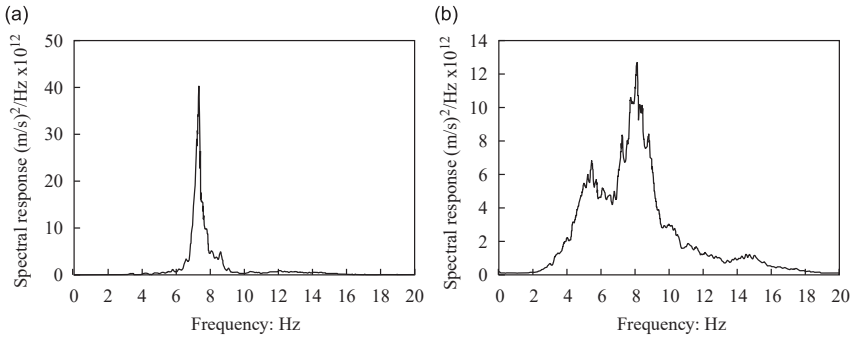


Figure 3.4: Autospectra from a grandstand when (a) empty and (b) occupied. From [32]

**Effects of Occupants on Structures**

Other than excitation on structures the human merging increases the dampening of the structure. Lenzen [35] found that four people increased the dampening by 300 % in a test on a concrete slab floor. Ellis and Ji [19] found that human excitation on structures would not change the modal properties of the structure. The study did, however, assume a synchronised crowd being in the air at the same time, despite the fact that a crowd at a stadium would be unable to be be airborne wholly synchronised. The Canadian guidance [11] suggests a damping ratio between 6 and 12 per cent when a structure is densely occupied by a crowd.

### 3.2.5 Acceptability of Vibrations

Two different criteria are proposed when determining the accepted levels for vibrations which are the levels for 'comfort' and the levels for 'panic'. The comfort criteria consider low-frequency vibrations which most people do not experience as dis-comfortable. The panic criterion has a higher level, but has a strict upper limit as one person panicking is enough to spread it to several other parts of the crowd. The fact that a situation with panicking amongst the crowd might cause hazardous situations, as they are uncontrollable and irrational, might be caused by vibrations that not necessarily are unsafe, as long as they are perceived as unsafe by the crowd. Most limits presented are based on surveys, observations, and statistical data, as inciting panic in a crowd is not an experiment easily carried out ethically.

### Root Mean Square Acceleration (RMS)

RMS of acceleration is one way of processing the vibrations to measure against given criteria used as limits. RMS is obtained using equations like

$$a_{\mathrm{RMS}} = \left( \frac{1}{T} \int_0^T a^2(t) \mathrm{d}t \right)^{0.5}. \tag{3.11}$$

ISO 10137 [28] suggests using a sample period of 1s for the panic criterion and 10s for the comfort criterion, whereas Kasperski and Agu [33] suggests 30s for for comfort and "a few cycles" for panic.

### Vibrations Dose Value (VDV)

This method focuses more on the magnitude of the vibrations than RMS. It is a cumulative exposure method and focuses more on the tolerance of vibration rather than perceptibility, which is the focus of RMS. VDV may be calculated by the following formula

$$\mathrm{VDV} = \left( \int_0^T a^4(t) \mathrm{d}t \right)^{0.25}. \tag{3.12}$$

### Vibration Criteria

The ISO, Canadian, and UK standards all have a few criteria for acceptable vibrations. These are not intended for in-service measurements, but to be used in the development of new structures. The proposed acceptable levels for $a_{\mathrm{RMS}}$ are found in Table 3.7, Table 3.8 shows the possible VDV ranges proposed by Ellis and Littler, and Table 3.9 shows their suggested acceptable vibrations levels and their extrapolation to VDVs based on experiments from Germany, with people jumping on cantilever grandstands [33].

| Code | Assesment method | Limit type | Limit |
|---|---|---|---|
| Commentary D [11] | Peak value | Absolute | 18%$g$ |
| ISO 10137 [28] | 10 s RMS | Comfort | 10%$g$ |
| | 1 s RMS | Panic | 20%$g$ |
| UK Working Group [29] | RMS | Scenario 3[a] | 7.5%$g$ |
| | RMS | Scenario 4[b] | 20%$g$ |

[a] All crowd considered active. Moderate bobbing
[b] The whole crowd highly active. Loading taken to be twice that for the commonly occurring events of scenario 3

Table 3.7: Proposed acceptable levels of vibrations

| VDV range | Reaction |
|---|---|
| $< 0.3$ | May be perceptible |
| 0.6 - 1.2 | Low probability of adverse comment |
| 1.2 - 2.4 | Adverse comment possible |
| 2.4 - 4.8 | Adverse comment probable |
| $> 4.8$ | Unacceptable |

Table 3.8: Possible VDV ranges for grandstands proposed by Ellis and Littler [21]

| Vibration level: %$g$ | Reaction | Event VDV: m/s$^{1.75}$ |
|---|---|---|
| $< 5$ | Reasonable for passive persons | $< 0.66$ |
| 5 - 18 | Disturbing | 0.66 - 2.38 |
| 18 - 35 | Unacceptable | 2.38 - 4.64 |
| $> 35$ | Probably causing panic | $> 4.64$ |

Table 3.9: Suggested acceptable vibration levels and their extrapolation to VDVs by Ellis and Littler [21]

### 3.2.6 Evaluation

The report by Jones et al. covers most of the relevant theory concerning crowd induced dynamics on stadia and is useful for giving a general understanding of the complexity of analytically describing the situation and the different approaches for modeling them. The digital twin approach will be a counterpart to the modeling of forces from a crowd; however, the modeling is useful for verifying the finite element model, as well as to show the viability of solving the dynamic response from measurements, rather than through an analytical representation of the load.

## 3.3 Sensing and Monitoring for Stadium Structures: A Review of Recent Advances and Forward Look [12]

The review aims to update the article by Jones et al. [32], with developments happening in the past decade. The new review by Catbas et al. from 2017 presents and discusses the general findings of the prior review, and focuses on the latest developments concerning the modeling of loads, monitoring of stadia, and on analysis vibration serviceability.

### Measurement and Sensing

Most of the advances in the crowd load estimation come from the use of computer vision to estimate the load from individuals and crowds. The method for an individual is based around the partitioning of the human body and tracking the acceleration of each of the parts with a camera, and distributing a mass partition of the total mass among them. The summations of these values provide a force estimate made by the human body as an alternative to using a simple slab measurement. The use of visual monitoring is also shown to estimate loads from the crowd using varying degrees of precision. This would enable a less expensive way of monitoring a crowd during real events. The method is not without disadvantages. The authors summarise these four disadvantages of the new approach: generation of large data sets, inability to place a camera in front of crowd, lighting and flashing cameras disturb the recordings, and no accounting effects from induced vibrations on the recorded movement.

The most critical development in sensing the behaviour is the introduction of wireless sensor networks which allows for a significant decrease in complexity for instrumentation of the structures.

### Load Regeneration, Human-Structure Interaction, and Structural Identification

The stochastic modeling of an individual's effect has improved the ability to recreate loads compared to the previously used half-sine and Fourier series methods. The method is better than the two others because of its ability to capture intra-personal variations throughout the load event, such as changes in intensity and changes in posture due to exhaustion from the activity. The next step in this develop-

ment is therefore presented as developing several models for different ratios of an active/inactive crowd that are active by jumping or bobbing periodically.

Another development presented is the progress on investigating the effect of a crowd on the natural frequencies, dampening, and the ability to store the energy of the human-structure interaction. Most studies showed that a higher mass decreased the frequencies and increased the dampening ratios.

The review also concludes that the use of operational modal analysis is a questionable method for determining the behaviour of a stadium and that this is an area that needs attention in the future, with focus on slender structures, time-variant excitation, and harmonics.

#### Vibration Serviceability

The authors present the idea of forming new criteria for vibrations that are based on recordings of a significant amount of events. The Issue with the criteria used today is their inability to reflect the actual state of the vibrations of the structure. No further information is presented in this area.

### Evaluation

The follow-up review shows that the field still has room for the development of new methods. The use of the digital twin methodology avoids the issue of accurately modeling the load to execute a simulation, and simplifies the process significantly. The update information is not as interesting as the in-depth review as performed by Jones et al.

## 3.4 Real-Time Vibration-Based Structural Damage Detection Using One-Dimensional Convolutional Neural Networks [3]

Abdeljaber et al. presents their development of using a neural network to identify structural damage in a grandstand. The group has a physical grandstand simulator in a laboratory instrumented with a random excitation generator, and accelerometers at each joint in their model. They have trained a neural network to identify damage in the different joints of their construction where the training and problems mostly have been focusing on detecting changes in a single joint. The results of the experiment are that the network was able to learn to identify the damage based

solely on the acceleration signal. The Network also managed to identify combinations of faults if two joints were loosened. This system, if developed further, could be used to detect defects in real time for more massive structures. The challenge, however, is that the training of a neural network would increase in complexity along with the size of the structure.

## 3.5 Long-Time Monitoring of the G. Meazza Stadium in a Pattern Recognition Prospective [16]

Datteo et al. investigates a system for structural health monitoring by using historical data over an extended period of monitoring a football stadium. The stadium used is the Guiseppe Meazza stadium in Milan, also known as San Siro, where seismic accelerometers are instrumented beneath the 2nd and 3rd tier of the grandstand. The two tools used in the solution are autoregressive models(AR) and Principal Component Analysis(PCA). An AR-model is used to estimate a stationary process based on earlier samples and a random term to provide a function of estimation over time. In combination with PCA, they are able to represent the behaviour of the structure through a small set of variables, here being the three first principal components(PCs) of the behaviour. PCs are the peaks of a frequency spectra showing the magnitude of each frequency contribution. The results presented from the procedure is a set of graphs that show the change in the principal components value across the period of the investigation, which covers eight months from August to April. These principal component values are combined with monitoring of average temperature and show that there is a strong correlation between the first PC and temperature and humidity, while the two remaining PCs are correlated, although less so than the first. The correlation shows that the PC increases with increased temperature, meaning the vibration frequency peak increases with a rise in temperature. The authors conclude with a statement that the monitoring of temperature is a suitable inclusion for a structural health monitoring system.

# Chapter 4

# System Description

This chapter will give a brief description of the planned system which components will be explored throughout the rest of this project. The system that is explored will be based on the components described in subsection 2.1.1. The three components in the digital twin system will be the edge capabilities, the core runtime, and the consumption layer. The ideal system would work as a closed loop that automatically performs the necessary steps to enable consumption of the system results. Figure 4.1 is a diagram that shows a sketch of how a structural health monitoring system would be set up with the three components. These components and their challenges will be explored in the following chapters at various degrees to find a solution suitable for a grandstand based on the general description given.

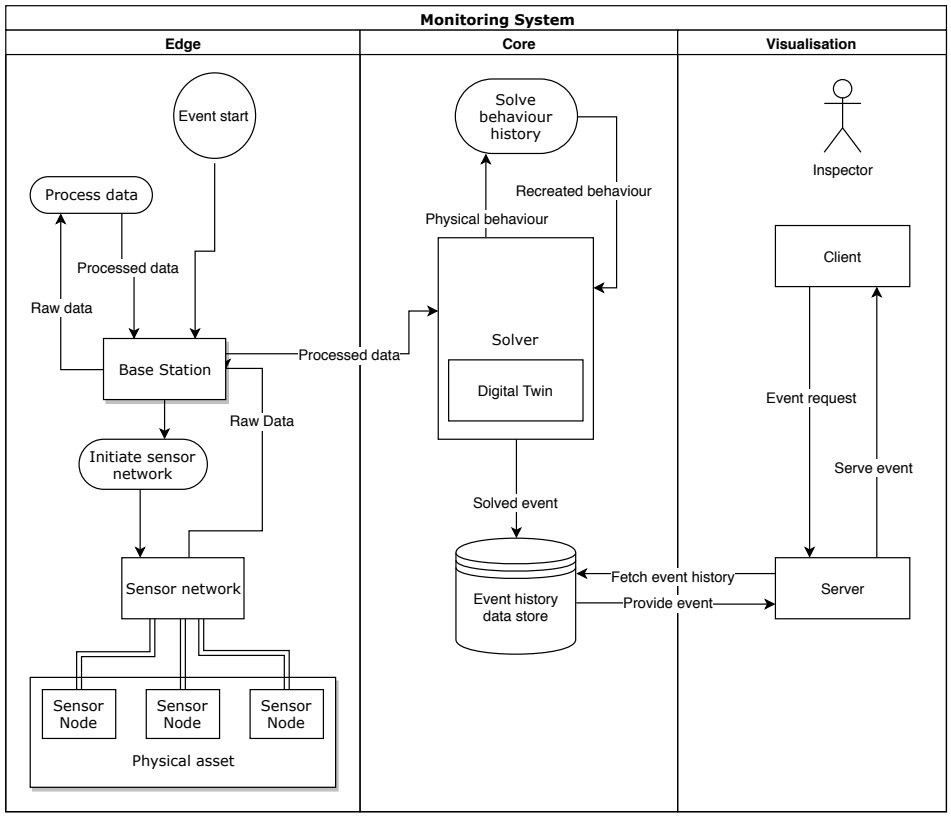


Figure 4.1: UML diagram of the system description

## 4.1 Edge Capabilities

The first step of the system is to capture the behaviour of the physical asset. In this case, the motion of interest is the vertical displacement of a cantilever grandstand. The sensor must necessarily be able to capture this behaviour. Seeing as the excitation may be described as a vibratory situation, the accelerometer is the sensor most fit for the job. The signal from the sensor set up must be synchronised and collected by a base station for further processing. This processing involves transforming the raw signal from the sensors into a format that the core runtime consumes. The process will involve filtering and integration as the signal used in the core runtime is displacement, which is obtained through double integration of acceleration.

## 4.2 Core Runtime

What is defined as the core runtime, is the part of the system that enables the recreation of the state and behaviour virtually on the digital twin. The recreation necessitates a digital version of the physical asset, i.e. an FE model. This is the digital twin and represents the core of the concept where one solves an event's time history based on the behaviour recorded from the physical asset. Depending on the resources available for running the simulation and the complexity of the FE model the solution might be available in close to real-time as the behaviour is recorded, a more complex model would most likely require a significantly longer time to complete a solution. The system explored in this thesis is the latter with a focus on the review of a recorded history of events. After solving the time event histories, they would be saved in a data store.

## 4.3 The Consumption Layer

The consumption layer is the part of the system an inspector would use and consists of a client and a server. The client-server relationship would enable inspection unrestrained from the geographical location by the use of a web interface, which connects to a server on-site. Exactly what the inspector would request from a solution could be tailored for the specific structure at hand. An example, and the one strived for in this project, is the ability to inspect the virtual recreation as an animation of displacement and stress distribution across the most critical elements. Another could be an overview of changes in behaviour between matches notify the inspector if there is an unnerving development in the behaviour.

# Chapter 5

# 3D Geometry and Finite Element Model

The construction of the four current grandstands at *Lerkendal Stadion* was completed in 2002, a time when architects and civil engineers usually did not make 3D models of constructions. The modeling is therefore based on drawings in the .dwg-format which was made available by the operations manager. The structure consists of three tiers of seating. The seating elements are supported by girders. The upper tier is supported by nine girders. The seven inner girders are supported by three beams each, whereas the two outer girders are supported by two beams each, as seen in 5.5a.


Figure 5.1: Photograph of grandstand D

## 5.1 Schematics

The representatives from *RBK* provided the available plans and schematics. There were no 3D models of the construction, so the model is recreated based on the schematics available. The schematics consists of sectional cuts seen from the south, floor plans seen from above, and façades from four directions. The cuts are located according to what is shown in Figure 5.3. The cuts are equivalent to what can be seen in Figure 5.2. The floor plans are equivalent to what can be seen in Figure 5.4. All of the schematics can be found in appendix E.

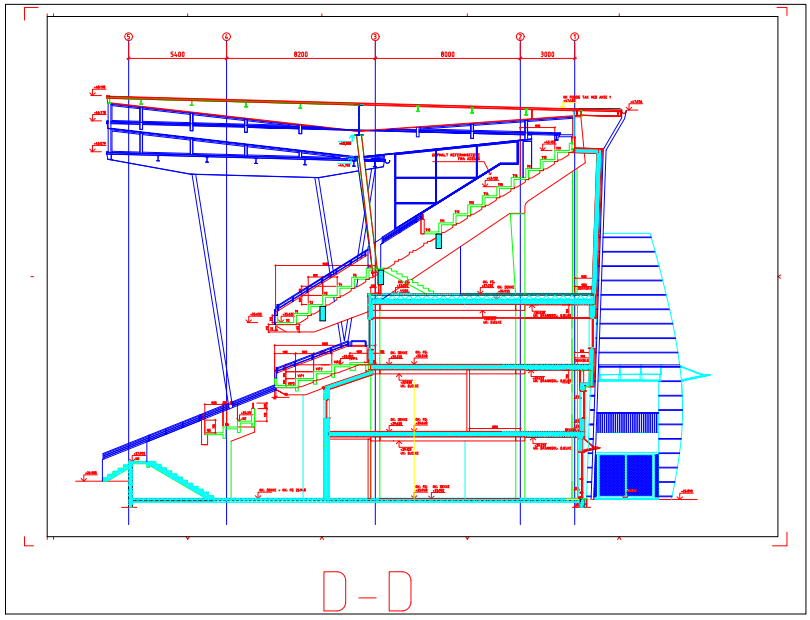


Figure 5.2: Sectional cut D

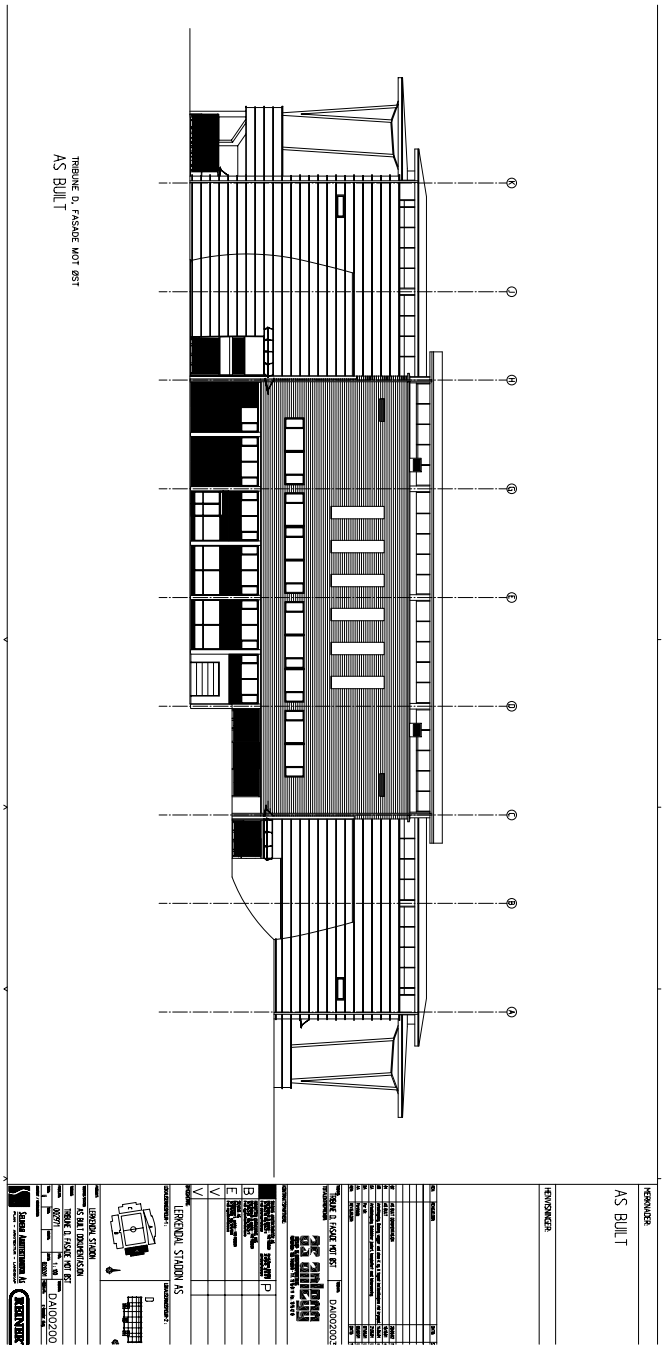


Figure 5.3: Eastern façade with the sectional cut locations and main girder locations

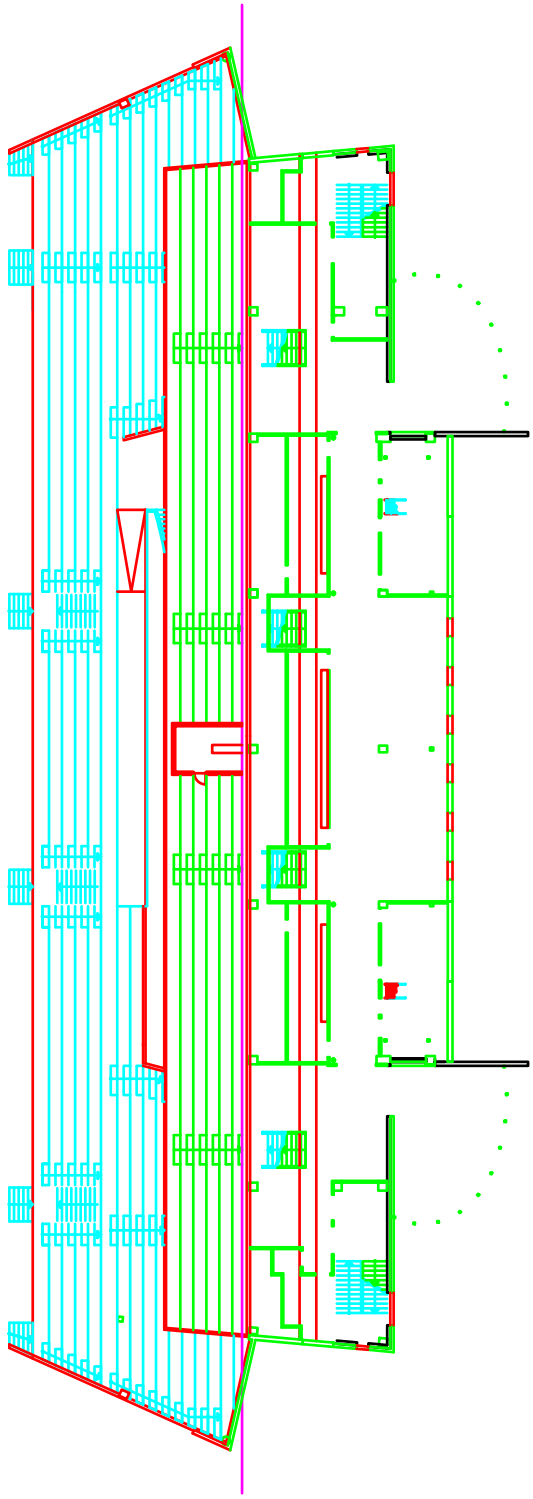

Figure 5.4: Floor plan 4

## 5.2 Modeling Geometry

The 3D geometry modeling of the structure is performed using Siemens NX 11.0. The process consists of importing the essential layers of the AutoCAD drawings and extruding the features into a 3D space. Seeing as the model is to be run in an FE-based simulation, most of the smaller details are omitted. Figure 5.5a and Figure 5.5b shows the result of the modeling.

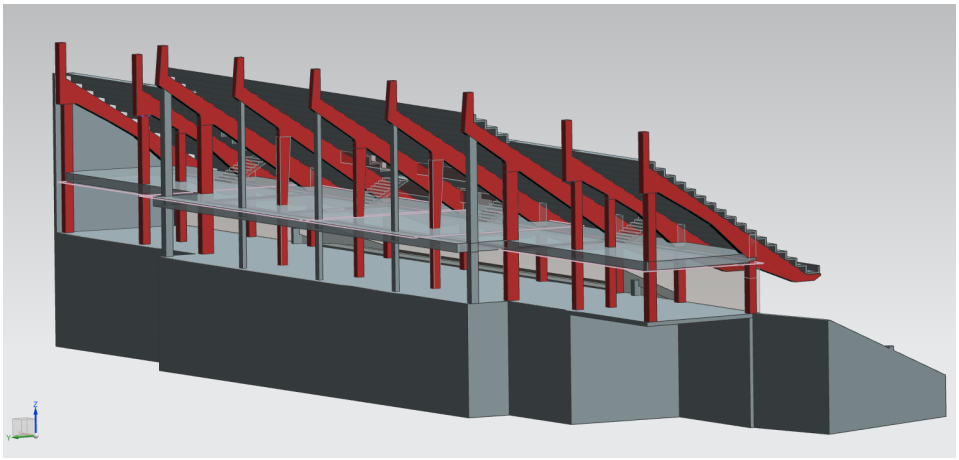

(a) Geometry as seen from the North-East

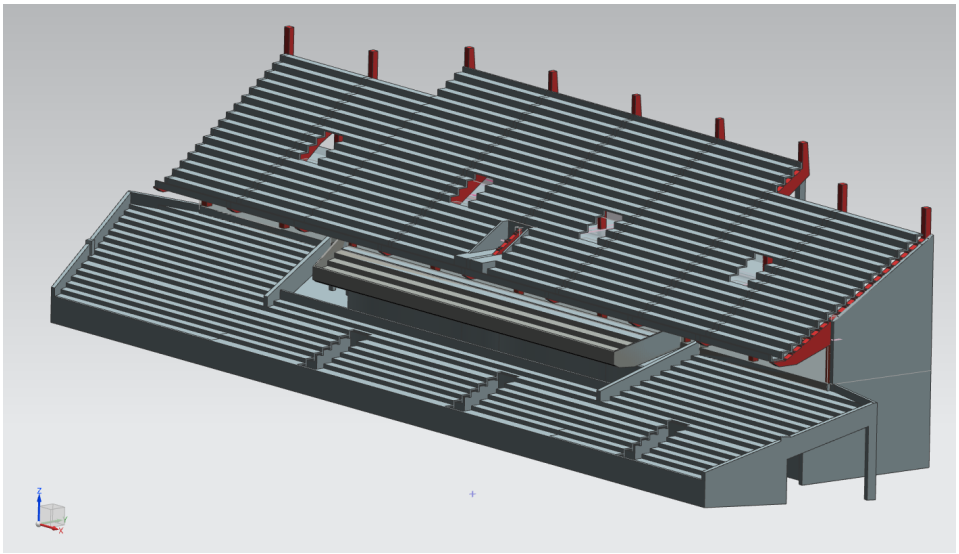

(b) Geometry as seen from the South-West

Figure 5.5: 3D geometry in Siemens NX

## 5.3 FE Mesh Parts

The geometry is idealised by removing minor details that would require smaller element sizes. All parts are presented in Table 5.1, with their meshing properties and element count. The material is a custom concrete for all meshes, with the properties presented in Table 3.2. These properties are based on the ones given in the *Reinertsen* report from 2001 found in Appendix C. The geometry is meshed as separate parts before being exported. RBE2 elements are added where the various parts connects. The lower level has an RBE2 element representing connection with solid ground, as seen in Figure D.1. The upper tier seating elements have an RBE3 elements covering most of the seats as seen in Figure D.25. An overview of all parts is found in Table 5.1

| **Part** | **Size** | **Type** | **Count** | **Geometry** |
|---|---|---|---|---|
| Lower level | 500 mm | CTETRA(10) | 180577 | Figure D.1 |
| Frame | 500 mm | CTETRA(10) | 5336 | Figure D.2 |
| Floor | 500 mm | CTETRA(10) | 44175 | Figure D.3 |
| Column A | 250 mm | CHEXA(20) | 112 | Figure D.4 |
| Column B front | 250 mm | CHEXA(20) | 92 | Figure D.5 |
| Column B back | 250 mm | CHEXA(20) | 112 | Figure D.6 |
| Column C | 250 mm | CHEXA(20) | 144 | Figure D.7 |
| Column D | 250 mm | CHEXA(20) | 36 | Figure D.8 |
| Column E | 250 mm | CHEXA(20) | 36 | Figure D.9 |
| Column G | 250 mm | CHEXA(20) | 36 | Figure D.10 |
| Column H | 250 mm | CHEXA(20) | 144 | Figure D.11 |
| Column J front | 250 mm | CHEXA(20) | 92 | Figure D.12 |
| Column J back | 250 mm | CHEXA(20) | 112 | Figure D.13 |
| Column K | 250 mm | CHEXA(20) | 112 | Figure D.14 |
| Girder A | 250 mm | CHEXA(20) | 692 | Figure D.15 |
| Girder B | 250 mm | CHEXA(20) | 694 | Figure D.16 |
| Girder C | 250 mm | CHEXA(20) | 888 | Figure D.17 |
| Girder D | 250 mm | CHEXA(20) | 888 | Figure D.18 |
| Girder E | 250 mm | CHEXA(20) | 888 | Figure D.19 |
| Girder G | 250 mm | CHEXA(20) | 888 | Figure D.20 |
| Girder H | 250 mm | CHEXA(20) | 888 | Figure D.21 |
| Girder J | 250 mm | CHEXA(20) | 698 | Figure D.22 |
| Girder K | 250 mm | CHEXA(20) | 690 | Figure D.23 |
| Seating element | 500 mm | CTETRA(10) | 55549 | Figure D.24 |

Table 5.1: Meshed parts overview

## 5.4 Fedem Model

The meshed parts are imported to Fedem where the simulations and the recorded events are solved.

### 5.4.1 Assembling Model

All parts are connected by fixed joints via RBE2 elements, as seen in Figure 5.6. The boundary condition of the assembled model is the *lower level* of the grandstand where all surfaces at ground level are connected to an RBE2 element which is connected to *ground* via a rigid joint as seen in 5.7. The *frame* and all *columns* are connected with the *lower level*. The upper level *floor* is connected with the the *frame* and each *column* which can be seen in 5.8. Each *girder* is connected with their respective *column* and with the *floor* in front. The middle *girders* are also connected with the columns that are part of the *frame* as can be seen in Figure 5.9 The *seating element* is connected to each *girder* at every second step as seen in Figure 5.10.

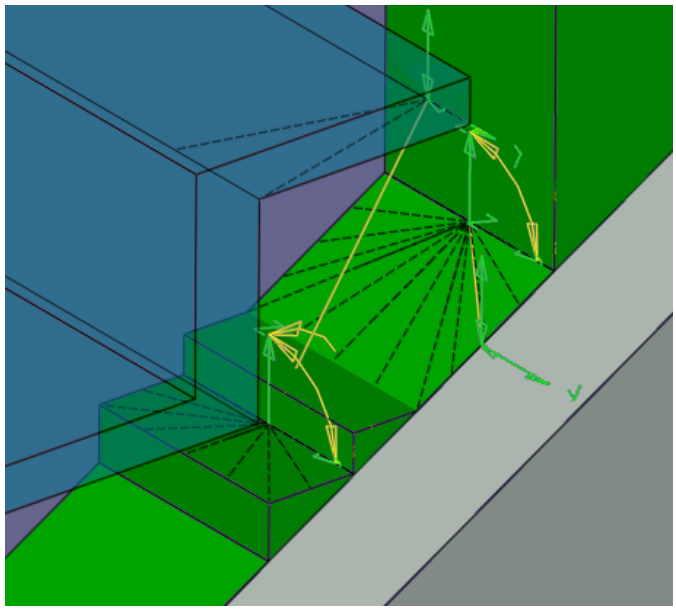

Figure 5.6: Joint connections

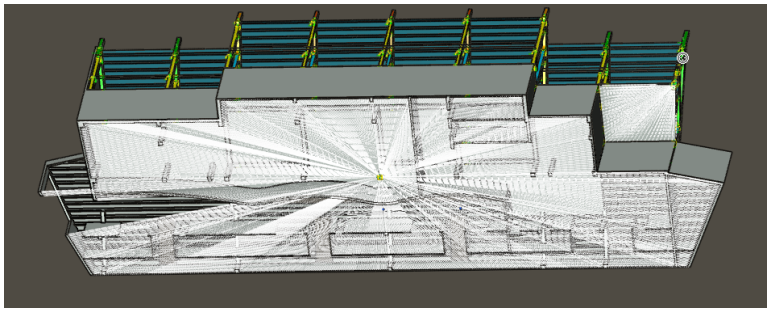

Figure 5.7: RBE2 spider in Fedem connecting the assembly to ground as a boundary condition

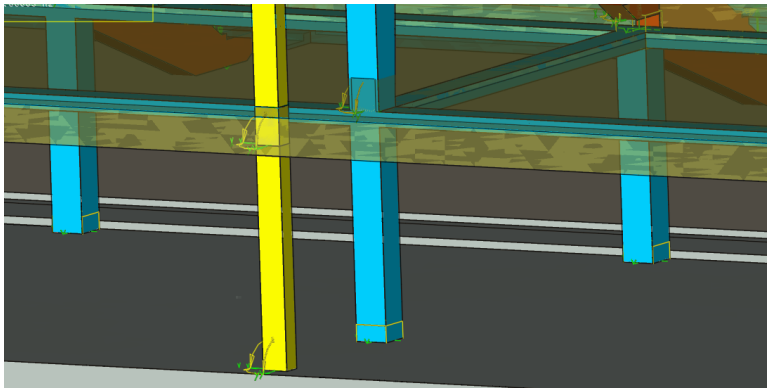

Figure 5.8: Frame and column joints, and upper level floor

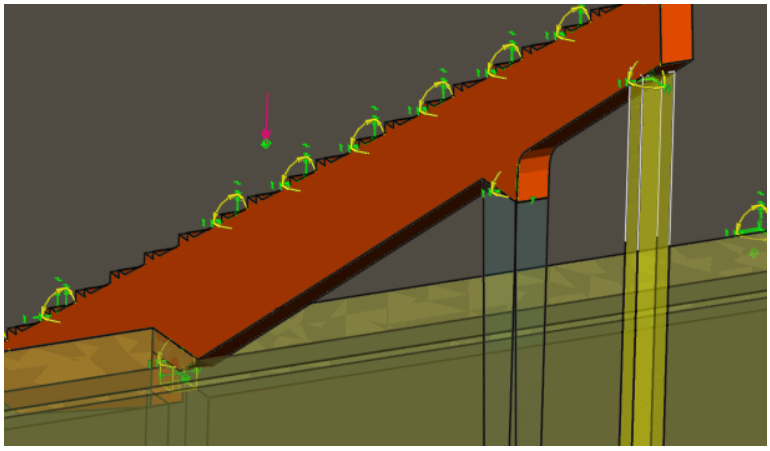

Figure 5.9: Girder connections joints

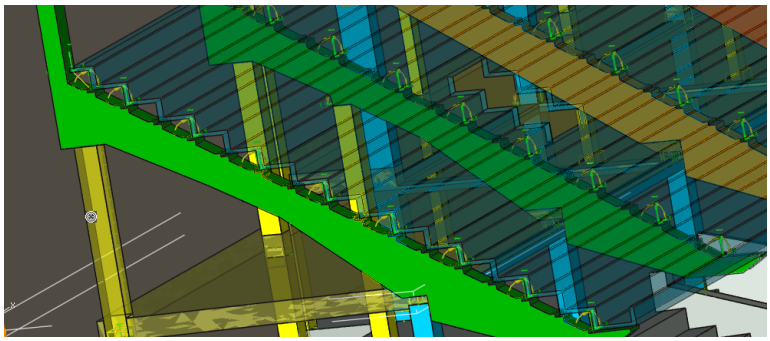

Figure 5.10: Seating joints

### 5.4.2 Scaling Stiffness

The stiffness of the construction is tuned based on the measurements of displacement of girder D during a match. The distance $h_{\text{full}} = 2778.9\text{mm}$ was measured at the start of the match with approximately $n = 2200$ people in the crowd on the upper level of the grandstand and the distance $h_{\text{empty}} = 2780.4\text{mm}$ was measured 15 minutes after the match when all seats were empty. This gives a difference $\Delta h$ as described in the following equation

$$\Delta h = h_{\text{empty}} - h_{\text{full}} = 1.5\text{mm}, \tag{5.1}$$

caused by the load from the crowd. By running a simulation with stiffness scaling factor $X_s = 1.0$ and a limited ramp function from 0N to $F_{\text{crowd}}$, which is the total load of the crowd mass given by

$$F_{\text{crowd}} = gnm_{\text{avg}} = 9.82\text{m/s}^2 \times 2200 \times 75\text{kg} = 1620\text{kN} \tag{5.2}$$

where $m_{\text{avg}} = 75\text{kg}$ is an assumption of the average supporter mass based on what *Reinertsen* used in their report, found in Appendix C, resulted in a $\Delta h = 1.06\text{mm}$ as seen in Figure 5.11a. With $k = X_{\text{s}} = 1.00$, the stiffness scaling factor is given by the relation between the initial simulations $\Delta h_{\text{init}}$ and wanted $\Delta h$ from equation 5.1, the following calculation

$$f = k\Delta h_{\text{init}} = 1 \times 1.06 \tag{5.3}$$

then a tuned $k_{\text{tuned}}$ would be given by

$$k_{\text{tuned}} = \frac{f}{\Delta h} = \frac{1.06}{1.5} = 0.707 = X_{\text{s}_{\text{new}}}, \tag{5.4}$$

where $X_{s_{new}}$ is the new stiffness scaling factor. Running the simulation again with the new stiffness scaling factor added to the parts shows, as seen in Figure 5.11b, that $\Delta h$ now is the same as the one measured during the match.

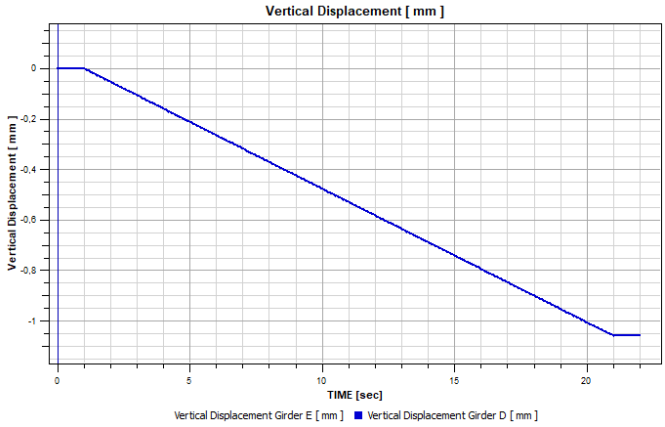


(a) Plot of displacement with $X_{\mathrm{s}} = 1.00$

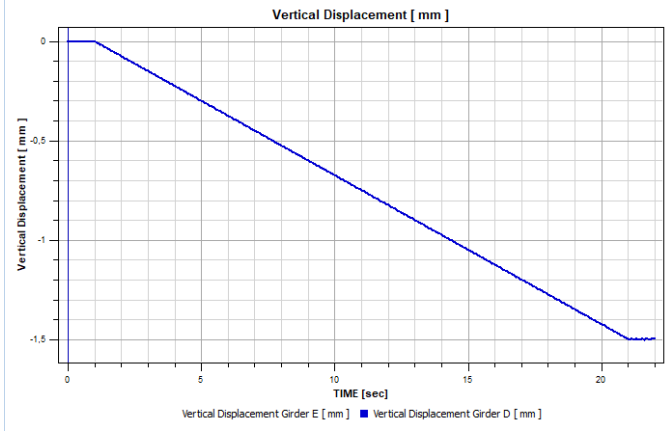


(b) Plot of displacement with $X_{\mathrm{s_{new}}} = 0.707$

Figure 5.11: $\Delta h$ before and after tuning

# Chapter 6

# Simulations and Modal Analysis

## 6.1 Modal Analysis

Performing modal analysis found the ten first eigenmodes of the grandstand. The respective eigenfrequencies differed between the two simulations based on depending on whether or not the mass of the crowd is accounted for. The eigenfrequencies from both simulations are found in table 6.1. The three first eigenmodes are horizontal, and therefore not of any particular interest, seeing as the behaviour of interest is in the vertical direction. The rest of the modes, excluding mode 9, have deformations at the tip of the cantilever. Neither of the two situations simulated is an accurate of the real load case, seeing as the mass of the supporters disconnect from the seating elements when they jump. Ellis and Ji [19] has found that the presence of a crowd does not affect the modal properties for perfectly synchronised jumping. The situation at *Lerkendal*, however, is not synchronised to such a degree that the properties would be unaffected. One might, therefore, assume that a modal analysis would give frequencies that define a range where the actual frequencies would lie within.

| Mode | Eigenfrequency empty[a][Hz] | Eigenfrequency full[b][Hz] | Difference [Hz] | Figure | Direction |
|---|---|---|---|---|---|
| 1 | 2.84 | 2.70 | 0.14 | A.1 | Vertical |
| 2 | 3.15 | 3.01 | 0.16 | A.2 | Vertical |
| 3 | 4.35 | 4.15 | 0.20 | A.3 | Vertical |
| 4 | 7.10 | 6.34 | 0.76 | A.4 | Horizontal |
| 5 | 7.82 | 7.05 | 0.77 | A.5 | Horizontal |
| 6 | 8.32 | 7.61 | 0.71 | A.6 | Horizontal |
| 7 | 8.60 | 7.96 | 0.64 | A.7 | Horizontal |
| 8 | 9.13 | 8.21 | 0.92 | A.8 | Horizontal |
| 9 | 9.60 | 8.51 | 1.09 | A.9 | Rotational |
| 10 | 9.79 | 9.08 | 0.71 | A.10 | Horizontal |

[a] Without crowd
[b] Mass of seating elements scaled to include mass of crowd

Table 6.1: Eigenmodes and eigenfrequencies from both simulations

## 6.2 Impulse Response

The impulse response of the system shows its 'preferred' motion after being struck by a triangle pulse lasting 0.2s with a load of 1 000 000N, which is a strike with the mass of roughly 1300 supporters. The impulse response is shown in Figure 6.1 with the FFT plot shown in Figure 6.2. The response is the activation of the first horizontal mode, mode 4, as the dominant frequency is at around 6.34Hz. As expected the highest amplitude is in girder E, as it is the one in the centre of the cantilever.

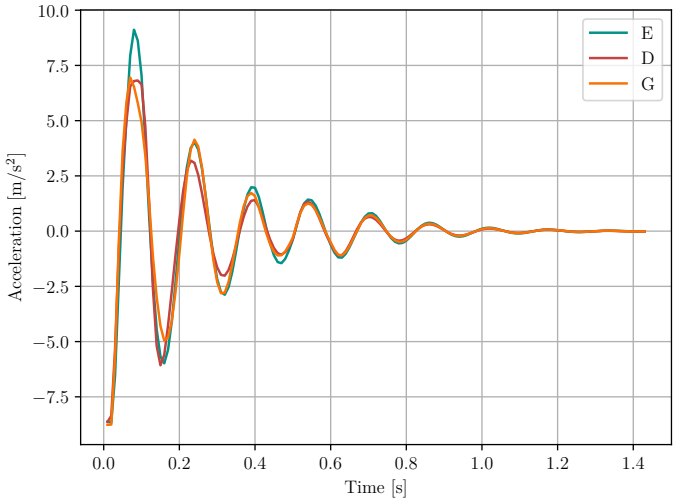


Figure 6.1: Impulse response of the grandstand

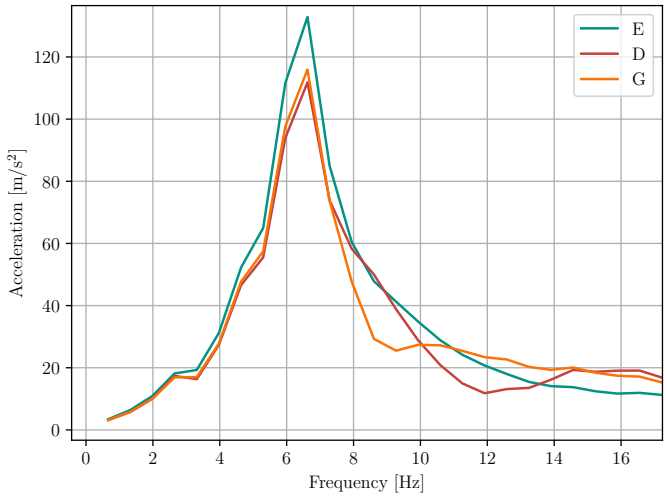


Figure 6.2: Impulse response of the system Fourier transformed

## 6.3 Periodic Loading Simulations

This sections will compare several similar loads that aim to recreate the observed load that occurs during the Pippi song at *Lerkendal*. The load represents a crowd of $n = 2200$ people with an average weight of $w = 750$N, with combined weight $Q = nw = 1650$kN rhythmically jumping at a frequency of 2Hz. The loads are based on the ones presented in section 3.2 by Jones et al. [32], that is the simple, limited sine load, an increased mean sine load, and loads using Equation 3.9 with dparameters from the ISO recommendation [28]. The biggest difference compared to the two first loads and the ones that precede them is that the amplitude is considerably higher than the weight of the crowd, as is noted by several authors and presented in Table 3.3. The loads are applied to the entire upper tier of the grandstand bye using an RBE3 spider as seen in Figure 6.3. The results of the simulations is presented in Table 6.2

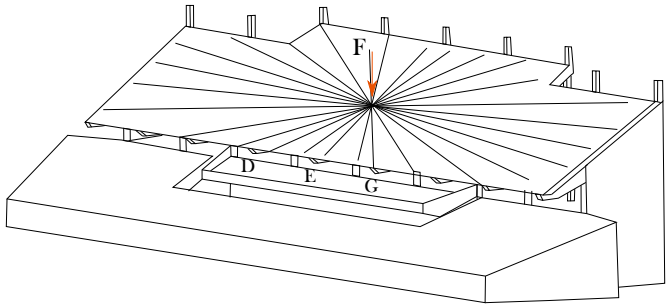


Figure 6.3: Force application for simulations

### 6.3.1 Simple Limited Sine

Applied load is a sine wave with a floor limitation of 0, an amplitude of $1Q$, and mean value of 0 as seen in Figure 6.4. The response is shown in Figure 6.5 and Figure 6.6.

### 6.3.2 Sine Load with Increased Mean

The increased mean value of the sine load enables more frequencies to be activated and represents a more substantial contact period for the crowd. The wave has a limited floor of 0, an amplitude of $0.8Q$ and, and a mean value of 0.2. The load function can be seen in Figure 6.7, and the response can be seen in Figure 6.8 and Figure 6.9.

| Simulation | Girder | Acceleration [m/s$^2$] | Velocity [m/s] | Displacement [m] |
|---|---|---|---|---|
| Limited sine | D | -0.54 | -0.023 | -0.0018 |
| | E | -0.46 | -0.021 | -0.0017 |
| | G | -0.44 | -0.021 | -0.0016 |
| Increased Mean | D | -0.59 | -0.023 | -0.0014 |
| | E | -0.55 | -0.021 | -0.0012 |
| | G | -0.55 | -0.021 | -0.0013 |
| ISO | D | -1.50 | -0.072 | -0.0034 |
| | E | -1.66 | -0.067 | -0.0032 |
| | G | -1.47 | -0.067 | -0.0032 |

Table 6.2: Peak values from simulation

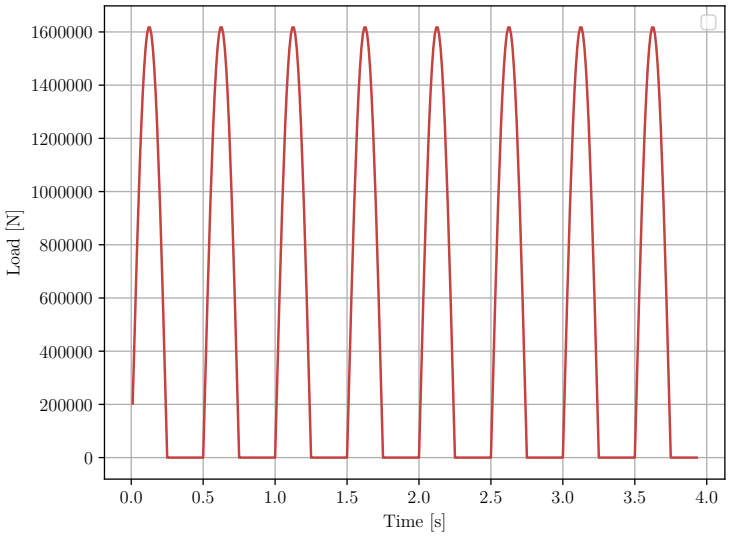


Figure 6.4: Simple limited sine load

### 6.3.3 ISO Parameters

The load used is based on Equation 3.9 and uses the parameters proposed by International Organization for Standardization [28], with three harmonics. The coordination factors are $C_1 = 0.67, C_2 = 0.50, C_3 = 0.40$, the weight is $Q$, and the DLFs are $\alpha_1 = 1.7, \alpha_2 = 1.0, \alpha_3 = 0.4$. The biggest difference compared to the two previous loads is that the amplitude is considerably higher than the weight of the crowd as is noted by several authors as presented in Table 3.6.

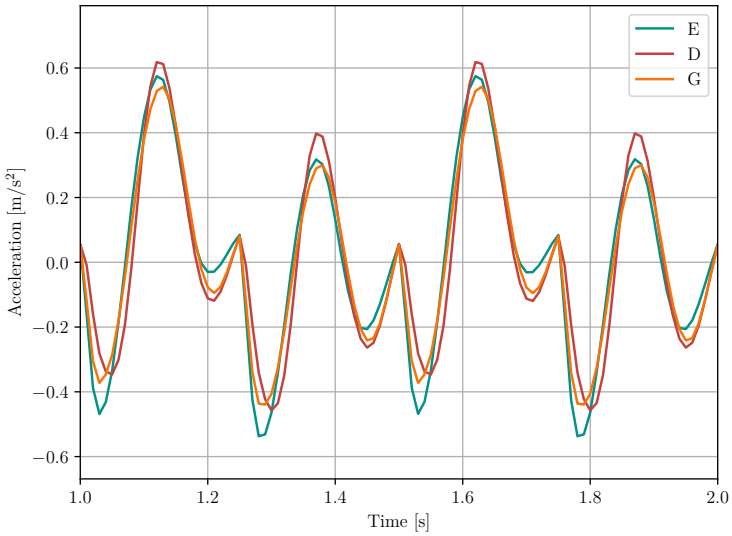


Figure 6.5: Simple limited sine load response

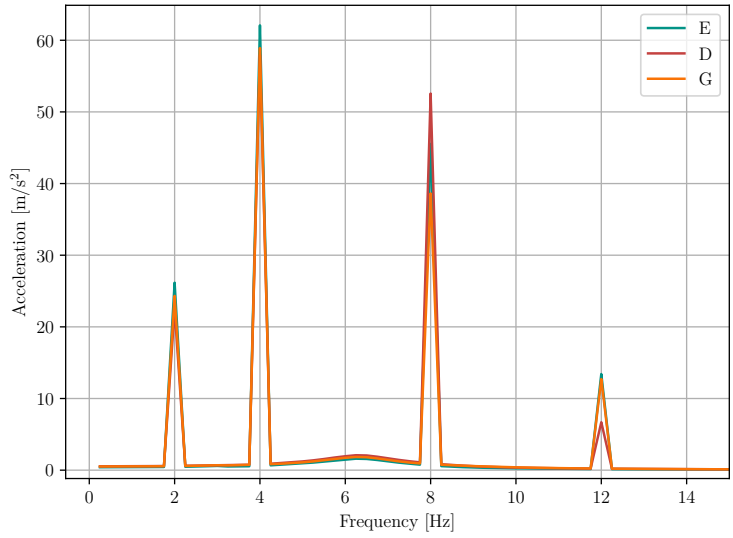


Figure 6.6: Frequency plane plot of simple limited sine load response

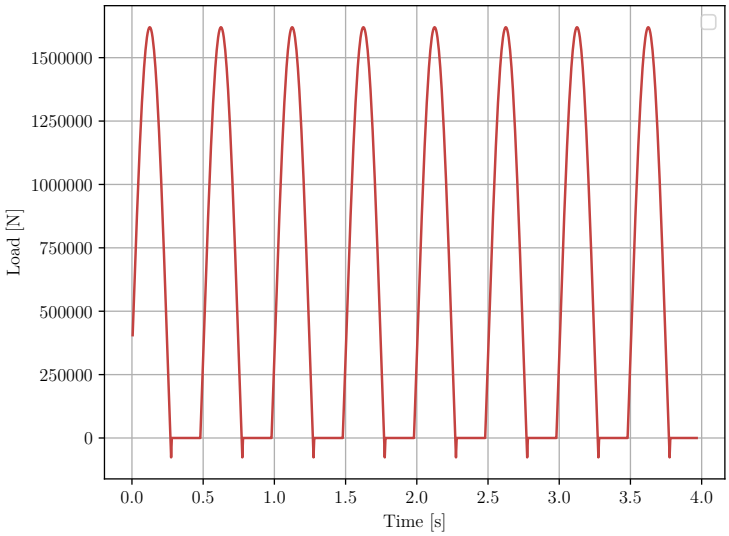


Figure 6.7: Limited increased mean sine load

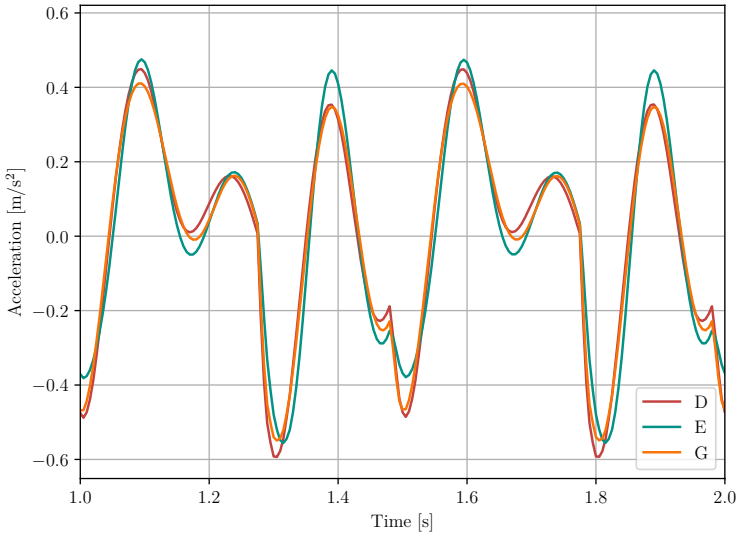


Figure 6.8: Limited increased mean sine load response

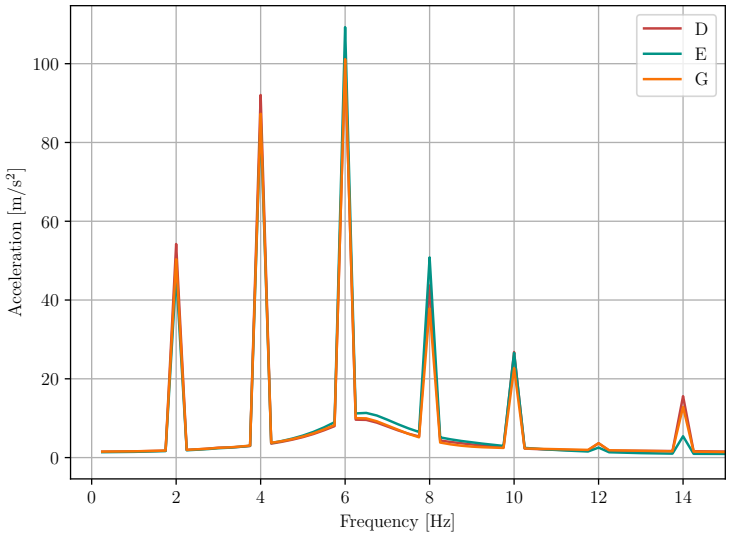


Figure 6.9: Frequency plane plot of limited increased mean sine load response

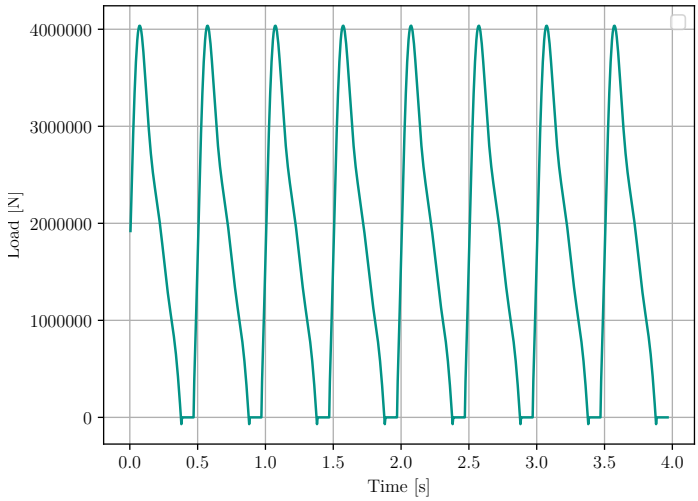


Figure 6.10: ISO parameters load

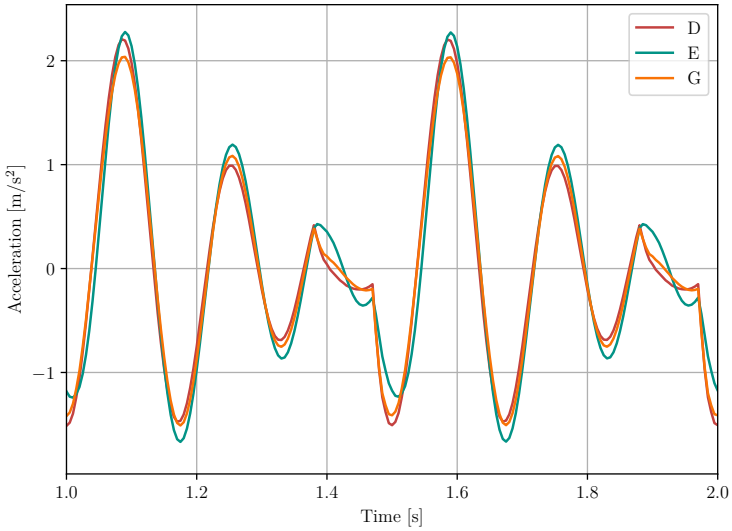


Figure 6.11: ISO parameters load response

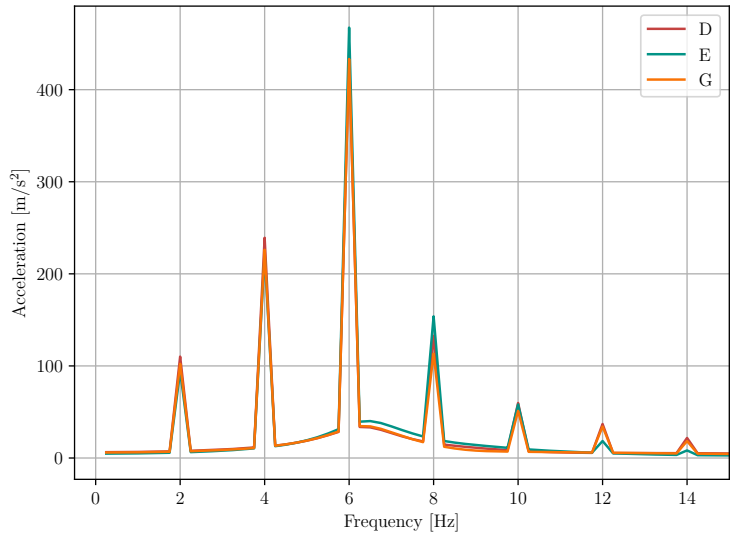


Figure 6.12: Frequency plane plot of ISO parameters load response

## 6.4 Simulation Results and Observations

The first thing to note is the fact that there is no response at 6 Hz for the first simulation seen in Figure 6.6, from the field measurements one knows this is not representative. The two following simulations do on the other hand have their highest amplitude at 6Hz as this is relatively close to an eigenfrequency of the model version which is used in the simulation.

Another observation is the fact that the largest displacement for all of the simulations is for girder D, to the side of the centre. This coincides with the results from the physical results as discussed in section 9.4, and might imply that there is a geometrical factor causing the asymmetry.

The amplitudes from the ISO simulation is significantly higher than the two preceding simulations but does not quite reach the amplitudes produced by the measured during the actual physical events presented later, in Table 10.1.

Based on the simulations and the measured response the model seems adequate for use in a recreation of the physical behaviour. The eigenmode shapes of the model are likely to coincide with the physical grandstand. However, the eigenfrequencies are most likely not representative of the physical structure. The structure is stripped for all non-bearing walls and interior and does not include the roof. This means that the eigenfrequencies most likely are higher on the physical structure than the ones found in the modal analysis.

# Chapter 7

# Recording Setup

During the matches, three nodes are set up to record the acceleration of three different girders. The nodes transmit the signal to the base station seen in Figure 7.2, and is recorded directly on a computer. The software used for operating and recording data is SensorCloud made by the provider of the sensor nodes [36]. The software handles all communication with the nodes as well as visualisation of the recorded data. The data can be monitored live when nodes are set to transmit data. Figure 7.1 shows how the view is set up during the recording of the data.


Figure 7.1: Screen grab of the data monitoring view in SensorConnect


Figure 7.2: Base Station

## 7.1 Sensors

The sensors used are in the accelerometer nodes *G-Link-200* produced by *Lord MicroStrain*. The nodes contain a tri-axial accelerometer with low noise and drift. The nodes may be set to sample continuously, in periodic bursts, or after an event trigger. Sampling rates vary between 1 sample per hour and 4096 samples per second. Further specifications are found in [37]. The accelerometer is shown in Figure 7.3, the sensor node is shown inFigure 7.4, and the base station is shown in Figure 7.2. The sensors transmit on a radio frequency between 2.4GHz and 2.5GHz. The thousands of devices connected to the LTE network could have been a complication for the transmission. However, the LTE frequency used in Norway is on the 1.8GHz and 2.6GHz bands, and should therefore not interfere with the signal [48].

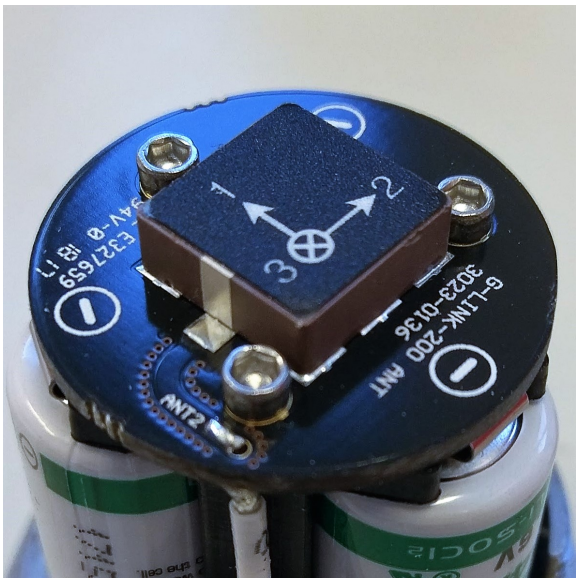


Figure 7.3: Accelerometer

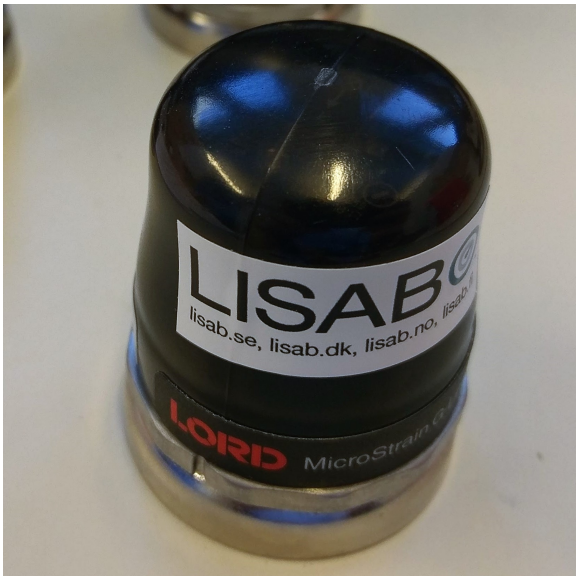


Figure 7.4: Sensor Node

## 7.2 Sensor Placement

The three sensor nodes are attached to an angle iron bolted to the aluminium beam that supports a safety net suspended beneath the upper stands, as seen in Figure 7.5. Seeing as the nodes are connected using strong magnets, the angles were necessary as aluminium is non-magnetic. The three sensors are placed on girder D, E, and G, as in Figure 7.6. These three girders are chosen based on their accessibility rather than their ability to reproduce the behaviour optimally. They are the only three girders that are reachable using a ladder that is safe to use for installation by unprofessional personnel. The cost of the sensors limited the amount to three nodes. Further, the digital twin concept intends to reduce the cost and recreate behaviour based on a few measurements. This means that the number of sensors could be reduced to one if the dynamic behaviour behaves in an adequately linear manner.

Figure 7.5: Attached sensor

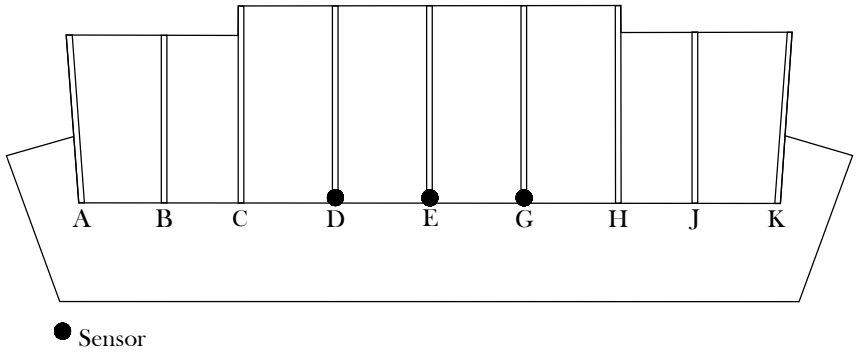


Figure 7.6: Girder overview

## 7.3 Exporting Data

Data is exported to CSV-files from the SensorConnect software. The files are readable by the scripts used for signal processing in the subsequent part of the system. *Lord* has provided an API for controlling the sensors through a few chosen programming languages, which enables an automated process for exporting the data while recording, as well as concurrently processing the data.

# Chapter 8

# Signal Processing

The files containing the signal is stored in the CSV-format, with a header containing the recorded channels, the data type, and the sample rate. The CSV-files used when developing the integration is exported from *Lord MicroStrain*'s software *Sensor-Connect* [36]. Each row of data contains a timestamp, on the format MM/DD/YY h:mm:ss.nnnnnnnnn, and the corresponding readings from each channel. The signal from the sensor is a measurement of the absolute acceleration recorded by the accelerometer measured in $g$, where $1g = 9.80665\text{m/s}^2$ [8]. Figure 8.1 shows a three-second snippet of the signal recorded during the Pippi load case.

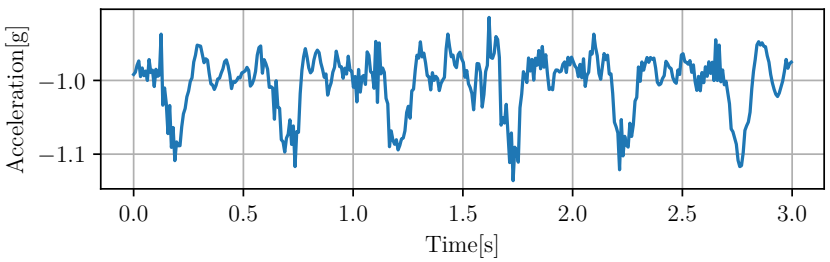


Figure 8.1: Raw signal example

## 8.1 Integration

The desired unit of the signal is displacement measured in m. The original signal has the unit g which is converted into $\text{m/s}^2$. The signal is then integrated twice using the cumulative trapezoid method to produce a signal showing displacement per

time. The integration is performed in using the `cumtrapz` function from the `SciPy` module [50]. Performing integrations without any additional processing results in sensor drifting, caused by the accumulation and increased sensitivity to the error in the signal. The drifting is observable in Figure 8.2 where the signal snippet from Figure 8.1 is normalised and scaled by $g$ seen in the first plot. The two following are the result of one and two integrations. One may observe that the two inferred signals are not oscillating about a mean value and tend to drift away from the expected path. This issue is a common problem described by Han and Lee [27] and Thenozhi et al. [52] amongst others.

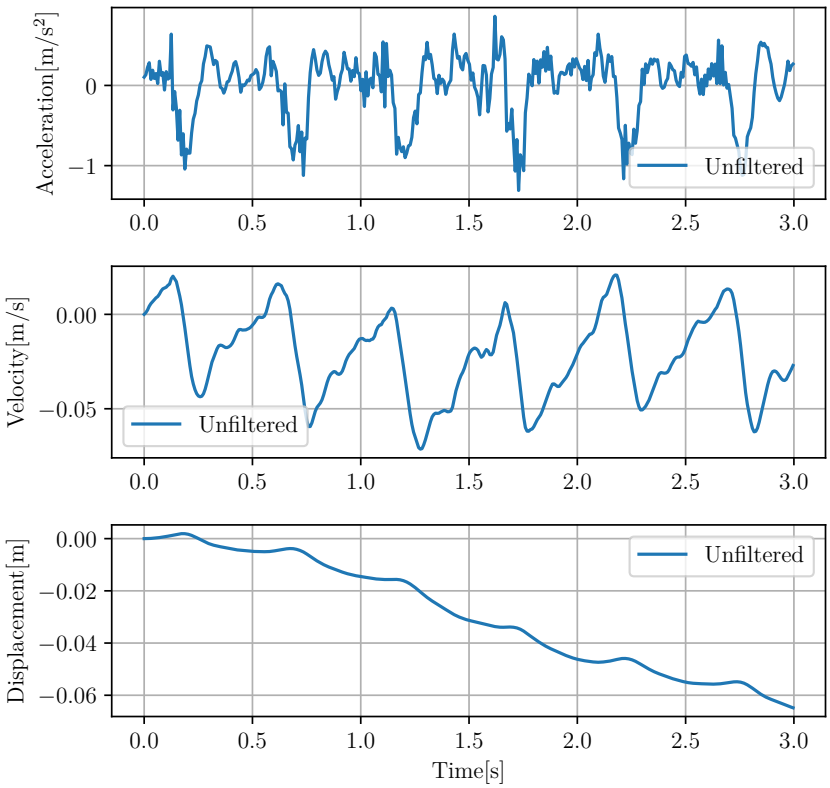


Figure 8.2: Nominal acceleration, velocity, and displacement after integration

## 8.2 Filtering Signal

The signal is filtered for two reasons and with two different filters. The raw acceleration signal is filtered with a low pass filter to remove noise, whereas the

velocity and displacement are filtered to avoid unwanted drifting. Parameters for the three filters applied is presented in Table 8.1. The frequency response of the filters is shown in Figure 8.3. The results of all three signals filtered are shown in Figure 8.4. The signals for both displacement and velocity are now oscillating about the 0 amplitude line. For longer samples, the offcuts frequency will not necessarily produce a signal that behaves identically. It is important to note is that this by no means is the exact motion of the girders, but a representation that is adequate to create the displacement series used when solving for the digital twin.

| **Signal** | **Filter Type** | **Cutoff [Hz]** | **Order** |
|---|---|---|---|
| Acceleration | Butterworth Low Pass | 30 | 6 |
| Velocity | Butterworth High Pass | 0.25 | 4 |
| Displacement | Butterworth High Pass | 0.65 | 4 |

Table 8.1: Filter Parameters

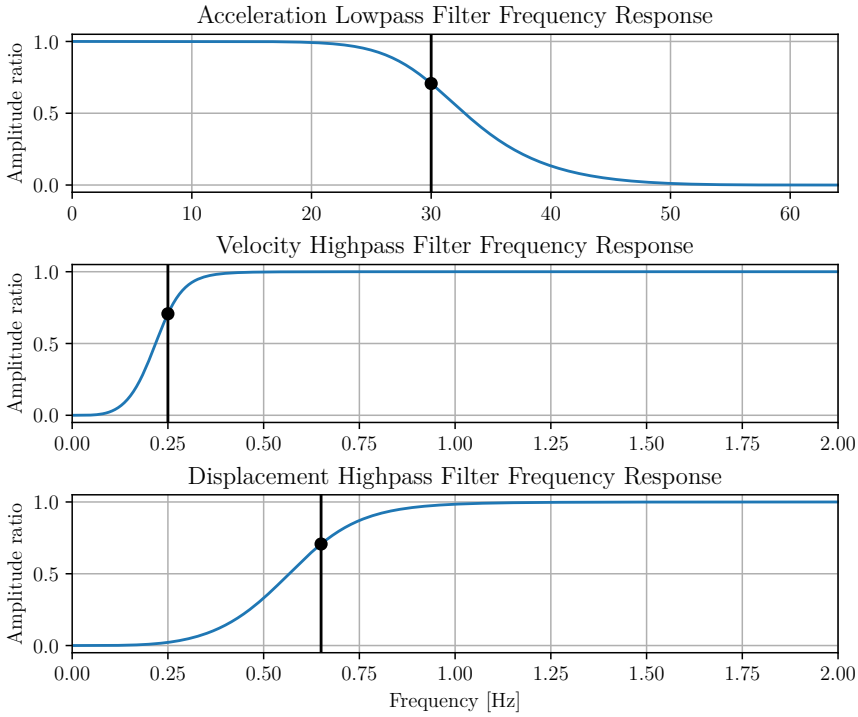


Figure 8.3: Frequency response of the three filters applied to the signal

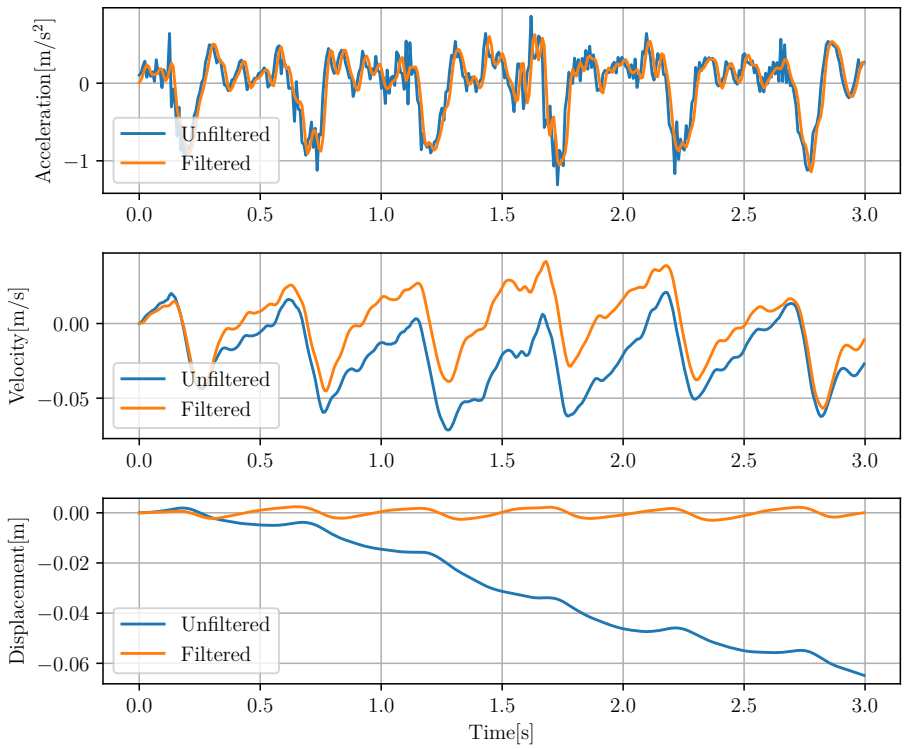


Figure 8.4: Comparison of filtered and unfiltered signals

# Chapter 9

# Dynamic Behaviour During Crowd Excitation

## 9.1 The Pippi Load Case

The load case that causes the most significant response in the grandstand, and that has caused reactions from attendants and employees. The upper part of the grandstand houses a crowd of about 2200 people based on reports from representatives from RBK. The crowd situated at the cantilever is equipped with a single dedicated drummer who is situated directly on a plateau on girder E. About once every half of the match the crowd put their arms on the shoulders of their seat-mates and jump the beat of the Pippi song. The drummer ensures that the crowd keeps their beat, which has been measured to be about 120 BPM, or equivalent to a frequency of around 2Hz. The frequency is further observable in the many frequency series plots found in Appendix B. The beat of the song is significantly lower than the actual theme song. This is likely because the beat by the drummer is adapted to play a frequency that a crowd is able to coordinate their jumping to. This frequency of around 2Hz is therefore no surprise as it is found that groups only are capable of maintaining their rhythm with frequencies between 1.8-2.3Hz [24].

## 9.2 Observability and Effect

The motion of the cantilever is observable for all attendants in the stadium. The crowd that is particularly exposed to the motion is the attendants seated in the VIP section directly beneath the cantilever, as visible in [1] and [2]. When seated in the VIP section the vibration is also palpable in the seats. Inside the structure, all glass windows vibrate and utensils in the kitchen rattles. Effects are not only reserved to the stadium, as the student housing across the road experience swinging lamps in the ceiling and shaking in the floor. This means that the vibrations propagate into the ground and below the playing field, the facing grandstand and under the street, before exciting the structures in its proximity.

## 9.3 Vibration Components and Resonance

The vibration components of the acceleration signal mostly consist of 2Hz and 4Hz. This is expected based on the earlier work presented in Jones et al. [32], where the load has been shown to consists of the harmonic frequencies of the periodic load frequency. Furthermore, as mentioned in subsection 3.2.2 the second harmonic is the most prominent as reported in [4]. The prominence of the second harmonic is observable in two of the girders in Figure 9.1, shows the frequency components of a typically measured response signal. In addition to the two first harmonics, there are notable increases in the frequency for the third and fourth harmonics around 6Hz and 8Hz respectively. Seeing as these frequencies all are part of the integer multiples of the periodic load, and that there is no significant response in the area around the two latter harmonics, there are no signs of any resonance in the grandstand. The vertical eigenfrequencies that could cause resonance are all found to be above 6Hz. A resonance would have caused a response more similar to what is found in Figure 6.12, where the third harmonic is the most significant component of the dynamic response signal.

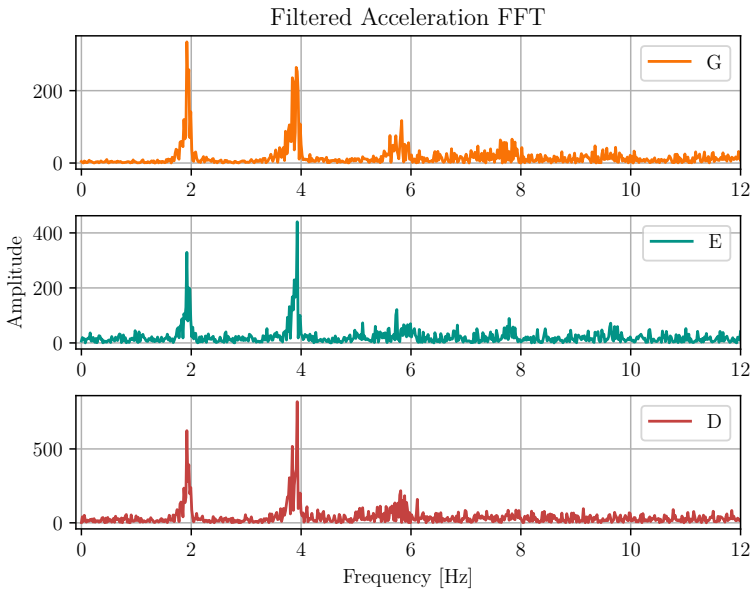


Figure 9.1: FFT plot of acceleration from Lillestrøm 1. Note the different scale of the y-axis

## 9.4 Asymmetry

All recorded matches show a distinct asymmetric behaviour present in the grandstand during the Pippi load case. This behaviour is the difference between the amplitude of the motion of girders D, and G, as well as the alteration of behaviour when the Pippi events occur. This asymmetry has no simple explanation, and as such, several hypotheses are presented and discussed. An initial assumption regarding the motion of the cantilever was that it would have a symmetric shape implying that one would need only one set of readings to reproduce the behaviour with the digital twin.

To provide a way of displaying the change in behaviour the acceleration signal from the three sensors has been plotted in a normal distribution using `matplotlib.mlab.normpdf(x,` $\mu$`,` $\sigma$`)` with parameters calculated using `numpy.mean()` and `numpy.variance()` in Python. The mean was normalised around 0 in the plot to ease the comparison of the three curves. What one may read from the two plots is the amplitudes of the signal as weighted amounts from the mean value. Figure 9.3 shows the distribution of the full first half of a match, whereas Figure 9.4 shows the same plot during the Pippi song. The different curves each represent the individual

| Girder | Peak positive displacement [mm] | Peak negative displacement [mm] |
|---|---|---|
| G | 2.21 | 2.36 |
| E | 2.50 | 2.78 |
| D | 4.38 | 4.81 |

Table 9.1: Max displacement values during Pippi from first half versus Ranheim

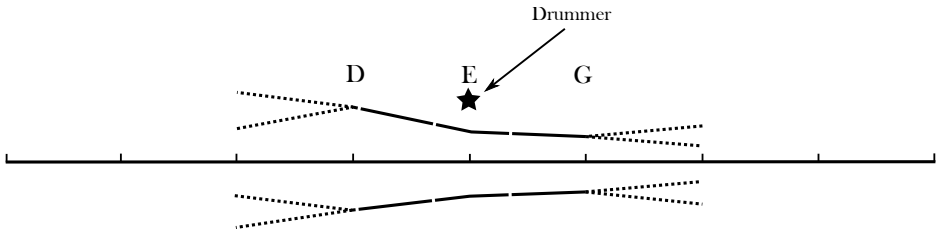


Figure 9.2: Girder displacement pattern with hypothetical continuation of displacement

sensors where D is the northern girder, and G is the southern girder, cf. Figure 7.6. One may read from the plot that the girder with the least amount of variation during the first half is G. Girder D has a higher variation in the motion whereas E, the centre girder, has the highest amount of variation in the samples. These curves imply the number of samples showing a high magnitude in the acceleration signal. During Pippi, the curves change, as can be seen in Figure 9.4 and girder E has the highest variation. This is also reflected in the resulting maximum displacements during the same Pippi load case, presented in Table 9.1. The measurements show that girder D has about twice the displacement as the other girders. The relative displacement is shown in Figure 9.2, where the relative position is represented as significantly up-scaled displacements.

### 9.4.1 Cause of Asymmetry

A definite cause of the asymmetry has not been pursued. However, several hypotheses present different factors that by themselves or in combination with others could be the cause. Most of them relate to the fact that the core of the supporter group *Kjernen* toward girder G than the centre, and that the remaining area has less enthusiastic and energetic behaviour.

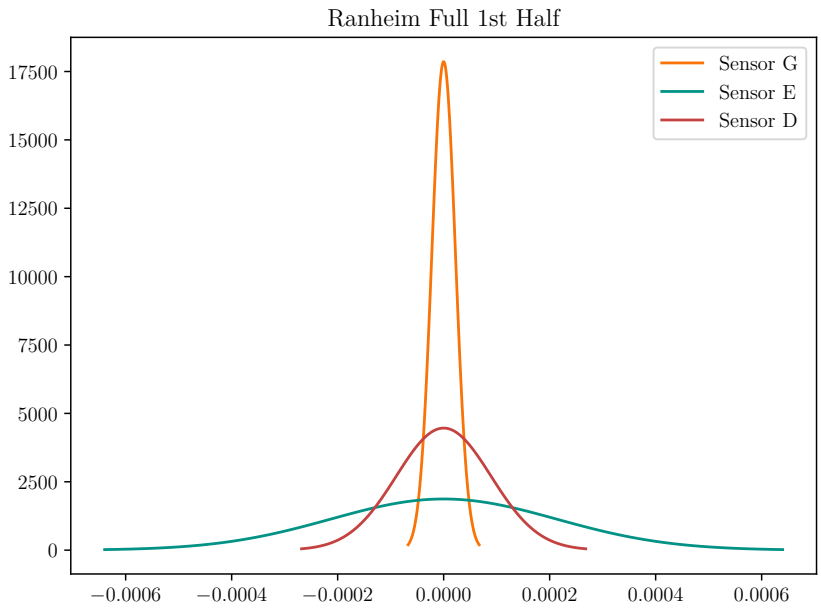


Figure 9.3: Normal distribution of measured acceleration during full first half versus Ranheim

### Constructional Asymmetry

A possible cause of asymmetry is that the structure in itself is not symmetrical. The northern side, towards D, is generally a more open structure than the southern part with more internal walls and stairwells. In Figure 9.5 shows a view from below where the asymmetry is quite evident. Another part visible in the figure is the elevated floor to the left in the as compared to the one on the right that continues all the way down, as the construction is built into a hill. Directly underneath the upper tier, there were no obvious differences visible on the structure.

### Rhythmical Capability

Seeing as the motion of the cantilever mostly consists of components matching the harmonics of the crowd load the crowd's ability to keep synchronised is relevant. This assumption is based on observations during the load event that the part of the crowd located more toward girder D was better at keeping in sync during the load event.

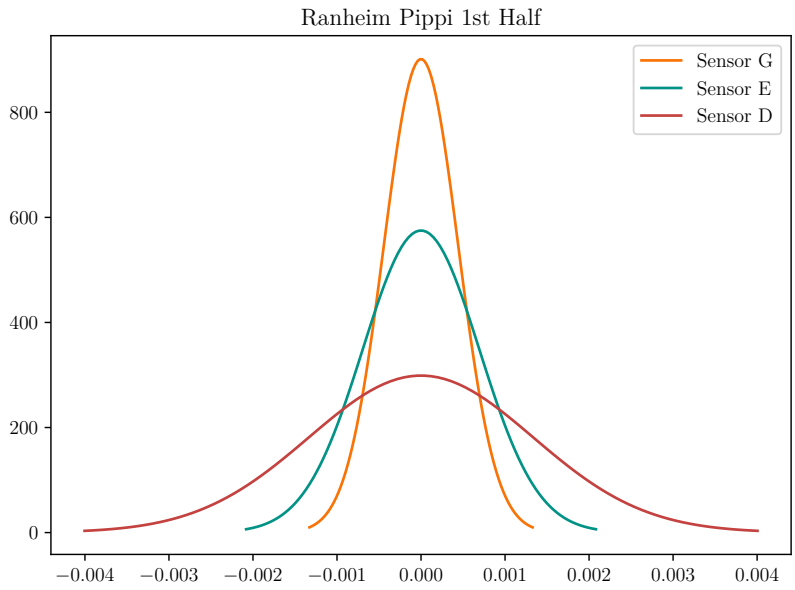


Figure 9.4: Normal distribution of measured acceleration during Pippi from first half versus Ranheim

### Reduced Dampening

The area towards girder D often has a more sparse distribution of people than the other side, which could reduce the dampening of the motion. In combination with the previous hypothesis, a more synchronised crowd would cause less dampening than their counterparts.

### Phase Difference

Seeing as the beat is kept by a drummer that is situated on a plateau directly above girder E there is likely a phase difference in the load applied. This is caused by the slight delay from the sound travelling through the air. This wave-like motion is observable on video as shown in [2], which could explain why D has a larger displacement than E. However, seeing as G has even smaller displacements than E this is likely not the cause in itself.

### Activation of Two Modes

Even though there are no signs of resonance or activation of eigenmodes in the recorded vibrations there are two of the modes that aligned could cause the asym-

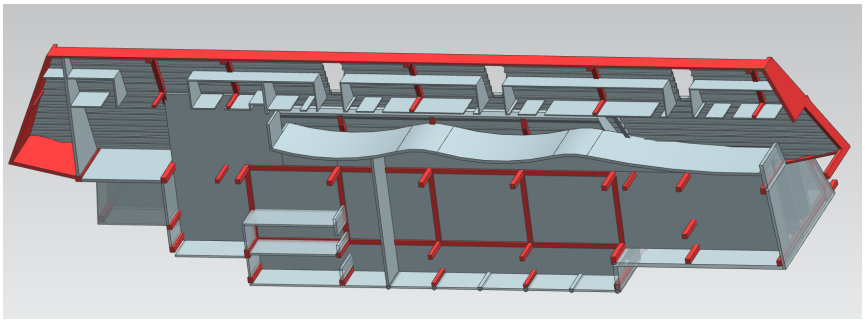

Figure 9.5: Asymmetry example seen from underneath

metry. The two first vertical modes, mode 4 and mode 5 shown in Figure A.4 and Figure A.5 respectively, are the two motions that are plausible to be activated at a correct frequency. Mode 4 is symmetric whereas mode 5 is antisymmetric, which can cause one side to be amplified while the other side is being reduced. Figure 9.6 shows a simplified possible combination of modes that could explain the shape of the vibration.

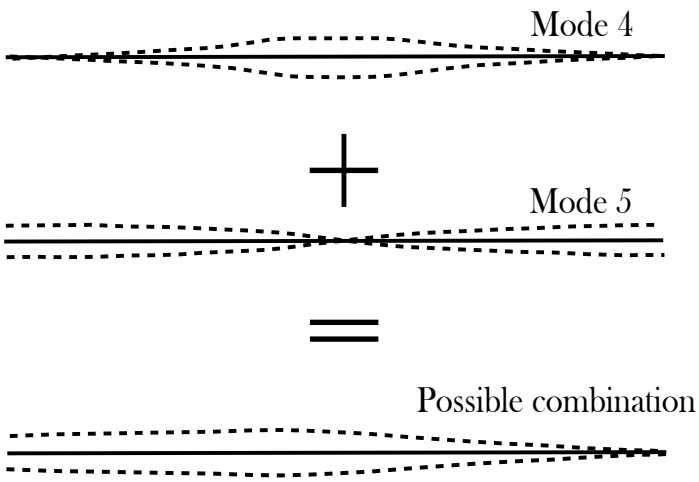


Figure 9.6: Possible mode combination

# Chapter 10

# Results of Measurements

Four of the matches played during the spring of 2018 was played with the system recording the behaviour of the grandstand. The sampling rate for most matches was 128Hz, except the Molde match which had a sampling rate of 512Hz. The vibration criteria used concerns the perception of vibration crowd and do not necessarily say anything about the acceptability of the mechanical behaviour.

## 10.1 Peak Values of Time Series

A measure of the highest amplitudes is an indication of how active the crowd has been during the different games. The peak values are the maxima of the recorded filtered signals and are presented in Table 10.1. The Kristiansund event stands out, seeing as the values are significantly higher in acceleration than the other games, and is therefore considered as an anomaly as the recording of the game had some technical problems. The next on the list is Lillestrøm 1 with the highest values across the board. The largest negative displacement is 10mm, whereas the highest velocity is 98mm/s. Both of these values are about 500% higher than the maximum values measured by *Reinertsen* in 2009, which were 2mm and 17mm/s accordingly. There is no exact report as to where the values were recorded, only that they were recorded on top of the seating elements and between two girders.

| Event | Girder | Peak Acceleration [m/s$^2$] | Peak Velocity [m/s] | Peak Displacement [m] |
|---|---|---|---|---|
| Kristiansund | D | -4.25 | -0.095 | -0.00982 |
| | E | -1.75 | -0.051 | -0.00571 |
| | G | -1.50 | -0.056 | -0.00368 |
| Molde 1 | D | -1.86 | -0.079 | -0.00481 |
| | E | -1.07 | -0.045 | -0.00278 |
| | G | -1.10 | -0.041 | -0.00235 |
| Molde 2 | D | -1.59 | -0.070 | -0.00422 |
| | E | -0.94 | -0.040 | -0.00249 |
| | G | -1.09 | -0.042 | -0.00245 |
| Molde 3 | D | -1.91 | -0.072 | -0.00365 |
| | E | -0.86 | -0.041 | -0.00240 |
| | G | -0.75 | -0.030 | -0.00175 |
| Ranheim | D | -1.21 | -0.064 | -0.00400 |
| | E | -1.05 | -0.045 | -0.00323 |
| | G | -0.93 | -0.032 | -0.00178 |
| Lillestrøm 1 | D | -2.35 | -0.098 | -0.00939 |
| | E | -1.28 | -0.056 | -0.00565 |
| | G | -1.14 | -0.042 | -0.00280 |
| Lillestrøm 2 | D | -1.86 | -0.088 | -0.00672 |
| | E | -1.08 | -0.046 | -0.00431 |
| | G | -1.04 | -0.032 | -0.00219 |

Table 10.1: Peak values from match day measurements

## 10.2 Largest Leap and Fall

The largest leaps and falls are defined based on the largest difference between two subsequent extremes in the deduced filtered displacement signal from sensor D, being the one with the highest amplitudes. The calculations were performed using the script found in section F.1.

| Event | Largest leap[a][mm] | Time of leap [s] | Largest Fall[a][mm] | Time of fall [s] | Figure |
|---|---|---|---|---|---|
| Kristiansund | 18.5 | 12.3 | 17.7 | 17.5 | Figure 10.1 |
| Molde 1 | 9.2 | 10.5 | 9.0 | 10.3 | Figure 10.2 |
| Molde 2 | 8.1 | 10.0 | 8.1 | 10.0 | Figure 10.3 |
| Molde 3 | 6.8 | 7.4 | 6.8 | 7.4 | Figure 10.4 |
| Ranheim | 7.9 | 19.7 | 7.9 | 19.7 | Figure 10.5 |
| Lillestrøm 1 | 17.7 | 9.1 | 17.7 | 9.1 | Figure 10.6 |
| Lillestrøm 2 | 12.5 | 30.5 | 12.5 | 30.5 | Figure 10.7 |

[a] Difference between subsequent valley and peak
[b] Difference between subsequent peak and valley

Table 10.2: Largest leap and fall per Pippi occurrence for girder D

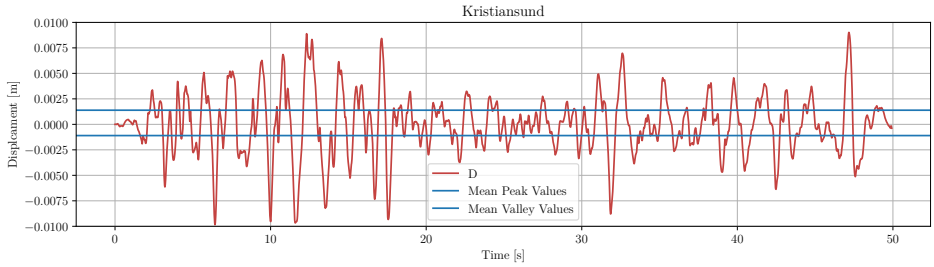


Figure 10.1: Girder D displacement with mean peaks and mean valleys during Kristiansund

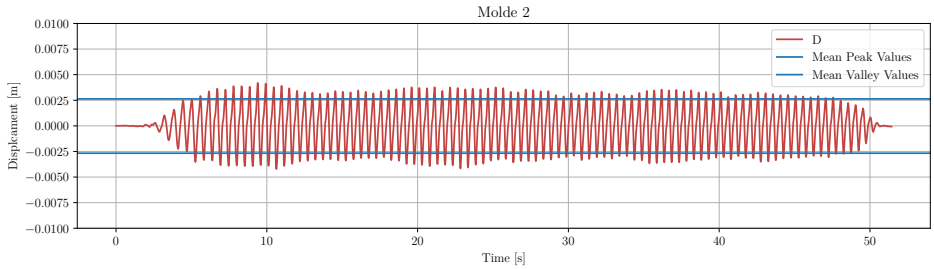


Figure 10.2: Girder D displacement with mean peaks and mean valleys during Molde 1

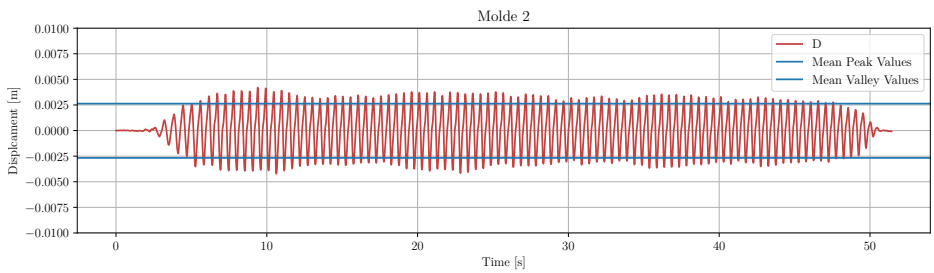


Figure 10.3: Girder D displacement with mean peaks and mean valleys during Molde 2

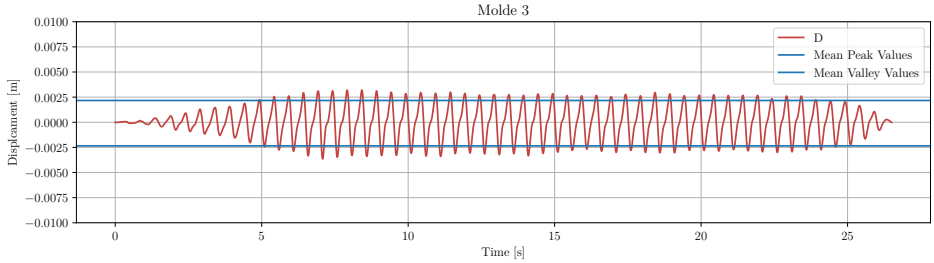


Figure 10.4: Girder D displacement with mean peaks and mean valleys during Molde 3

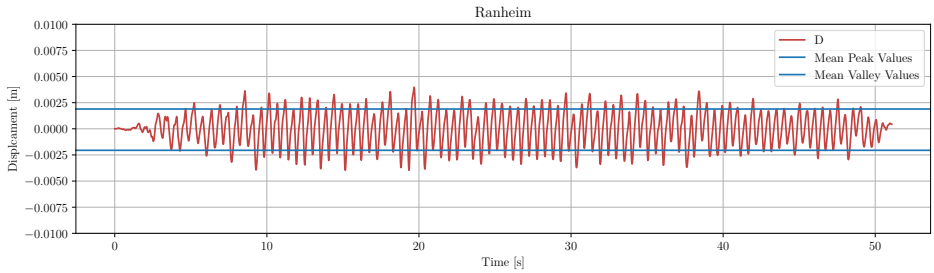


Figure 10.5: Girder D displacement with mean peaks and mean valleys during Ranheim

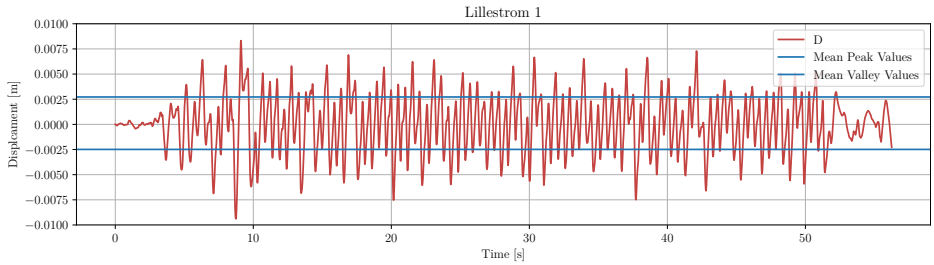


Figure 10.6: Girder D displacement with mean peaks and mean valleys during Lillestrøm 1

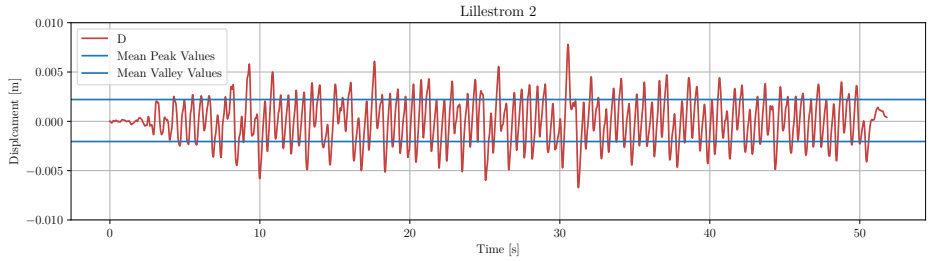


Figure 10.7: Girder D displacement with mean peaks and mean valleys during Lillestrøm 2

## 10.3 Vibration Criteria from RMS

Vibration criteria used for stadia structures using RMS are presented in Table 3.7. $a_{\text{RMS}}$ is calculated with Equation 3.11 using the script in section F.2. The levels proposed for comfort and or panic were, 10%$g$ and 20%$g$ respectively. The results are presented in Table 10.3.

Comparing the results with the criteria shows that only the Kristiansund event had levels that exceeded the limit, in both cases. However, this match was also the one with a considerable uncertainty of the measurements validity, and will therefore not weigh heavy in conclusion.

| Event | $a_{\text{RMS}}$ panic[b][%$g$] | Sample period [s-s] | $a_{\text{RMS}}$ comfort[a][%$g$] | Sample period [s-s] |
|---|---|---|---|---|
| Kristiansund | 26.0 | 10-11 | 11.1 | 10-20 |
| Molde 1 | 4.8 | 8.5-9.5 | 6.0 | 8-18 |
| Molde 2 | 6.1 | 25-26 | 5.6 | 10-20 |
| Molde 3 | 8.9 | 6.75-7.75 | 5.4 | 5.5-15.5 |
| Ranheim | 3.4 | 31-32 | 2.8 | 25-35 |
| Lillestrøm 1 | 12.0 | 19.25-20.25 | 8.3 | 12-22 |
| Lillestrøm 2 | 7.8 | 22.5-23.5 | 6.9 | 18-28 |

[a] 1 s RMS
[b] 10 s RMS

Table 10.3: RMS Vibration criteria calculation per Pippi occurrence for girder D

## 10.4 Vibration Criteria from VDV

The vibration dose value concerns a cumulative exposure to the vibrations, more than the amplitude of each vibration. The calculations are presented in Table 10.4, and shows that all VDV would cause individuals to experience the motion as "Disturbing". It is unclear whether this reaction is from the crowd exciting the structure or passive onlookers perceiving the structure. The vibration criteria are however intended for design purposes, and not for criteria used to tell whether or not a situation is safe.

| Event | VDV [m/s$^{1.75}$] | Probable reaction[a] |
|---|---|---|
| Kristiansund | 2.11 | Disturbing |
| Molde 1 | 1.99 | Disturbing |
| Molde 2 | 1.76 | Disturbing |
| Molde 3 | 1.43 | Disturbing |
| Ranheim | 1.26 | Disturbing |
| Lillestrøm 1 | 2.13 | Disturbing |
| Lillestrøm 2 | 1.81 | Disturbing |

[a] From Table 3.9

Table 10.4: VDV Vibration criteria calculation per Pippi occurrence for girder D

## 10.5 Vibration Servicability Summary

As mentioned all of the criteria that are proposed by the various standardisation groups are based on the crowds perceptiveness of the vibrations. The literature on the area does not specify to whom the criteria apply. If the criteria and the comments are based on the perception of the same crowd that is causing the excitation there is likely a higher threshold before any reaction occurs, compared to passive part such as the attendants of the VIP section below the cantilever. The probable reactions are fitting to the reactions observed among these attendants. Whereas the crowd causing the excitations does not seem to have any negative experience of their own activity.

If one is to use these criteria to make a decision it must be solely based on the crowds perceived danger, and not any actual structural danger. There is however, a possibility that the vibrations would cause panic among the crowd, which is another type of danger, which should be taken into account if in a process for evaluating the serviceability by the management of the stadium.

# Chapter 11

# The Digital Twin Solver

An essential part of utilising the digital twin concept is in connecting the sensor data to the virtual representation of the physical asset. The digital twin environment in which the recreation of behaviour is performed is the Fedem software. The digital twin is the finite element model presented in chapter 5. The process for recreation is to apply the behaviour history signal from the physical twin and produce a recreated history with the digital twin.

## 11.1 Inverse Fedem

The inverse Fedem solver requires a time history for $n$ known positions to retrieve $n$ unknown forces applied to the structure that would produce the given displacements. The solver uses displacement history from all three sensors and is applied as three distributed loads by utilising RBE3 elements. Figure 11.1 shows where the three forces are acting. The RBE3 spiders are limited to three parts symmetrically, where $F_1$ and $F_3$ are equal sizes. The solver utilises a YAML-file as a description for the properties of the solver [7]. The file contains identifiers and orientation for both the three unknown forces and the three known displacements, the size of the time step for the solver, as well as the path to the Fedem model. Although the general concept of the solver is known, the actual solver is treated as a black box as the no insight in to the underlying algorithm for confidentiality purposes.

One point of concern for the recreation is found by examining the forces used in the recreation as seen in Figure 11.2, where the values are nowhere near similar to the assumed periodic loads, and they also have negative values which would imply the crowd is pulling the grandstand up with the jumps. The solution, however, does

recreate the motion as intended.

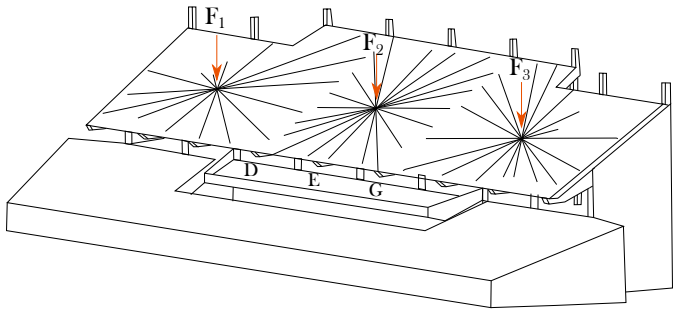


Figure 11.1: Application of forces in inverse solution

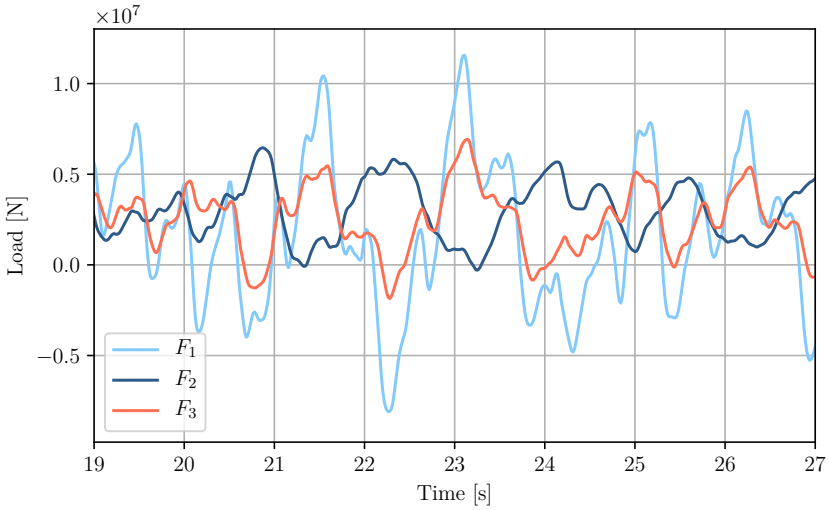


Figure 11.2: Applied forces in the solution for Lillestrøm 1 in between 19 and 27 seconds

## 11.2 I/O Comparison

A comparison of the two signals for input and output show that the solver can recreate the behaviour correctly. Figure 11.3 shows the two signals plotted on top of each other. The output signals oscillate about the same path as the input signal; however, it follows the same path for the most part. The oscillations occur because the FE model is not adequately dampened and has a response to the changes in applied loads.

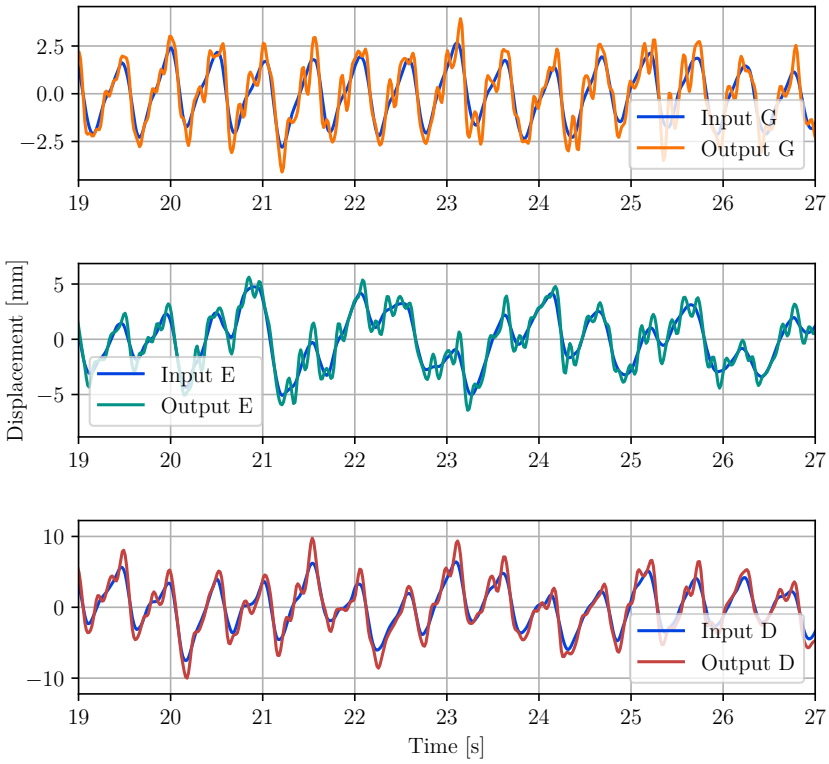


Figure 11.3: Plot of input signal and output signal for displacement from Lillestrøm 1

## 11.3 Measured Stresses

Recovering stresses from the solution shows that the critical areas are the three front columns at A, B and C, whereas the other area with the highest stresses are the two slim columns in the back at E and G. The stress distribution in Figure 11.4 is during the time-step with the highest negative displacement during Lillestrøm 1, which was the most extreme load event. The highest level of stress is around 14MPa in the three front columns, whereas the ones in the back experience peak stress of about 13Mpa. All stress levels in a solution like this should not be trusted as notches intensify the stress concentration where there are sharp transitions between elements, which causes the max reported stress by Fedem to be 21Mpa, even though no parts seemed to have areas experiencing this stress level.

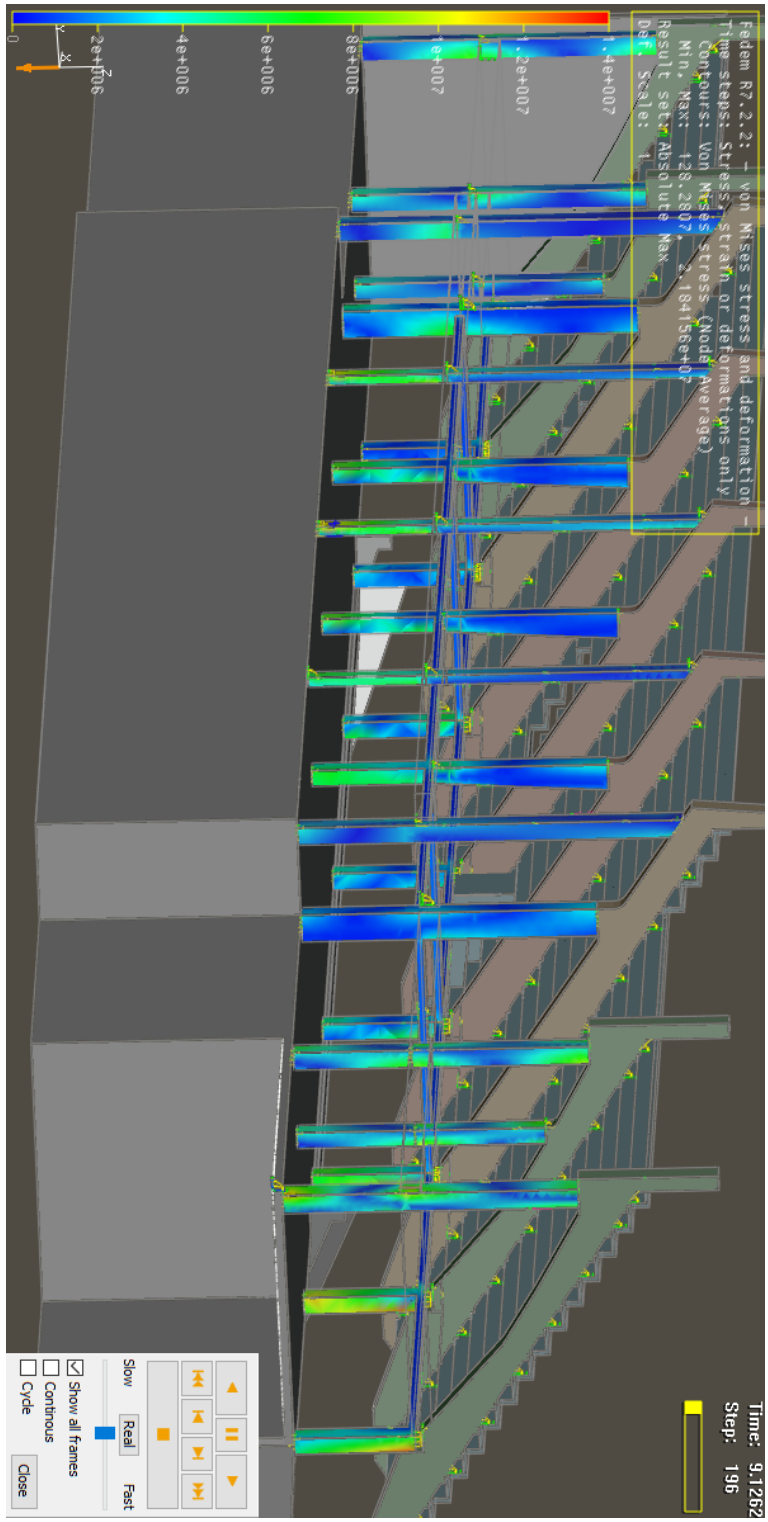


Figure 11.4: Stress distribution at peak displacement during Lillestrøm 1 at 9.1s

# Chapter 12

# The Consumption Layer

The consumption layer of the system is where the recreated history is made available for the user of the system. The digital twin component of the system is a recreated history where the stresses of several parts of the system are part of an animated recreation of the event. This animation is exported to the VTF-format to be usable for visualisation applications powered by Ceetron solutions. This particular visualisation uses the Ceetron Cloud Components [14] to create a web visualiser that would be available on any device through the browser.

## 12.1 Web Visualiser

The web application is made to visualise the animation of the solved event histories. Seeing as Fedem is able to export animations in the VTF-format [13] the use of a solution from Ceetron was a low hanging fruit compared to other options. The architecture for the web visualisation application is shown in Figure 12.1. The application developed for this thesis is based on the demo application provided by Ceetron. The server is run using Node.js which is a JavaScript run-time environment that runs both server side and client side, in the browser of the user. A screen capture of the web visualiser is shown in Figure 12.2 where the menu on the left shows the available events, and controls for orienting the model for inspection in 3D. The application has been run on a local server and not been hosted by a dedicated server for online access. The user interface used HTML5 and CSS, and the communication between the client and the cloud server uses socket.io.

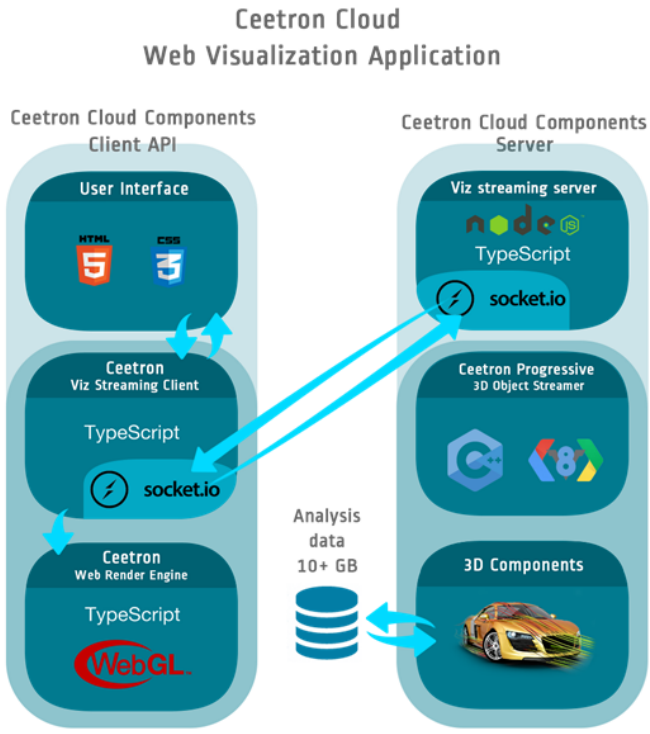


Figure 12.1: Ceetron architecture from [14]

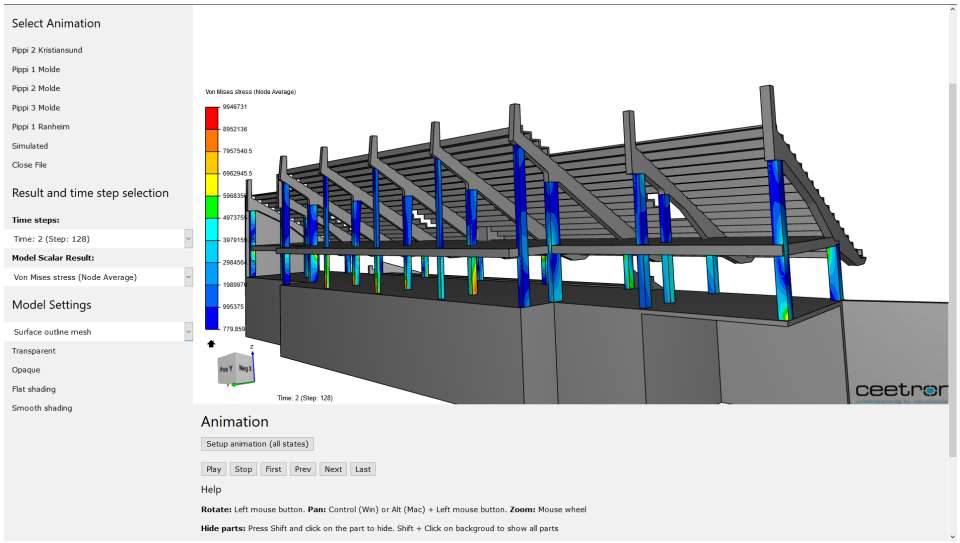


Figure 12.2: Screen capture of the web visualiser used for showing solved event histories

## 12.2 Additional Components for Inspection

The monitoring developed is solely based on a visual replay of the event histories of stress distribution and displacements using the digital twin model. In addition to the simple reenactment of past events, there are several other possibilities for additional components in a client used for inspection.

One of them could make use of the system developed by Datteo et al. [16] which used principal components of the recorded behaviour to monitor the change in behaviour caused by the climate over more extended periods of time.

The system could be connected to receive information about the number of attendants on the upper tier to identify any possible relationship between the number of people and the displacements.

Other possibilities include capturing more of the behaviour of the events, e.g. via recording sound, measuring temperature, and capturing video. The more information is available, the more representative the digital twin would be of the real structure.

# Chapter 13

# Discussion and Further Work

The discussion sections aims to summarise areas of interest to evaluate the results and the capabilities of the proposed system before propositions for areas requiring further work is presented.

## 13.1 Displacement Comparison

The only previous data that is usable as a comparison to the data measured during the field work of this project is the data from *Reinertsen* investigation in 2009. When comparing the data to their highest recorded values the largest increase for the displacement was a 500% increase, whereas all other largest measured displacement for each Pippi event was about twice that of *Reinertsen*'s. The problem is that their report did not state where the maximum displacement was recorded, and as such there are no grounds to assume the condition of the structure has deteriorated. This is because the values from the two other girders are more reasonable as a comparison.

## 13.2 FE model

The FE model was created in a preliminary project to this thesis and did not receive any drastic updates to the geometry or parameters after completion. The material data was based on printouts produces in the initial FE analysis in 2001 but does not necessarily mean that all material in the entire construction is uniform as is assumed in the model. The concrete used is most likely armed with steel, which has not been addressed to a sufficient degree. The stiffness of the model is based on

only one measurement with an uncertain load, which is means that it is no more than an educated guess at what the actual stiffness properties are. Furthermore, the stiffness of the structure was considered uniform and all parts received the same scaling of dynamic properties. All of the mentioned faults as well as the ones that are not mentioned have been presented in subsection 3.2.3, where Jones et al. describes common areas of fault in FE models used for simulating structures.

The ideal situation for future projects would be developing the FE model along with the production of the physical asset, and as such one would ensure the coherence between the twins. The uncertainty and lack of precision in this project mostly stem from the difficulty of recreating the digital twin correctly, as it is solely based on the original schematics without accounting for any changes during the construction or throughout its lifetime.

## 13.3 Resonance

As discussed in section 9.3 there is no evidence to support a claim that there is resonance in the cantilever caused by the dynamic load of the crowd. The claim does, however, not hold against a resonance in the structure in general. There are eigenfrequencies in other orientations than the vertical motion of the cantilever, and seeing as the vibrations are of such a significant magnitude that they are felt throughout the grandstand, it is possible that one of the horizontal eigenmodes is activated and causes resonance.

## 13.4 Asymmetry

The asymmetry might be one of the most peculiar results of recording the behaviour of the cantilever as it is counter-intuitive seeing as the cause of the asymmetry is a mystery despite the proposed hypotheses. The video showing the jumping from the front is at an angle that caused enough confusion to assume the drummer was located to the side over girder G. This erroneous assumption caused the hypothesis of hearing latency to rise as the most probable contender, consequently the confusion returned once the location was confirmed to be in the centre of the stands. This has highlighted the problem of recreating a load one is unable to model correctly.

## 13.5 Validity of Signal After Processing

When processing the signal, there are no validations that the deduced signals are correct, only that they are representative of the general motion of the cantilever. The acceleration is filtered to reduce the higher frequency spikes and noise, whereas the two deduced signals are filtered to remove their drifting. The method of using high pass filters for this task is not based on any previous work but seems to be a short-cut to produce adequate representations, seeing as the units two deduced signals are unmeasurable in their form. There are no easy ways of verifying the results except investigating the frequency spectra before and after the integration and filtering of the signals.

## 13.6 Molde Signal

The sensor data from the events recorded during the match against Molde had four times the sampling rate of the rest of the matches. The reason for the sampling rate was the fear of bandwidth of the data transmission. When all sensors were set to 512Hz, the bandwidth was at its, and any minor loss of connection would change the signal. This fear does not seem to outweigh the positive effect of the higher sampling rate. The difference is observable when comparing for instance Figure 10.2 and Figure 10.6. The signal from the Molde event seems more idealised and more synchronised whereas the other matches have a more chaotic signal. This might be explained by an unbelievably well-synchronised crowd in this one match, but it is more likely to do with the difference in sampling rate. According to the theorem in subsection 2.3.1 the sampling rate of 128Hz should be sufficient to represent the signal in discrete samples, as the principal components of the vibration are well beneath 64Hz. However, the Shannon-Nyquist theorem only concerns the ability to recreate the signal without any loss of information, but the time-steps of the signal is also used in the numerical integration where the $dt$ is defined as the time between samples. Furthermore, the displacement from the Molde game is similar in shape to the constructed load created using the ISO parameters seen in Figure 6.10. The similarity and an assumption that the Molde results are more representative than the rest would show a more direct connection between the analytical load models and the measured response from the field measurements.

## 13.7 Inverse Fedem Solver

The inverse Fedem solver is as expected capable of recreating the behaviour based on the comparison of the input and output displacement signals. The issue arises when investigating the method this behaviour is recreated. The basic idea was to find the load that results in the given behaviour, but the load is not the same as the actual load that caused the motion, as seen in Figure 11.2. The loads are mostly out of phase so that the three distributed crowd representations "jump" at different times. The other noteworthy issue is the forces crossing over into negative force, which is impossible without restraining the feet into the grandstand. The inclusion of a way to restrain the loads the solver is allowed to consider would be necessary for further development of the inverse Fedem solver when instrumenting structures that are subjected to loads by humans, such as bridges which is the area with the most potential at this time.

## 13.8 Lack of Standards and Regulations

A part of the project was to determine the safety of the load event at during matches. Through the literature, the vibration criteria using RMS and VDV are presented by the international standard whereas the Norwegian standard has no counterpart to this. The Norwegian standard covering the topic states that the standard does not consider dynamic loads caused by crowd activities [40]. This means that there are not many limits that apply to determine the safety based solely on the vibrations. A consequence of the lack of limits means that the perceived safety of a crowd is not easily accounted for in a decision. The use of the international standards will be the only source when considering the perception of safety. The results from the VDV calculations and their described response seem very fitting to the perception when attending matches. The vibrations are disturbing and have to some degrees caused comments from spectators. The staff at the stadium has told about comments from their clients about every match over the past years, which implies that the vibrations indeed are disturbing for the non-participating attendants of the crowd.

## 13.9 Usefulness of System

The last few sections of chapter 3 presents most of the theory and methods used for modeling the crowd dynamics on stadia, as well as some systems used for monitoring structural health. It is natural to weight the system developed in this project up

against what is presented in the most recent developments. Seeing as the digital twin system in its current form can avoid the need for a precise estimation of a crowd load, an advantage has been found.

Another advantage of the digital twin solution is the fact that the stress distribution of the complete structure is produced, whereas most systems thus far have been interested in detecting changes in vibrations patterns of random excitations. The ability to apply virtual sensors when the behaviour is recreated is of one of the valuable opportunities of the system. An automated version of the system that runs as a closed loop would make the inspection easier for any client that wanted to inspect the system.

## 13.10 Cumulative Uncertainty

Uncertainty is a common part of the entire system, and there is, therefore, a necessity to discuss all the areas where uncertainty is present. There are only three sensors used, which are placed in the three middle girders, and determining a precise behaviour of the entire cantilever is therefore not possible.

The next uncertainty comes from the signal processing. The integration of the acceleration signal into displacement is not a method that produces the correct signal, merely an indicator of the displacement. This is evident as the signal requires filtering to keep the mean value at zero. The problem with the signal processing is also the drifting of signals after integration. An ideal and more scientifically sound method would be to use a Kalman-filter or some other method that utilises an estimate to calibrate a most likely value based on the input signal.

The FE-model, as discussed in the chapter concerning the 3D modeling, is based on the architectural schematics. This means that the model is not an exact recreation of the physical grandstand. The further idealisation of the geometry was needed when the model was imported into the Fedem model where all parts needed to be split before they were attached by several different joints. The geometry was not the only uncertainty, as the mass, stiffness, and dampening properties of the model is based on printouts from a 17-year-old FE-analysis. The material data was assumed uniform across all parts of the model, which is most likely not representative of the physical twin. Mass is the dynamic property that is easiest to estimate as concrete does not vary significantly. One can estimate the stiffness by using a simple difference in static displacement with an assumed load of a crowd used to cause the displacement. The final property of the dampening ratio is nearly

impossible to find. The property is challenging enough for an empty grandstand as a hammer-test or equivalent could be conducted. However, as discussed by both Jones et al. [32] and Catbas et al. [12] the crowd has a significant effect on the dampening ratio, both by their mass and the merging of the human-structure relationship, that the task is as of yet undeterminable. The human body can quickly change from exuding energy into a system to absorbing the same energy. The effect of posture and degree of participation from the crowd also affects the dampening.

The last component is the actual solver of the event. The inverse Fedem is discussed earlier and would, therefore, be the final uncertainty to be presented.

The cumulative effect of these uncertainties is not investigated and makes a definite conclusion of the safety monitoring hard establish. Despite all these uncertainties, the system is capable of providing results that are reasonable and proves the viability of a system utilising the digital twin method.

## 13.11 Further Work

The following areas needs further work to make the solution a more complete product.

#### Closing the Loop

The endeavour with the most interest for this system is closing the loop, as in automating the process from start to finish. The path from cantilever motion to visualisation is a straight path that can be described as a pipe-and-filter process where there is a one way stream from input to output. The sensor network has an API which would enable control of the nodes in an application and can receive the transmitted data directly into a processing script.

#### Launching Web Application

The web application has only been hosted locally and has not been tested in a production environment. The process of hosting a web service a straight forward, but time-consuming process.

#### Identify the Exact Behaviour of the Cantilever Motion

The motion of the cantilever is not completely understood as only a third of the length has been recorded. By recording all girders a more complete understanding of the motion would be gained.

### Investigating the Critical Areas of the Construction

The areas of the structure that has experienced the greatest levels of stress has been identified and could be used for inspection of the state of the grandstands structural health.

### Developing the Inverse Fedem Solver

The Fedem solver does manage to produce a solution, but not necessarily the right solution. Adding rules for the allowed solution, such as no negative load from humans, would produce more accurate results.

# Chapter 14

# Conclusion

The goal of the edge is to capture the behaviour of the instrumented physical asset, and process this into a consumable behavioural history for the core. The three sensors used are able to capture the behaviour consistently. The processing set-up with conversion from an acceleration signal into a displacement signal appears to produce accurate representations of the motion that is expected by a periodic load from the crowd. A comparison to simulations and previous investigations show that the are of the measurements are of similar magnitude, but the peak values recorded during this process have been significantly higher. The increase of values does not imply that the situation has worsened, as the data is recorded on different locations from the previous investigation.

The goal of the core is to recreate the behaviour using the digital twin. A comparison of the input and output of the solver demonstrate that the model is able to recreate the motion it receives. The digital twin model through simulations and solving is not detailed enough, both by design and load application method, to correctly determine the load that causes the behaviour, despite the resulting motion being produced accurately. The FE model does not have the correct dynamic properties to precisely use represent the physical structures properties. The mass and stiffness have been estimated, but the dampening has not been identified as the property is dependent on the interaction between human and structure.

The goal of the consumption layer is to visualise the solved events. A web application for visualisation of the vent histories has been developed based on a solution for visualisation FE models on the web. The server has been hosted locally and is capable of visualising the events with both displacements and stress distribution present in the animation.

Vibrations serviceability criteria are used to determine situations where crowds experience vibrations of structures they occupy. The calculation of the vibrations present in the grandstand show that the are within the acceptable limits for the serviceability criteria and does not necessitate any remedial actions.

The usefulness of the system stems in its ability to recreate an event to such a degree that an investigation of the stress distribution in the structure is visualised after the said event has occurred. The system at the level of development managed in this project is not yet mature to be sold as a finished product, as is evident in the many uncertainties present in the system pipeline. Despite the system's current incompleteness is shows great potential for further development into a product capable of monitoring stadia and other structures, to the degree that comparable systems of today are not.

# Bibliography


[1] Vibrations caused by dynamic crowd load during RBK - Viking 19.11.17 - YouTube. URL https://www.youtube.com/watch?v=VW3mCZXHaG8.

[2] Pippi theme during RBK - Zenit 02.11.17 - YouTube, 2017. URL https://www.youtube.com/watch?v=6GjMJqqIod4.

[3] Osama Abdeljaber, Onur Avci, Serkan Kiranyaz, Moncef Gabbouj, and Daniel J. Inman. Real-time vibration-based structural damage detection using one-dimensional convolutional neural networks. *Journal of Sound and Vibration*, 388:154–170, feb 2017. ISSN 0022-460X. doi: 10.1016/J.JSV.2016.10.043. URL https://www.sciencedirect.com/science/article/pii/S0022460X16306204.

[4] E Agu and M Kasperski. A statistical approach to loads induced by bobbing. *Structural Dynamics EURODYN*, 2008.

[5] Hugo Bachmann and Walter Ammann. *Vibrations in Structures Induced by Man and Machines*. 1987. ISBN 3-85748-052-X.

[6] RC Batista and C Magluta. Spectator-induced vibration of Maracana football stadium. *Structural Dynamics–EURODYN*, 1993.

[7] Oren Ben-Kiki, Clark Evans, and Ingy döt Net. YAML Ain't Markup Language (YAML™) Version 1.2, 2009. URL http://yaml.org/spec/1.2/spec.html.

[8] Guillaume Bigourdan. *Le système métrique des poids et mesures: Son établissement et sa propagation graduelle, avec l'histoire des opérations qui ont servi à déterminer le mètre et le kilogramme*. Gauthier-Villars, 1901.

[9] A. Bodare and S. Erlingsson. Rock Music Induced Damage and Vibration at Nya Ullevi Stadium. *International Conference on Case Histories in Geotech-*

*nical Engineering*, jun 1993. URL http://scholarsmine.mst.edu/icchge/3icchge/3icchge-session04/7.

[10] J.M.W. Brownjohn, Pin-Qi Xia, Hong Hao, and Yong Xia. Civil structure condition assessment by FE model updating:: methodology and case studies. *Finite Elements in Analysis and Design*, 37(10):761–775, sep 2001. ISSN 0168-874X. doi: 10.1016/S0168-874X(00)00071-8. URL https://www.sciencedirect.com/science/article/pii/S0168874X00000718.

[11] Canadian Commission on Building and Fire Codes. *User's Guide—NBC 2005:Structural Commentaries (Part 4 of Division B)*. National Research Council of Canada, Institute for Research in Construction, Ottawa, 2006.

[12] Fikret Necati Catbas, Ozan Celik, Onur Avci, Osama Abdeljaber, Mustafa Gul, and Ngoan Tien Do. Sensing and Monitoring for Stadium Structures: A Review of Recent Advances and a Forward Look. *Frontiers in Built Environment*, 3: 38, aug 2017. ISSN 2297-3362. doi: 10.3389/fbuil.2017.00038. URL http://journal.frontiersin.org/article/10.3389/fbuil.2017.00038/full.

[13] Ceetron ASA. VTF - Binary GLview 7 REFERENCE GUIDE, 2006.

[14] Ceetron Cloud Team. Ceetron Cloud Components (C3), 2018. URL https://ceetron.com/docs/CloudComponents/index.html.

[15] W.T. Cochran, J.W. Cooley, D.L. Favin, H.D. Helms, R.A. Kaenel, W.W. Lang, G.C. Maling, D.E. Nelson, C.M. Rader, and P.D. Welch. What is the fast Fourier transform? *Proceedings of the IEEE*, 55(10):1664–1674, 1967. ISSN 0018-9219. doi: 10.1109/PROC.1967.5957. URL http://ieeexplore.ieee.org/document/1447887/.

[16] Alessio Datteo, Francescantonio Lucà, Giorgio Busca, and Alfredo Cigada. Long-time monitoring of the G. Meazza stadium in a pattern recognition prospective. *Procedia Engineering*, 199:2040–2046, jan 2017. ISSN 1877-7058. doi: 10.1016/J.PROENG.2017.09.470. URL https://www.sciencedirect.com/science/article/pii/S1877705817339644.

[17] Arya Ebrahimpour and Ronald L Sack. A Review of Vibration Serviceability Criteria for Floor Structures. *Computers and Structures*, 83(28):2488–2494, 2005.

[18] B Ellis, T. Ji, and J D Littler. THE RESPONSE OF GRANDSTANDS TO DYNAMIC CROWD LOADS. *ICE Proceedings, Structures and Buildings*, 140(4):355–365, nov 2000. ISSN 1751-7702. doi: 10.1680/istbu.2000.32800. URL `http://www.atypon-link.com/ITELF/doi/abs/10.1680/istbu.2000.32800`.

[19] B R Ellis and T Ji. Floor vibration induced by dance-type loads: verification. *The structural engineer : journal of the Institution of Structural Engineers.*, 72 (5):37, 1994.

[20] B R Ellis and T Ji. HUMAN-STRUCTURE INTERACTION IN VERTICAL VIBRATIONS. *Proceedings of the Institution of Civil Engineers - Structures and Buildings*, 122(1):1–9, feb 1997. doi: 10.1680/istbu.1997.29162. URL `http://www.icevirtuallibrary.com/doi/10.1680/istbu.1997.29162`.

[21] B. R. Ellis and J. D. Littler. Response of cantilever grandstands to crowd loads. Part 1: serviceability evaluation. *Proceedings of the Institution of Civil Engineers - Structures and Buildings*, 157(4):235–241, aug 2004. ISSN 0965-0911. doi: 10.1680/stbu.2004.157.4.235. URL `http://www.icevirtuallibrary.com/doi/10.1680/stbu.2004.157.4.235`.

[22] Fedem Technology AS. Digital Twin — Fedem, 2018. URL `http://www.fedem.com/digital-twin/`.

[23] Zhi-Fang Fu and Jimin He. *Modal Analysis*. Elsevier Science & Technology, 2001.

[24] D Ginty, J M Derwent, and T Ji. The Frequency Ranges of Dance-Type loads. *The Structural Engineer*, 79(6):27–31, 2001. ISSN 00392553.

[25] M Glackin. Stadia design rethink prompted by Cardiff fiasco. *Building*, page 11, 2000.

[26] Michael Grieves and John Vickers. Digital Twin: Mitigating Unpredictable, Undesirable Emergent Behavior in Complex Systems. In *Transdisciplinary Perspectives on Complex Systems: New Findings and Approaches*, pages 85–113. Springer International Publishing, 2017.

[27] S Han and J.-B. Lee. Analysis of errors in the conversion of acceleration into displacement. *Proceedings of the International Modal Analysis Conference - IMAC*, 2:1408–1413, 2001. ISSN 10466770. URL `http://www.scopus.com/`

inward/record.url?eid=2-s2.0-0035051506{&}partnerID=40{&}md5=ff8975a9b026e56e83a64f1b1a8c0417.

[28] International Organization for Standardization. *ISO 10137:2007*. International Organization for Standardization, 2007.

[29] IStructE/DCLG/DCMS Joint Working Group. *Dynamic Performance Requirements for Permanent Grandstands: Recommendations for Management Design and Assessment*. Institution of Structural Engineers, London, 2008.

[30] T. Ji and D. Wang. A SUPPLEMENTARY CONDITION FOR CALCULATING PERIODICAL VIBRATIONS. *Journal of Sound and Vibration*, 241(5): 920–924, apr 2001. ISSN 0022-460X. doi: 10.1006/JSVI.2000.3318. URL https://www.sciencedirect.com/science/article/pii/S0022460X00933182.

[31] Ragnar Johnsen. Impulsrespons, 2009. URL https://snl.no/impulsrespons.

[32] C.A. Jones, P. Reynolds, and A. Pavic. Vibration serviceability of stadia structures subjected to dynamic crowd loads: A literature review. *Journal of Sound and Vibration*, 330(8):1531–1566, apr 2011. ISSN 0022-460X. doi: 10.1016/J.JSV.2010.10.032.

[33] M. Kasperski and E Agu. Prediction of crowd-induced vibrations via simulation. *Proceeding of 23rd International Modal Analysis Conference*, 2005.

[34] Erwin Kreyszig. *Advanced engineering mathematics*. John Wiley & Sons, 2010.

[35] Kenneth H Lenzen. Vibration of Steel Joist-Concrete Slab Floors. *AISC. Eng. Jour.*, 3:133–136, 1966. URL https://ci.nii.ac.jp/naid/10004180533/.

[36] *SensorConnect*. LORD Corporation, 2016.

[37] *G-Link-200*. LORD Corporation, 2017.

[38] Manchester Evening News. Robbie fans in danger at cricket ground gig, 2007. URL https://www.manchestereveningnews.co.uk/news/greater-manchester-news/robbie-fans-in-danger-at-cricket-ground-1189766.

[39] R Moreland. The Weight of a Crowd. *Engineering*, 79:551, 1905.

[40] Norsk Standard. *NS-EN 13200-1_2012*. Standard Norge, 2012.

[41] Store norske leksikon. Resonans, 2018. URL https://snl.no/resonans.

[42] M. P. (Michael Peter) Norton and D. G. (Denis G.) Karczub. *Fundamentals of noise and vibration analysis for engineers*. Cambridge University Press, 2003. ISBN 0521499135.

[43] D Nyawako and P Reynolds. Active control of human induced floor vibrations. *Conference Proceedings of the Society for Experimental Mechanics Series*, 2008.

[44] Helmut Ormestad. Egenfrekvens, 2017. URL `https://snl.no/egenfrekvens`.

[45] Wolfgang. Rindler. *Essential Relativity : Special, General, and Cosmological*. Springer Berlin Heidelberg, 2012. ISBN 3642866506.

[46] D Rogers and R Thompson. Liverpool stand gets a red card. *Construction News*, 2000.

[47] Claude E Shannon. Introduction To "Communication In The Presence Of Noise". *Proceedings of the IEEE*, 86(2):442–446, 1947. ISSN 0018-9219. doi: 10.1109/JPROC.1998.659496. URL `http://ieeexplore.ieee.org/document/659496/`.

[48] Telenor. Raskest med 4G+, 2018. URL `https://www.telenor.no/privat/dekning/4g-pluss.jsp`.

[49] The Scipy Community. Discrete Fourier Transform (numpy.fft) — NumPy v1.14 Manual, 2016. URL `https://docs.scipy.org/doc/numpy/reference/routines.fft.html`.

[50] The Scipy Community. scipy.integrate.cumtrapz — SciPy v0.18.1 Reference Guide, 2016. URL `https://docs.scipy.org/doc/scipy-0.18.1/reference/generated/scipy.integrate.cumtrapz.html{#}scipy.integrate.cumtrapz`.

[51] The SciPy community. Signal processing (scipy.signal), 2018. URL `https://docs.scipy.org/doc/scipy/reference/signal.html`.

[52] Suresh Thenozhi, Wen Yu, and Ruben Garrido. A novel numerical integrator for velocity and position estimation. *Transactions of the Institute of Measurement and Control*, 35(6):824–833, 2013. ISSN 14770369. doi: 10.1177/0142331213476987.

[53] C. J. Tilden. Kinetic Effect of Crowds. *Proceedings of the American Society of Civil Engineers*, 39(3):325–340, 1913.

[54] Christopher Y. Tuan and William E. Saul. Loads Due to Spectator Movements. *Journal of Structural Engineering*, 111(2):418–434, feb 1985. ISSN 0733-9445. doi: 10.1061/(ASCE)0733-9445(1985)111:2(418).

# List of Figures

# List of Tables

# Appendix A

# Eigenmodes

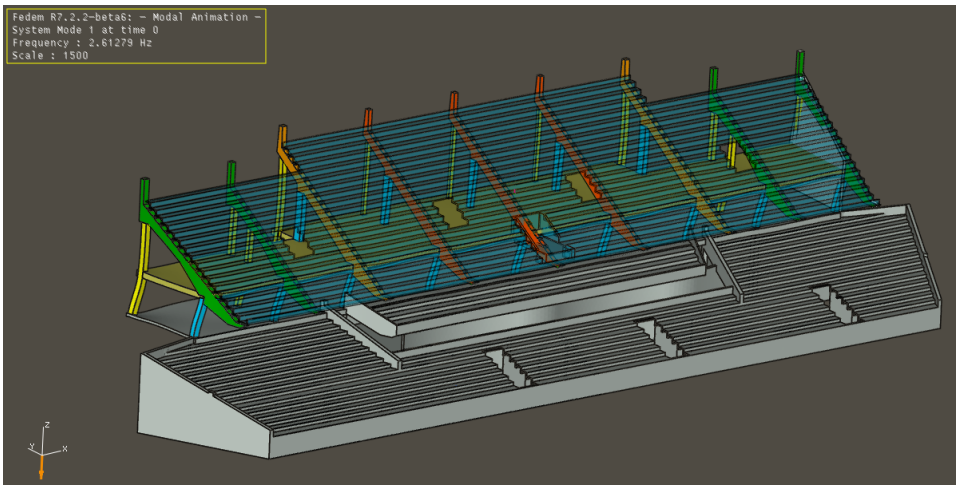


Figure A.1: Mode 1

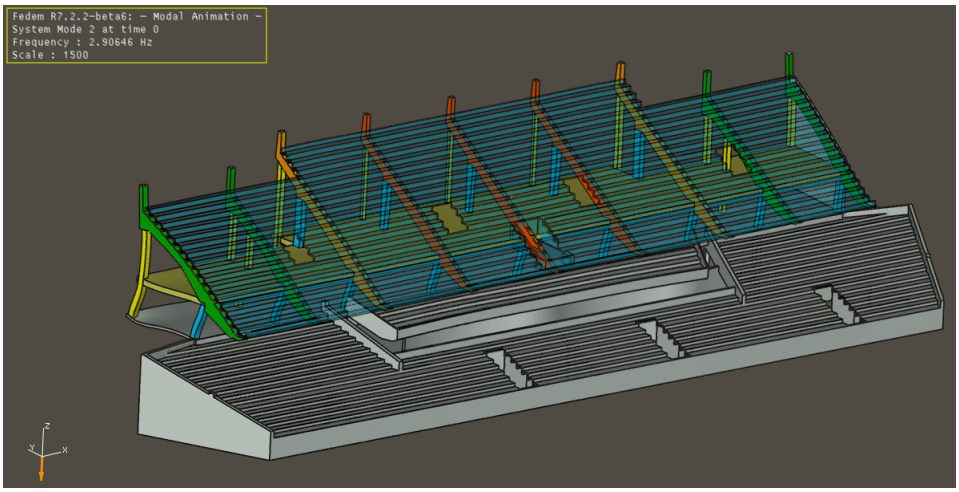


Figure A.2: Mode 2

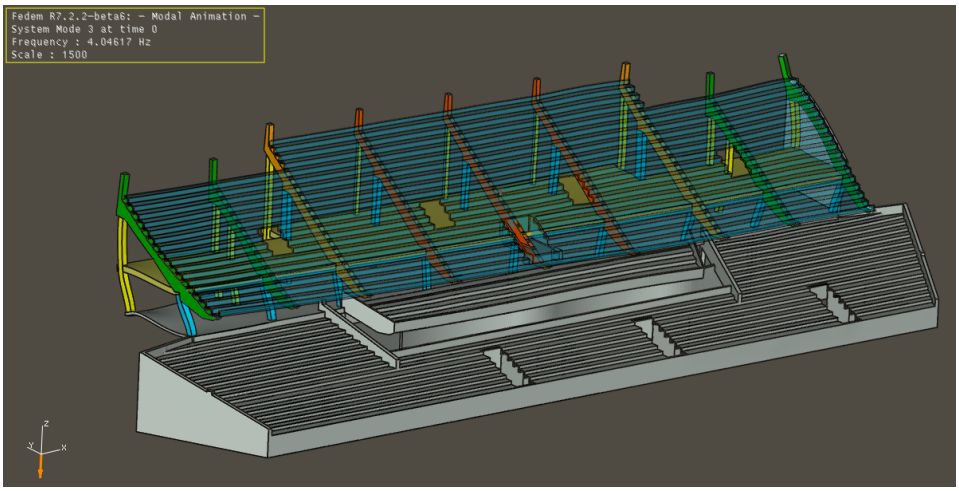


Figure A.3: Mode 3

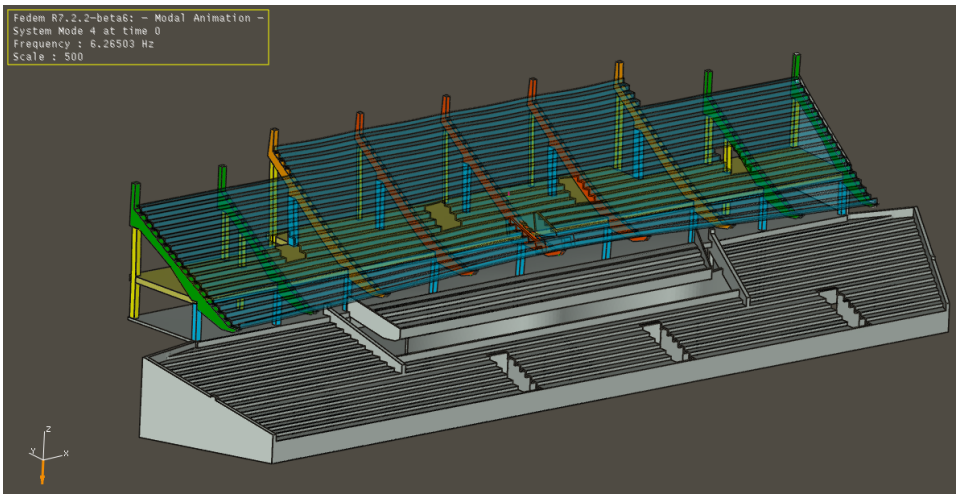


Figure A.4: Mode 4

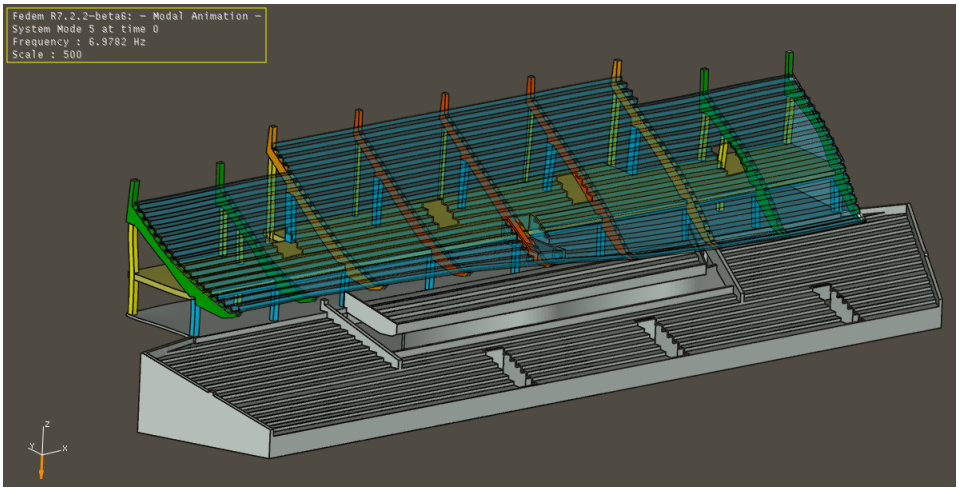


Figure A.5: Mode 5

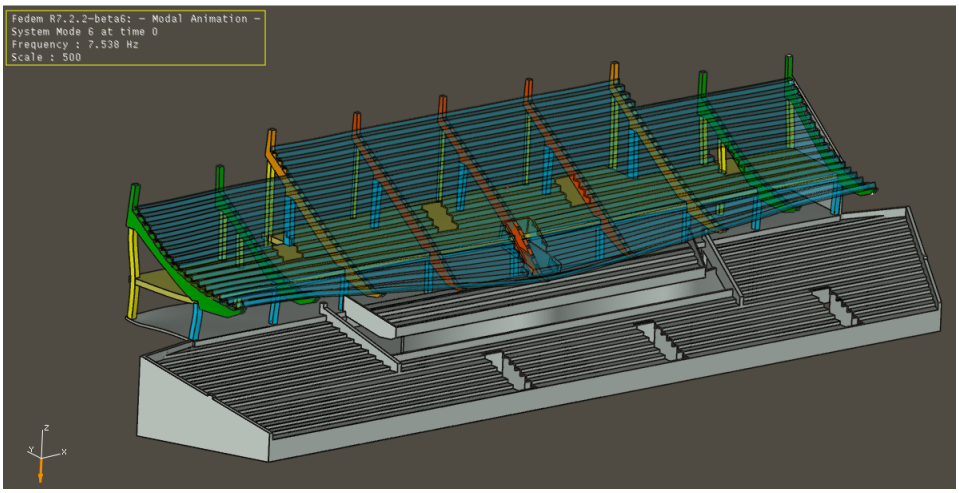


Figure A.6: Mode 6

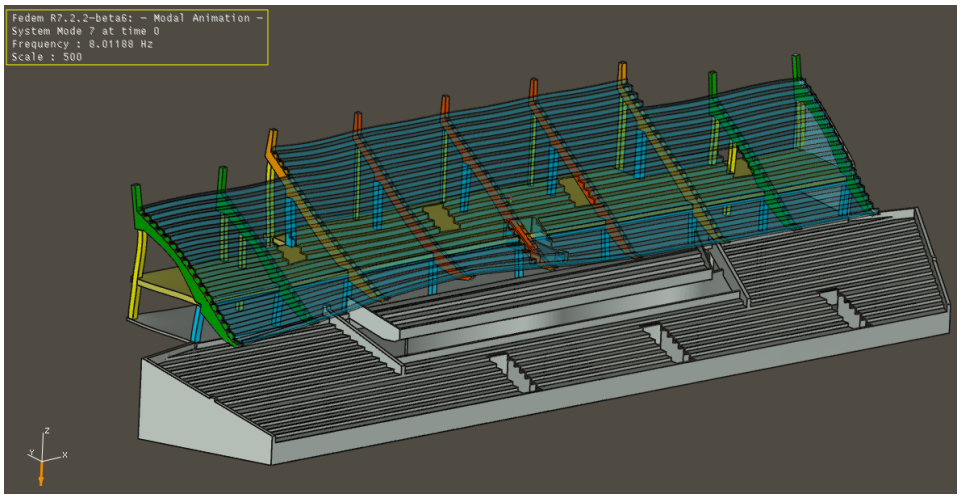


Figure A.7: Mode 7

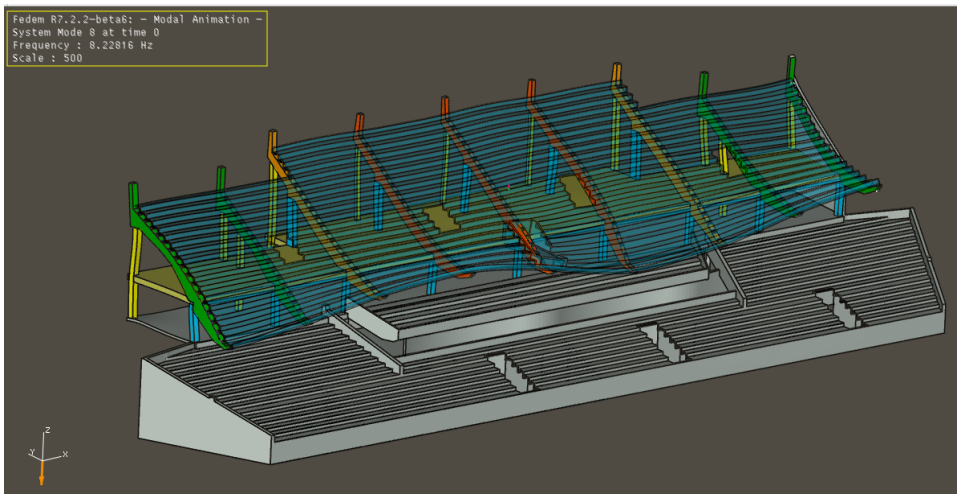


Figure A.8: Mode 8

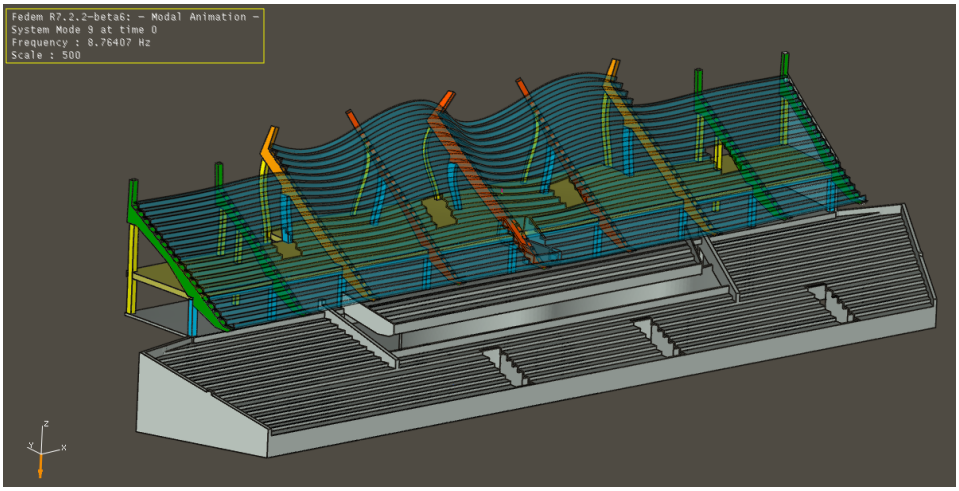


Figure A.9: Mode 9

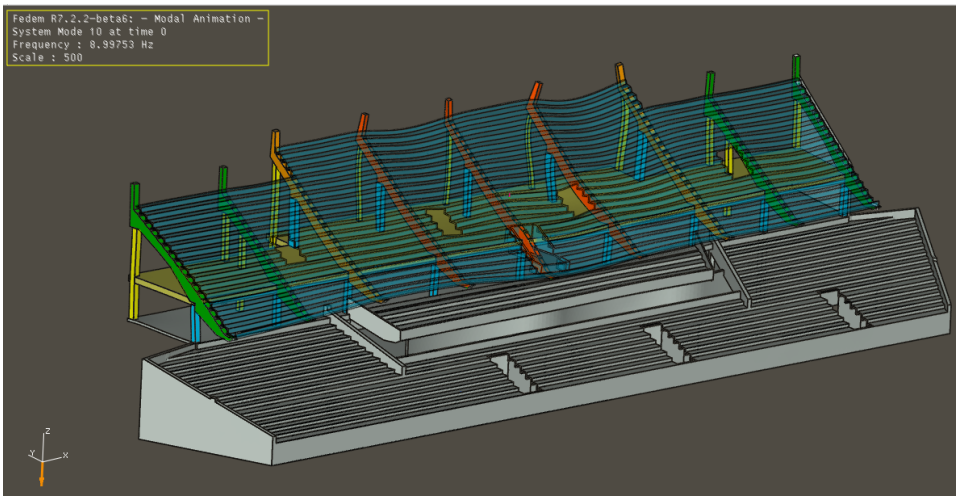


Figure A.10: Mode 10

# Appendix B

# Plots from all Matches

All recorded Pippi load cases are presented in this chapter, and are from the matches against Kristiansund, Molde, Ranheim, Lillestrøm, and Brann. When the title has a number it means there were several occurrences of the load case during a match. The plots include all plots both filtered and unfiltered and FFT plots from the same data.

## B.1 Kristiansund

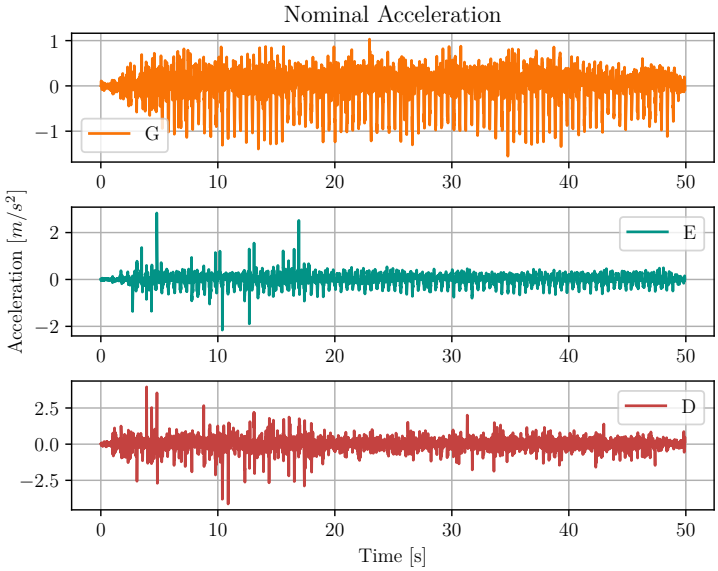


Figure B.1: Nominal Acceleration from Pippi vs Kristiansund

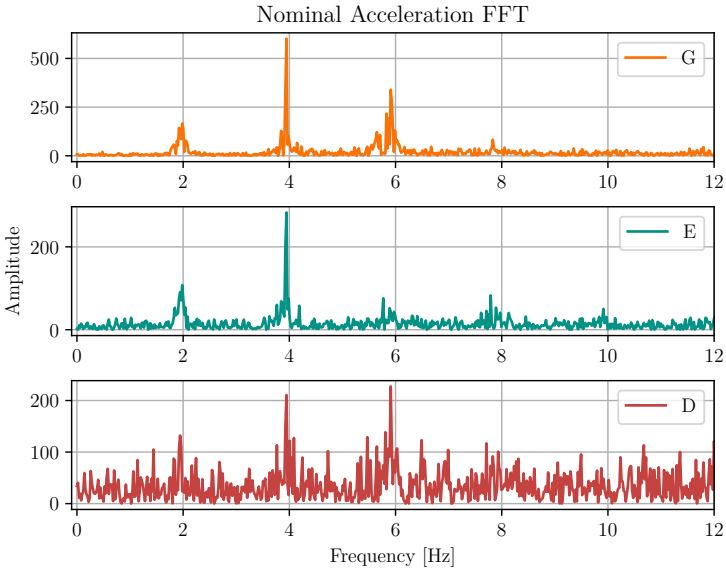


Figure B.2: FFT of Nominal Acceleration from Pippi vs Kristiansund

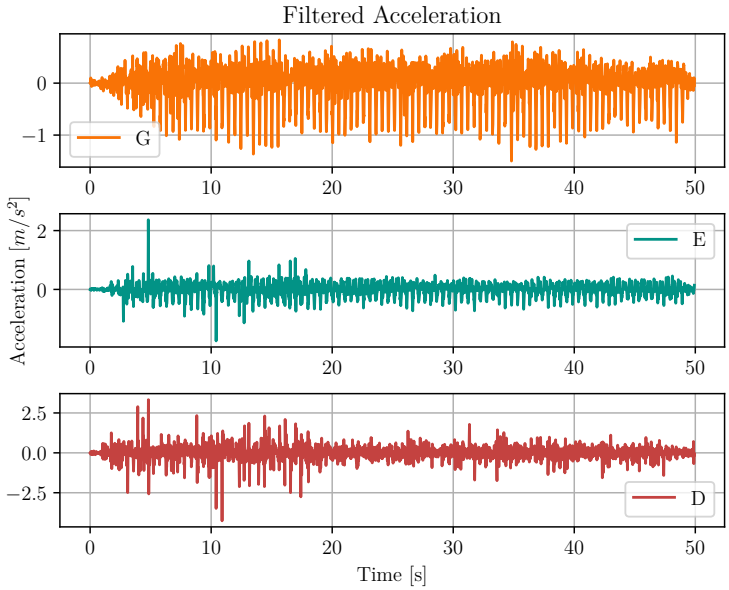


Figure B.3: Filtered Acceleration from Pippi vs Kristiansund

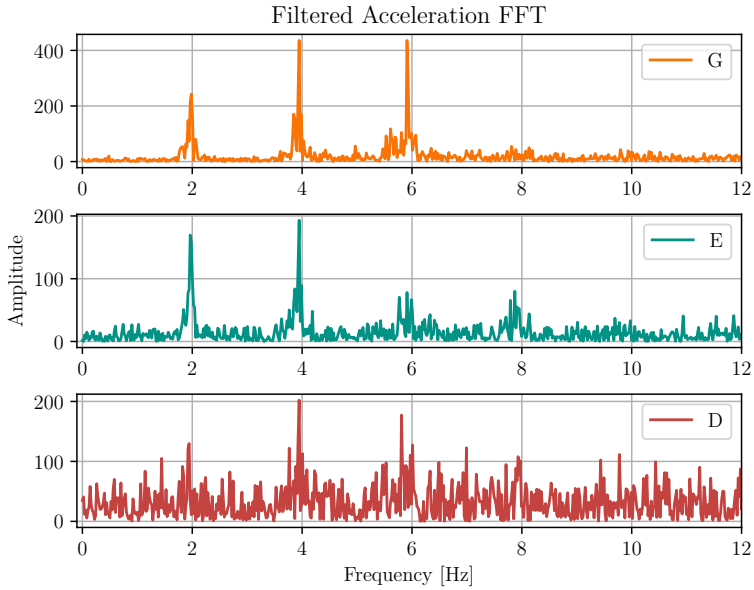


Figure B.4: FFT of Filtered Acceleration from Pippi vs Kristiansund

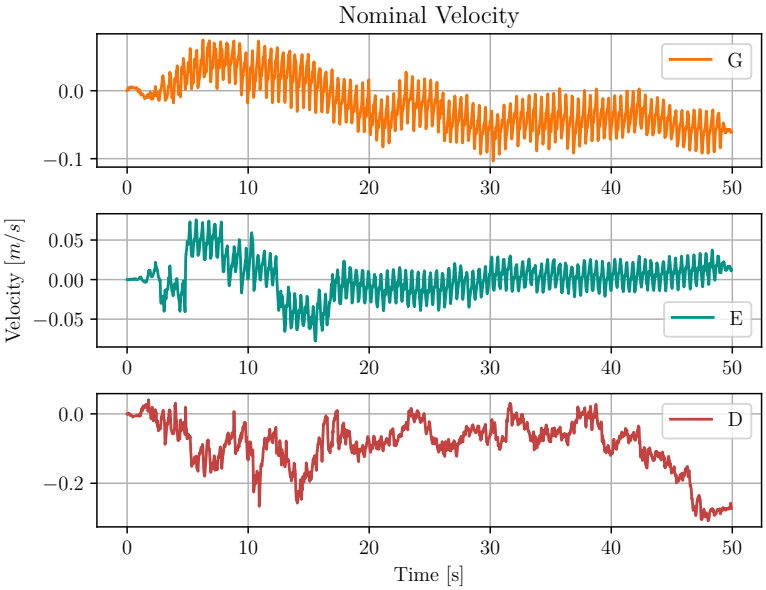


Figure B.5: Nominal Velocity from Pippi vs Kristiansund

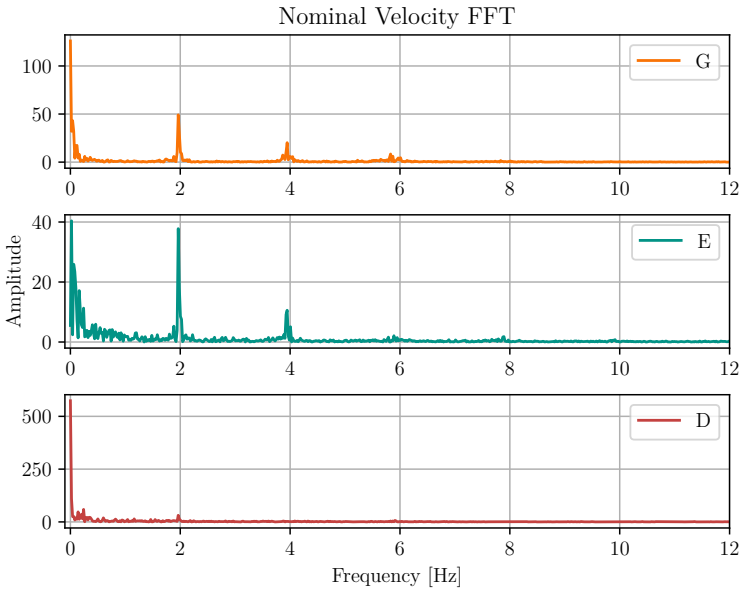


Figure B.6: FFT of Nominal Velocity from Pippi vs Kristiansund

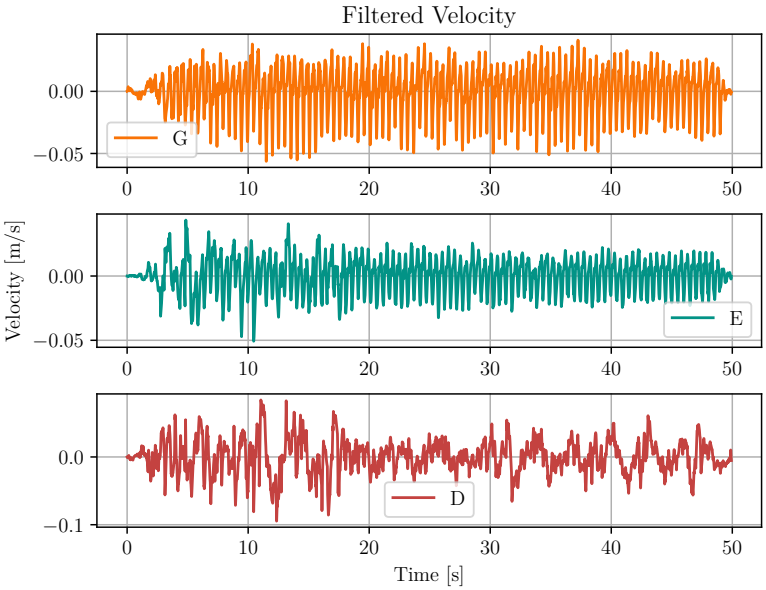


Figure B.7: Filtered Velocity from Pippi vs Kristiansund

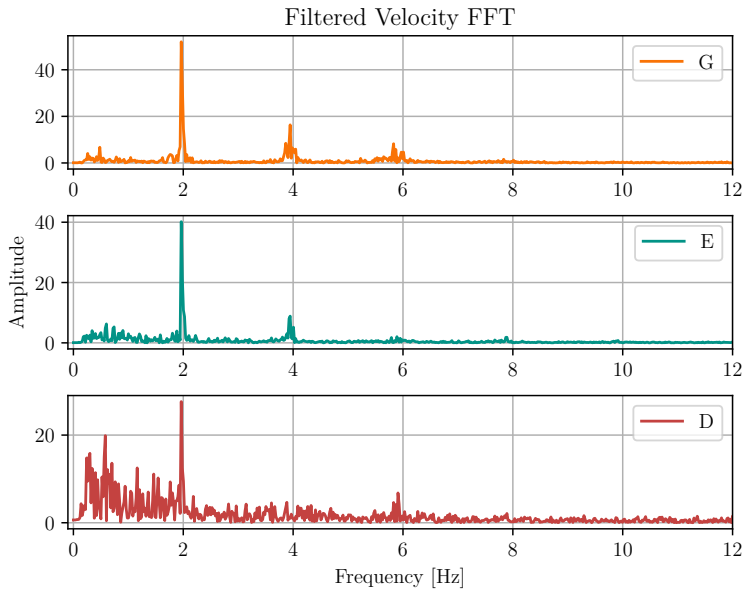


Figure B.8: FFT of Filtered Velocity from Pippi vs Kristiansund

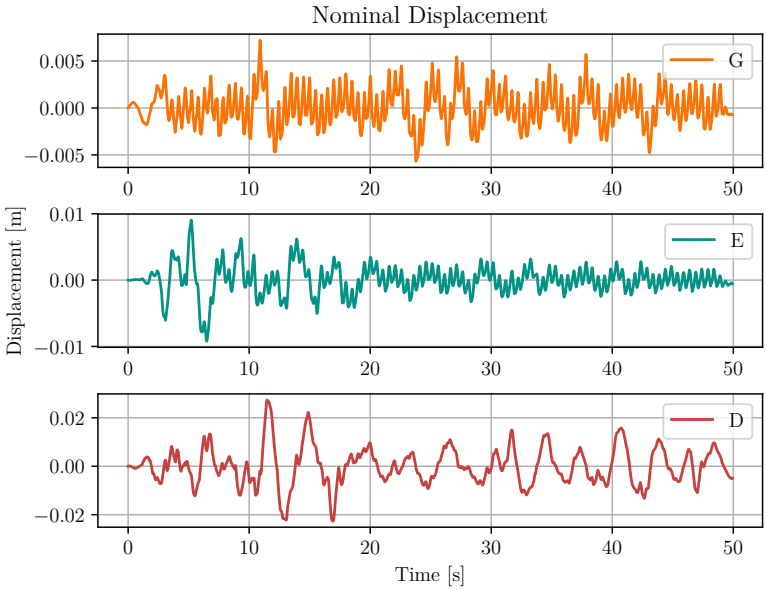


Figure B.9: Nominal Displacement from Pippi vs Kristiansund

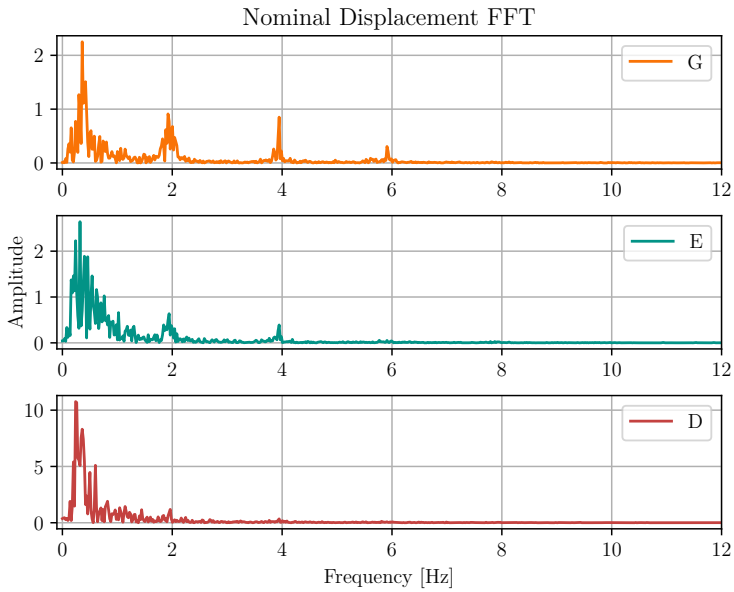


Figure B.10: FFT of Nominal Displacement from Pippi vs Kristiansund

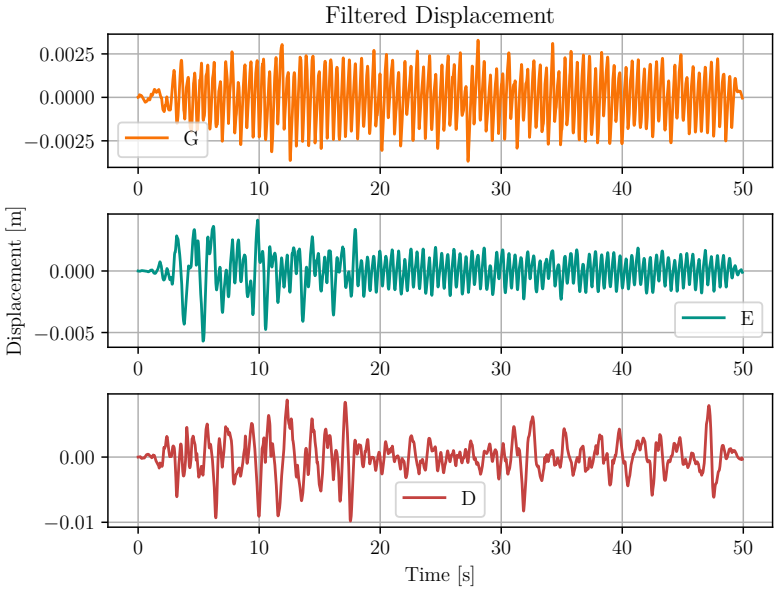


Figure B.11: Filtered Displacement from Pippi vs Kristiansund

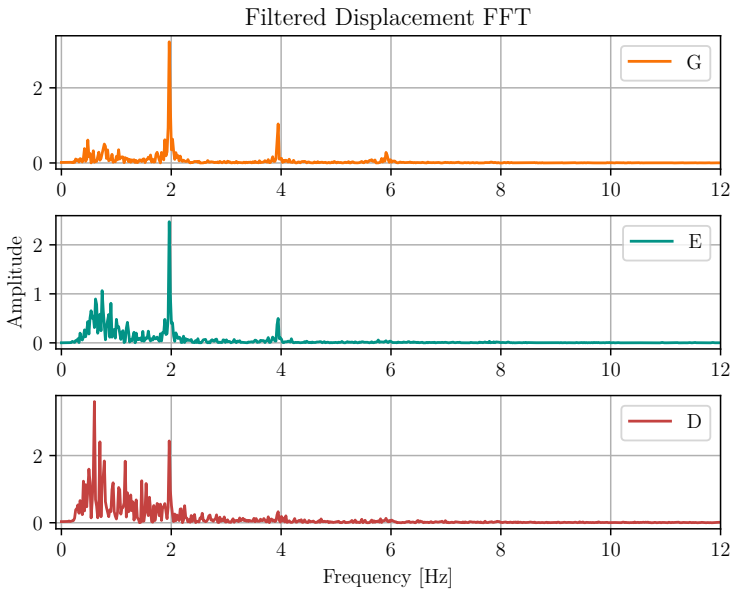


Figure B.12: FFT of Filtered Displacement from Pippi vs Kristiansund

## B.2 Molde 1

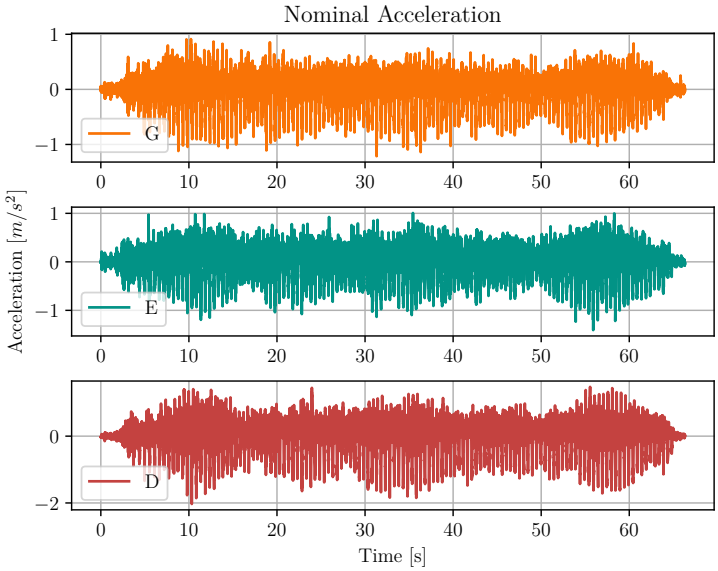


Figure B.13: Nominal Acceleration from Pippi 1 vs Molde

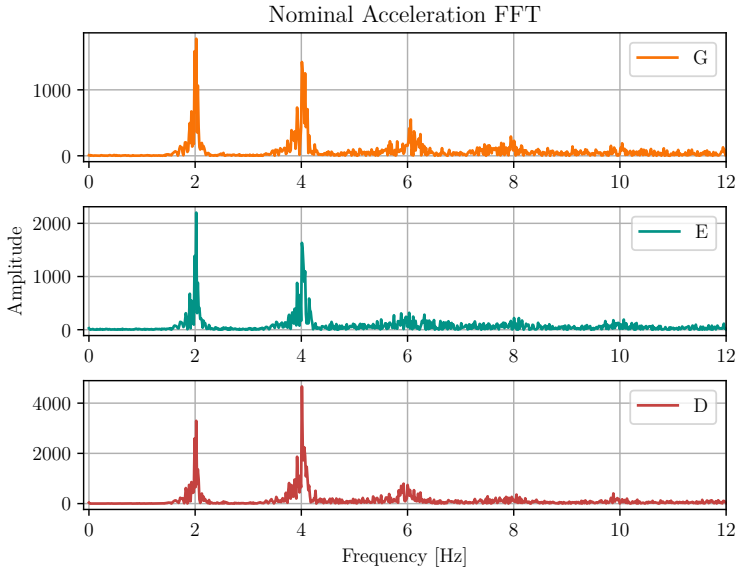


Figure B.14: FFT of Nominal Acceleration from Pippi 1 vs Molde

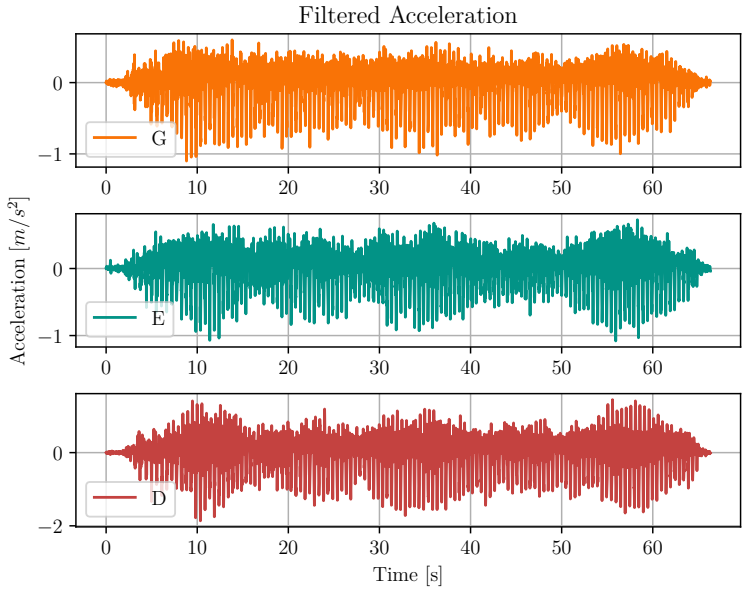


Figure B.15: Filtered Acceleration from Pippi 1 vs Molde

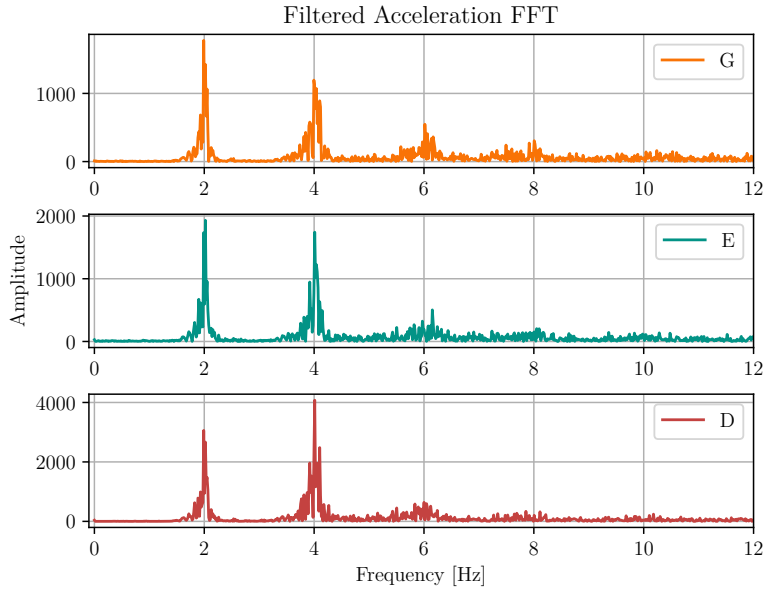


Figure B.16: FFT of Filtered Acceleration from Pippi 1 vs Molde

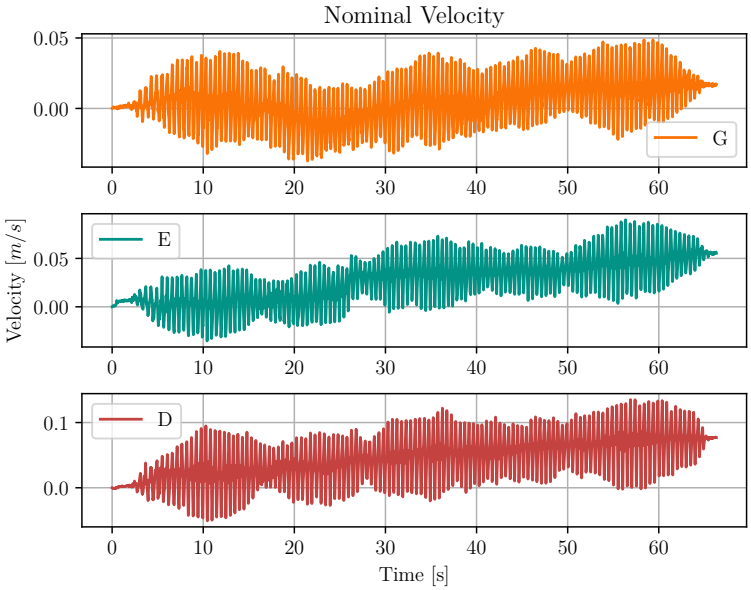


Figure B.17: Nominal Velocity from Pippi 1 vs Molde

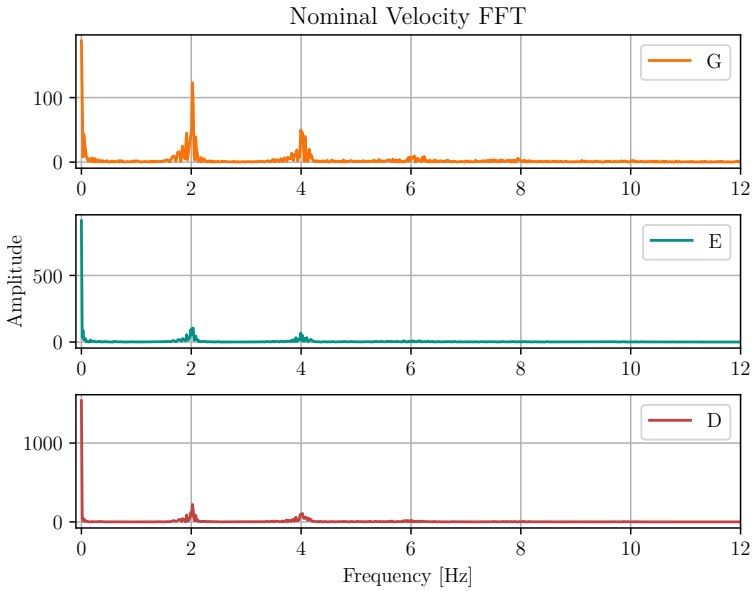


Figure B.18: FFT of Nominal Velocity from Pippi 1 vs Molde

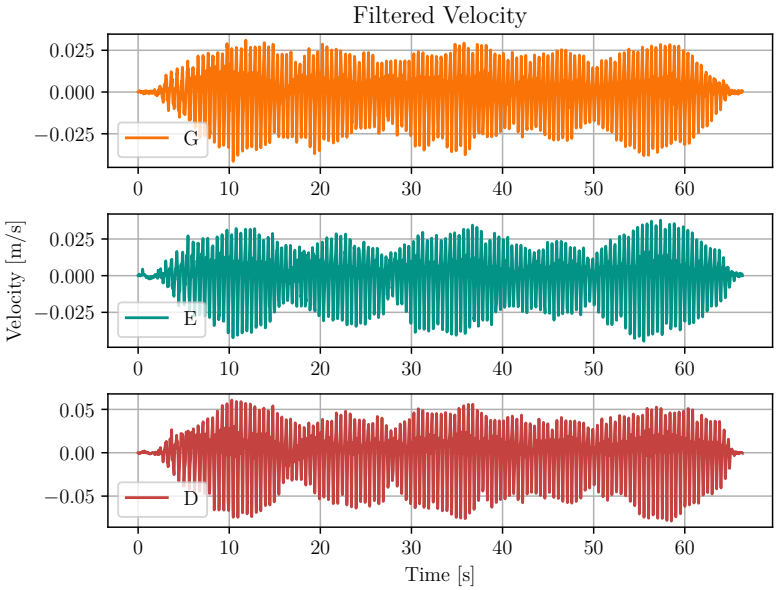


Figure B.19: Filtered Velocity from Pippi 1 vs Molde

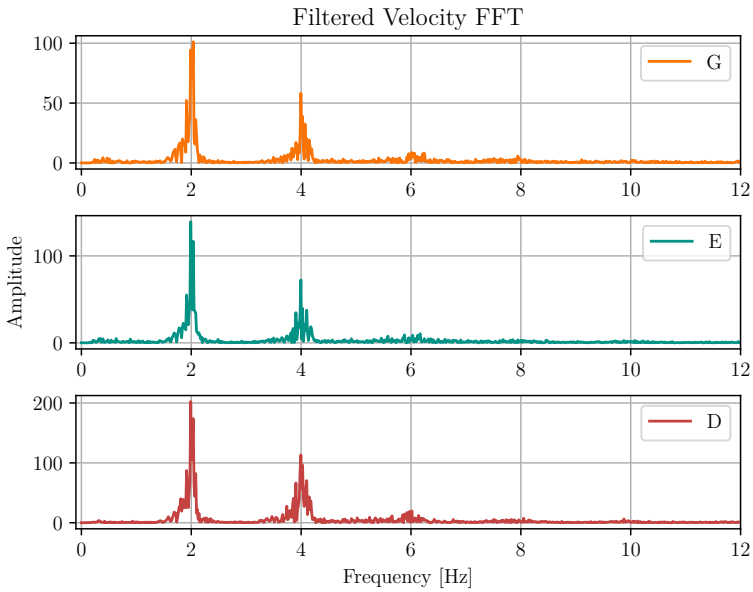


Figure B.20: FFT of Filtered Velocity from Pippi 1 vs Molde

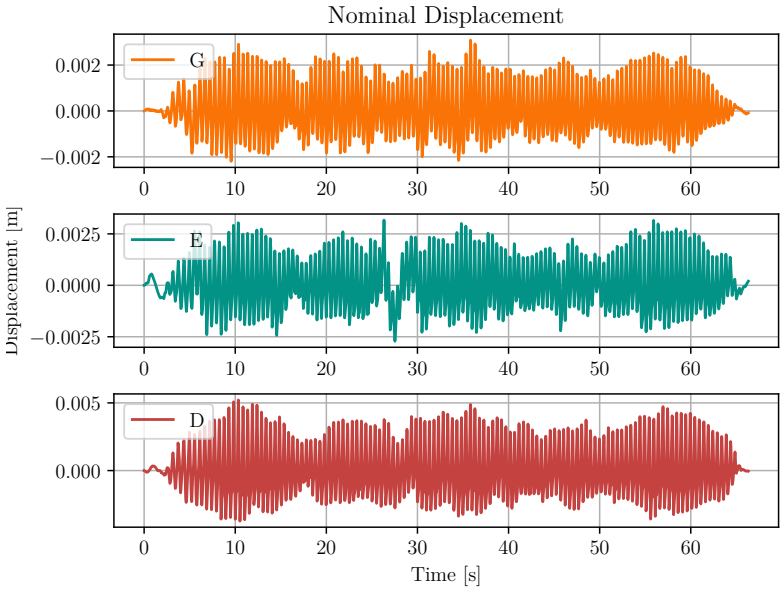


Figure B.21: Nominal Displacement from Pippi 1 vs Molde

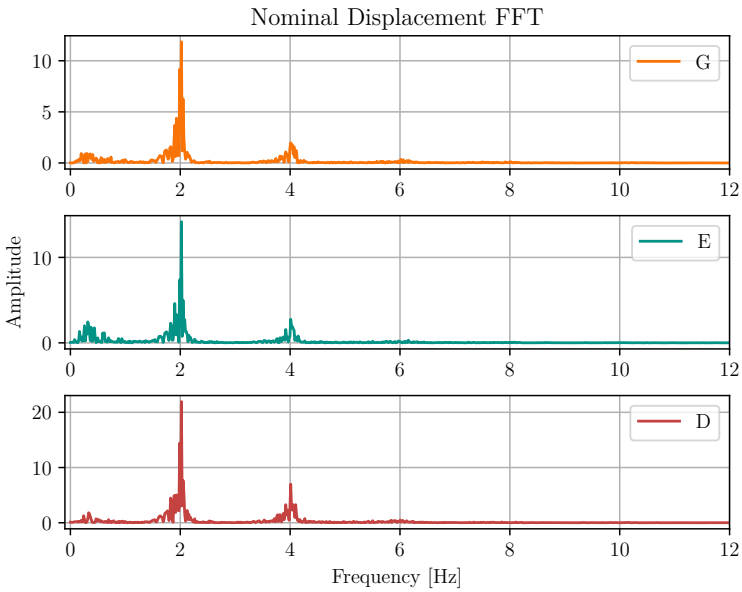


Figure B.22: FFT of Nominal Displacement from Pippi 1 vs Molde

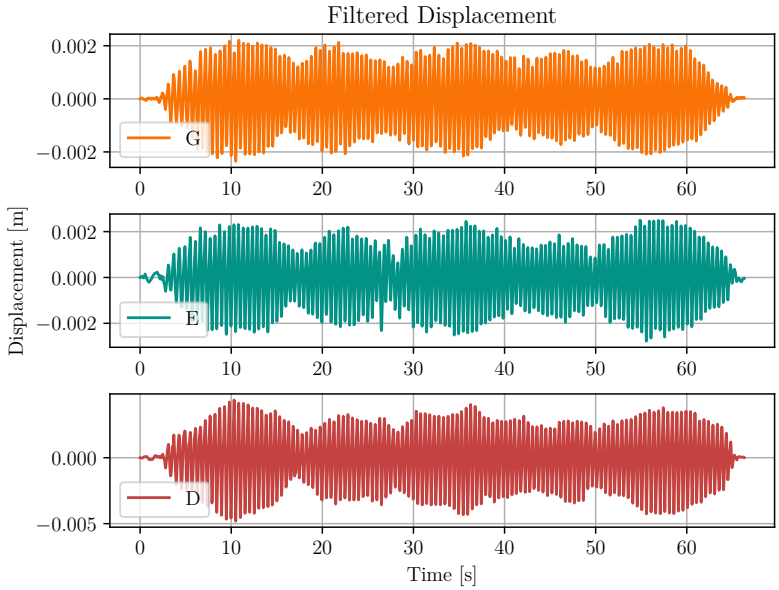


Figure B.23: Filtered Displacement from Pippi 1 vs Molde

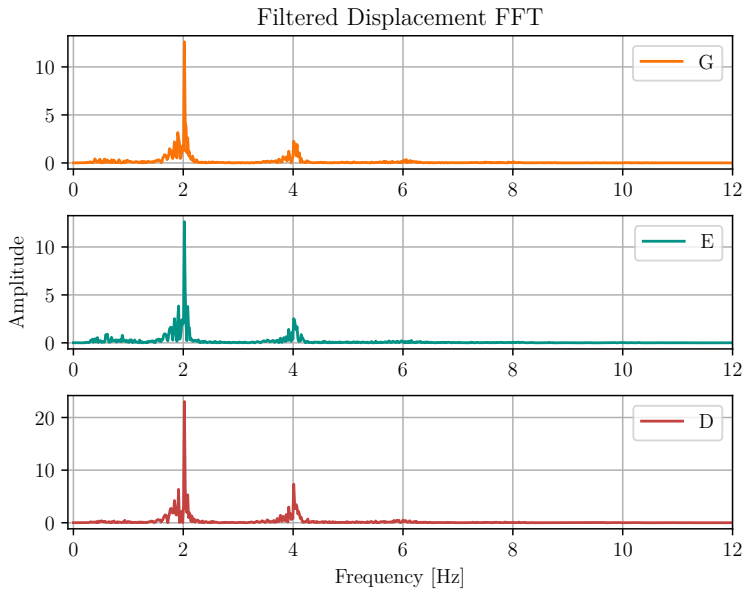


Figure B.24: FFT of Filtered Displacement from Pippi 1 vs Molde

## B.3 Molde 2

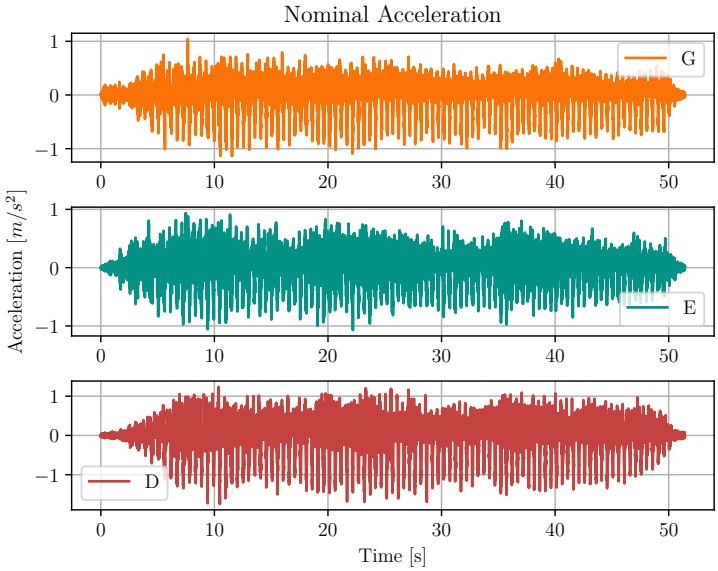


Figure B.25: Nominal Acceleration from Pippi 2 vs Molde

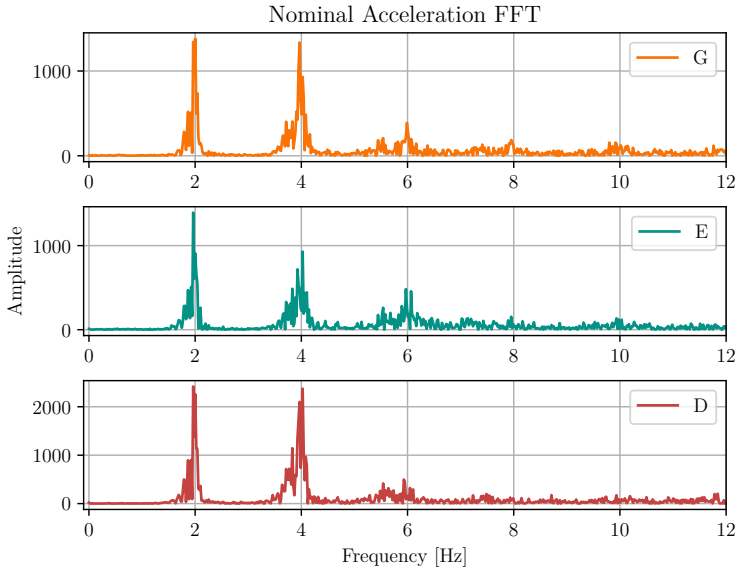


Figure B.26: FFT of Nominal Acceleration from Pippi 2 vs Molde

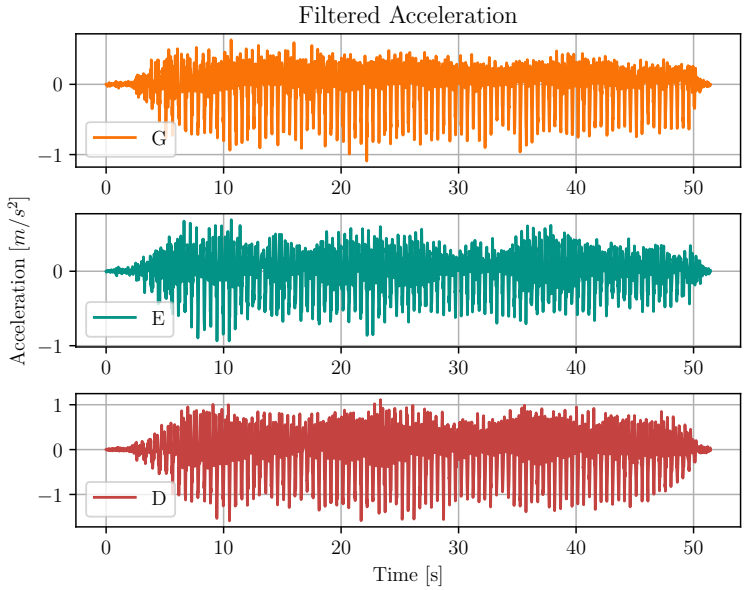


Figure B.27: Filtered Acceleration from Pippi 2 vs Molde

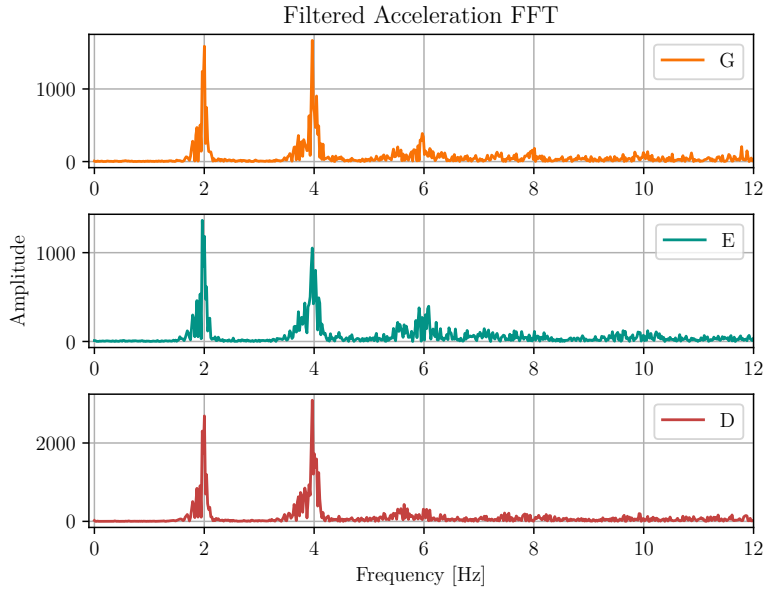


Figure B.28: FFT of Filtered Acceleration from Pippi 2 vs Molde

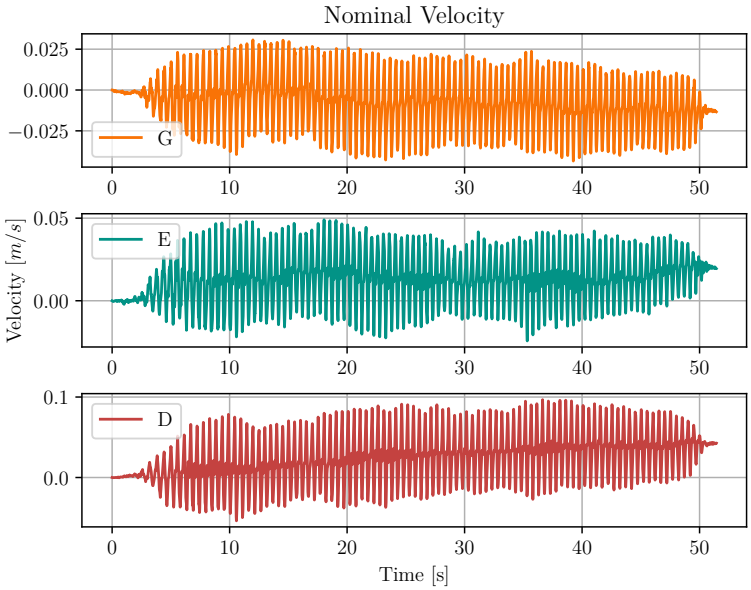


Figure B.29: Nominal Velocity from Pippi 2 vs Molde

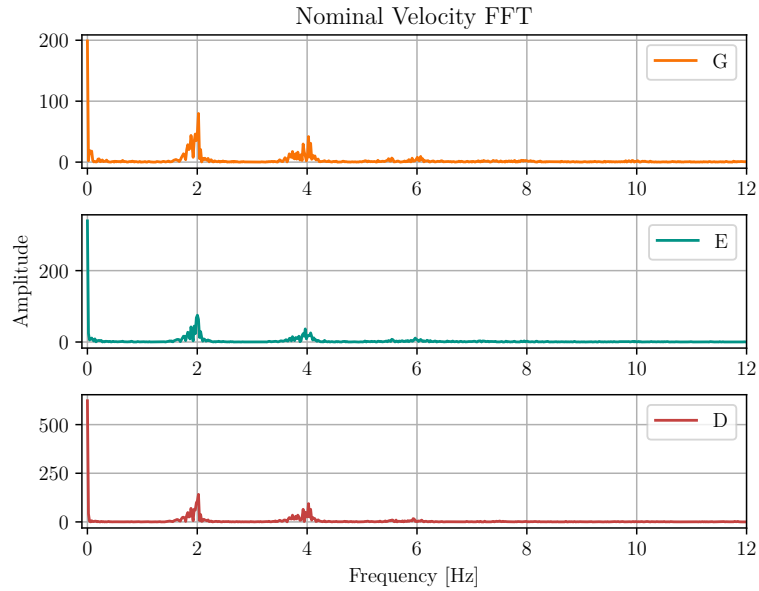


Figure B.30: FFT of Nominal Velocity from Pippi 2 vs Molde

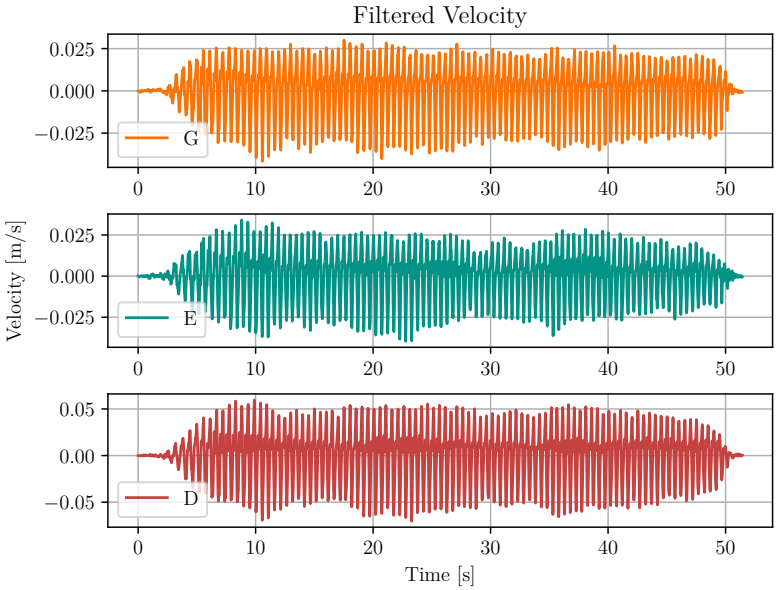


Figure B.31: Filtered Velocity from Pippi 2 vs Molde

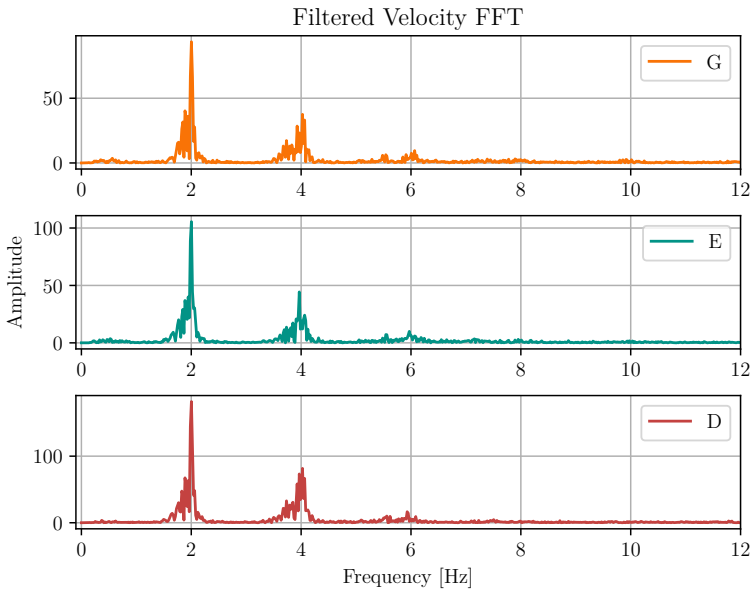


Figure B.32: FFT of Filtered Velocity from Pippi 2 vs Molde

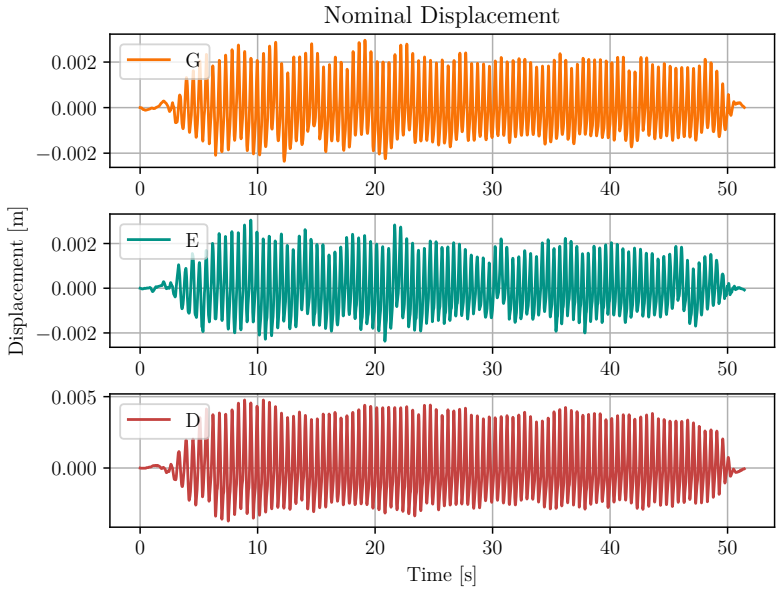


Figure B.33: Nominal Displacement from Pippi 2 vs Molde

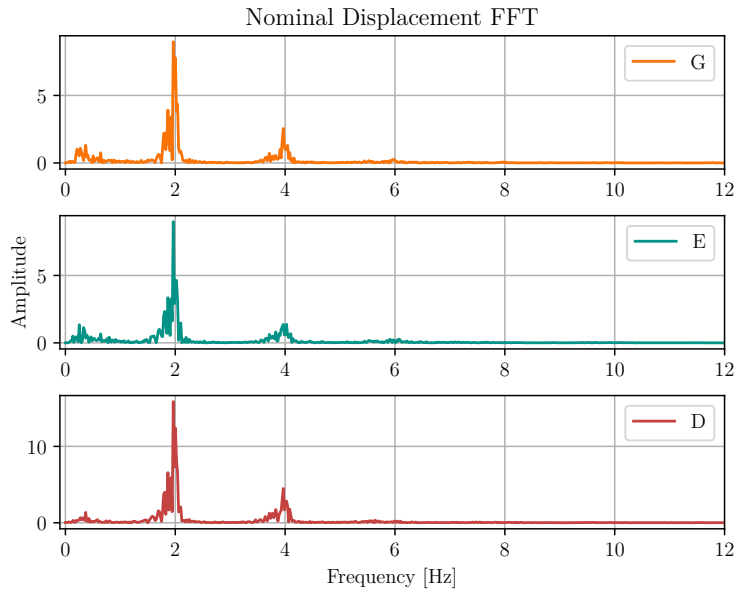


Figure B.34: FFT of Nominal Displacement from Pippi 2 vs Molde

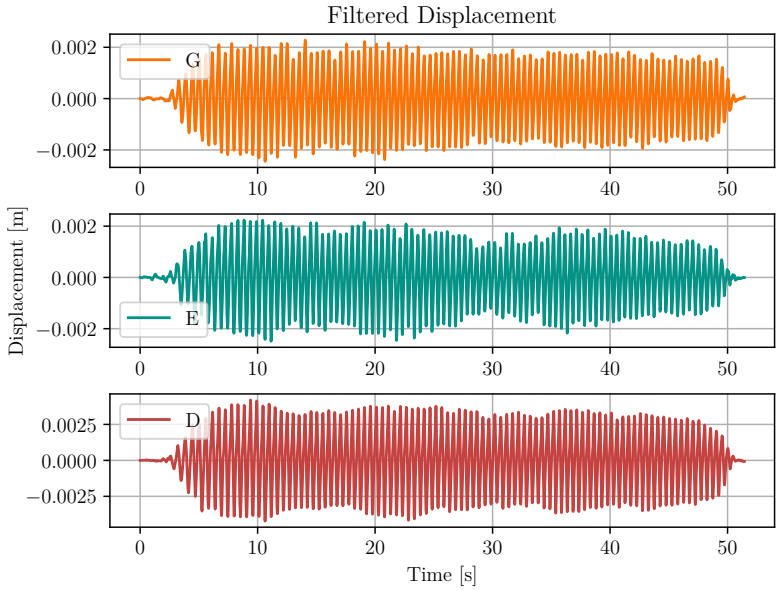


Figure B.35: Filtered Displacement from Pippi 2 vs Molde

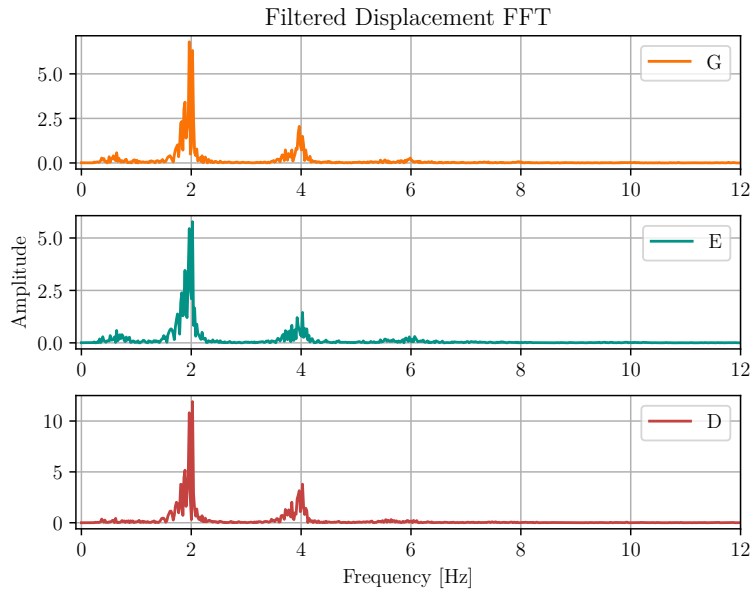


Figure B.36: FFT of Filtered Displacement from Pippi 2 vs Molde

## B.4 Molde 3

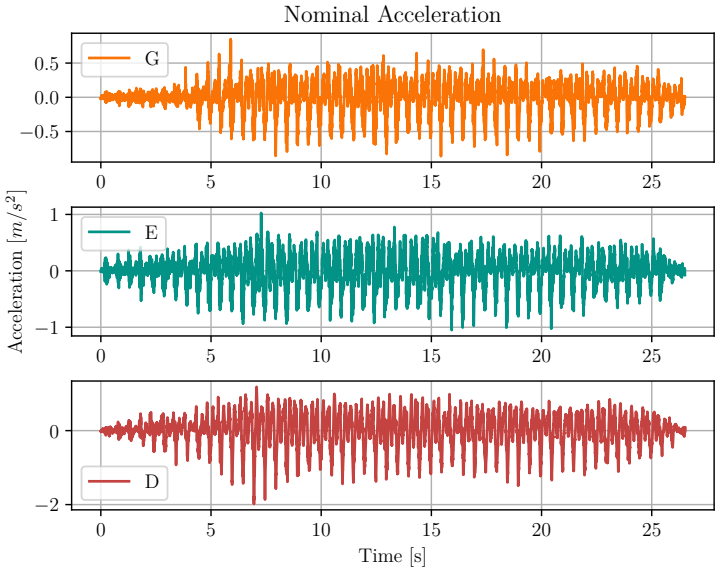


Figure B.37: Nominal Acceleration from Pippi 3 vs Molde

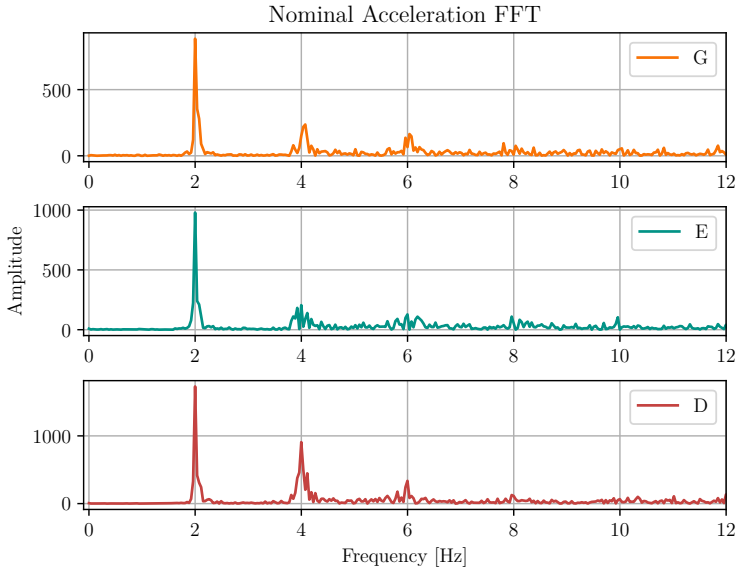


Figure B.38: FFT of Nominal Acceleration from Pippi 3 vs Molde

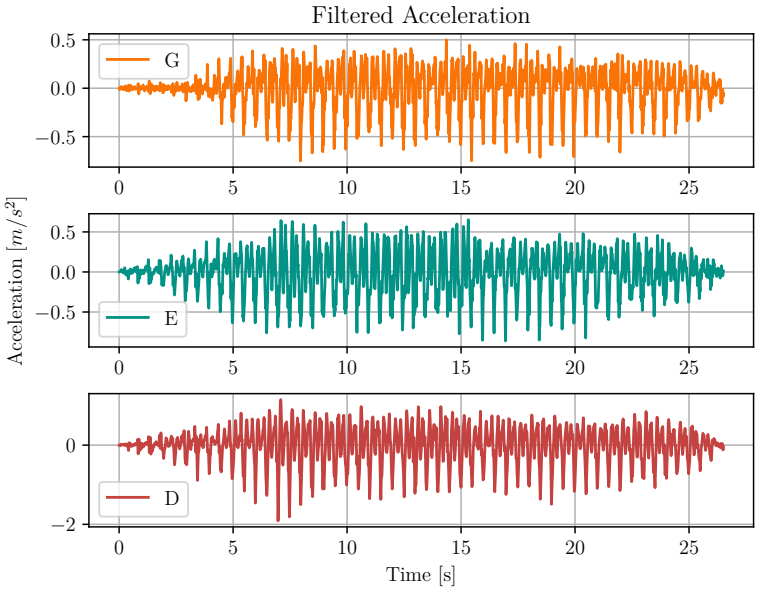


Figure B.39: Filtered Acceleration from Pippi 3 vs Molde

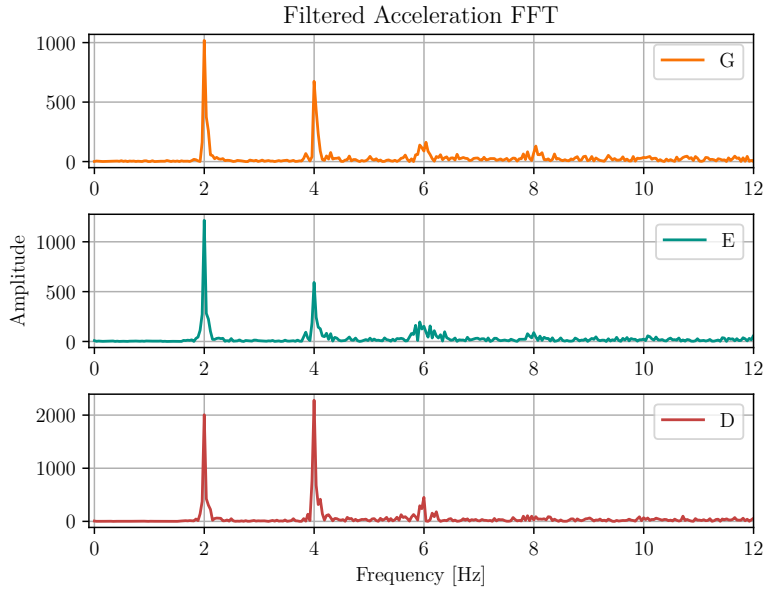


Figure B.40: FFT of Filtered Acceleration from Pippi 3 vs Molde

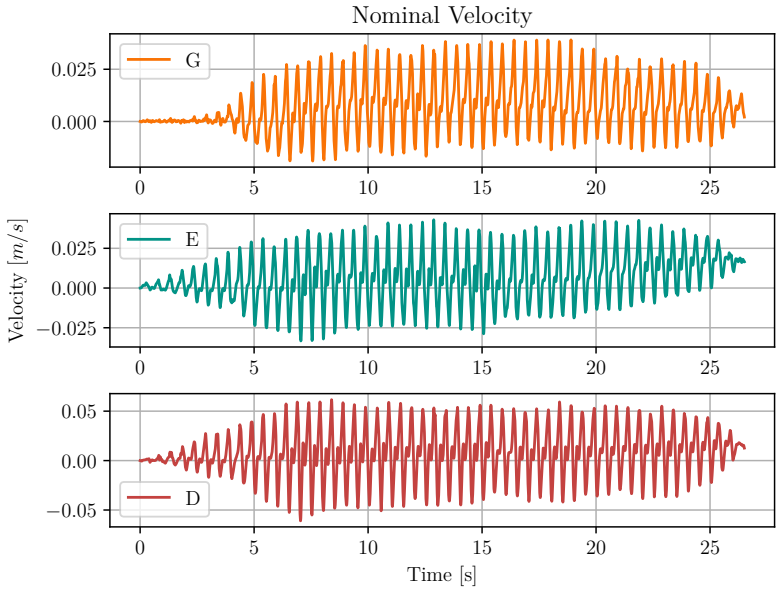


Figure B.41: Nominal Velocity from Pippi 3 vs Molde

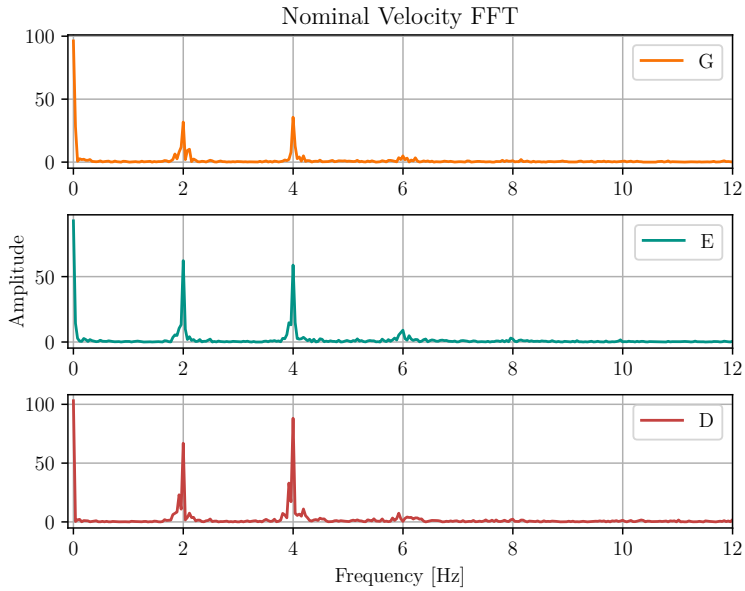


Figure B.42: FFT of Nominal Velocity from Pippi 3 vs Molde

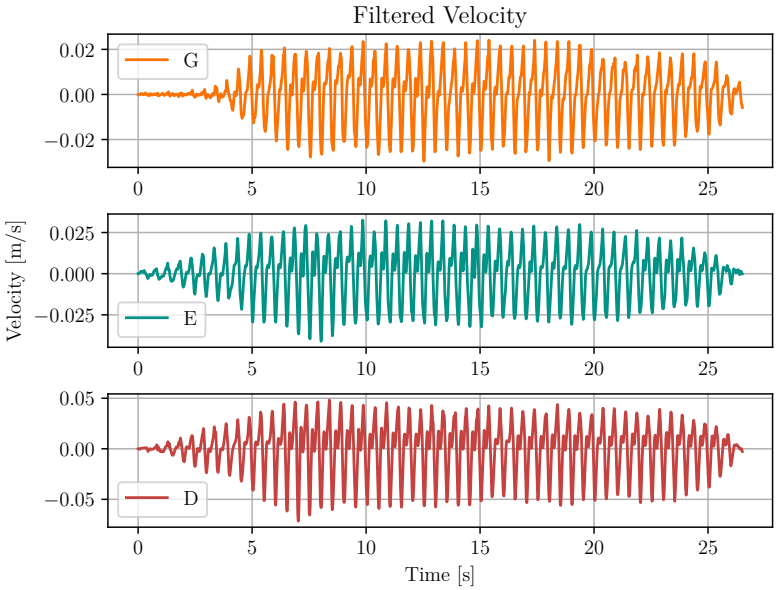


Figure B.43: Filtered Velocity from Pippi 3 vs Molde

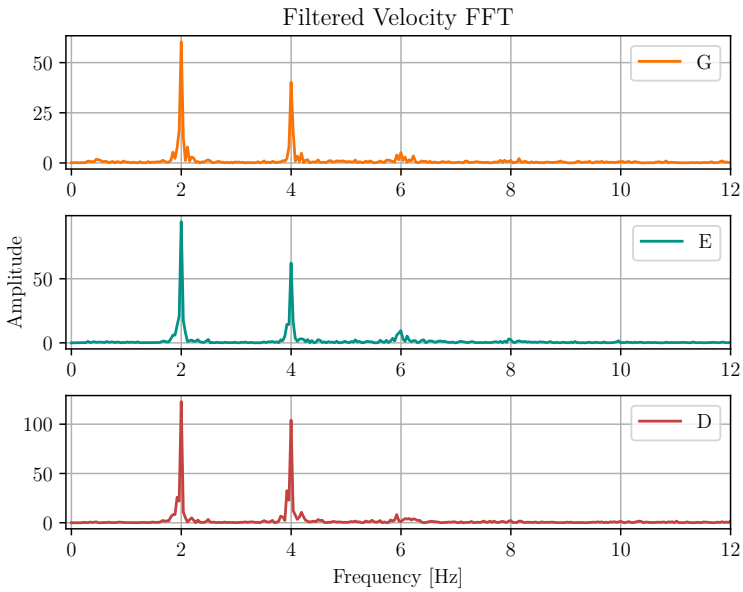


Figure B.44: FFT of Filtered Velocity from Pippi 3 vs Molde

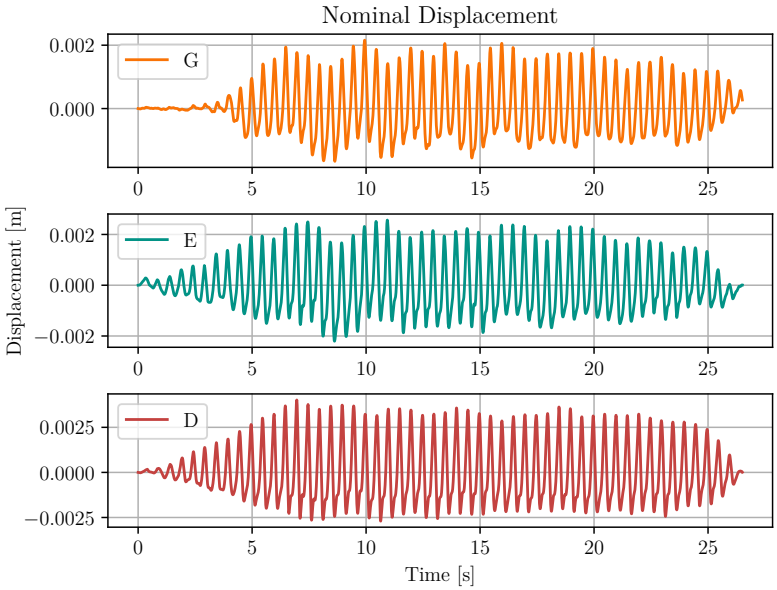


Figure B.45: Nominal Displacement from Pippi 3 vs Molde

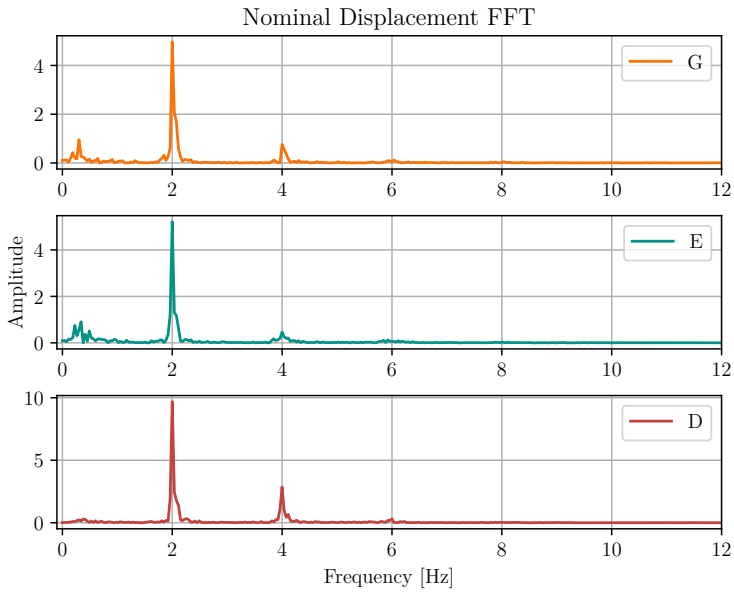


Figure B.46: FFT of Nominal Displacement from Pippi 3 vs Molde

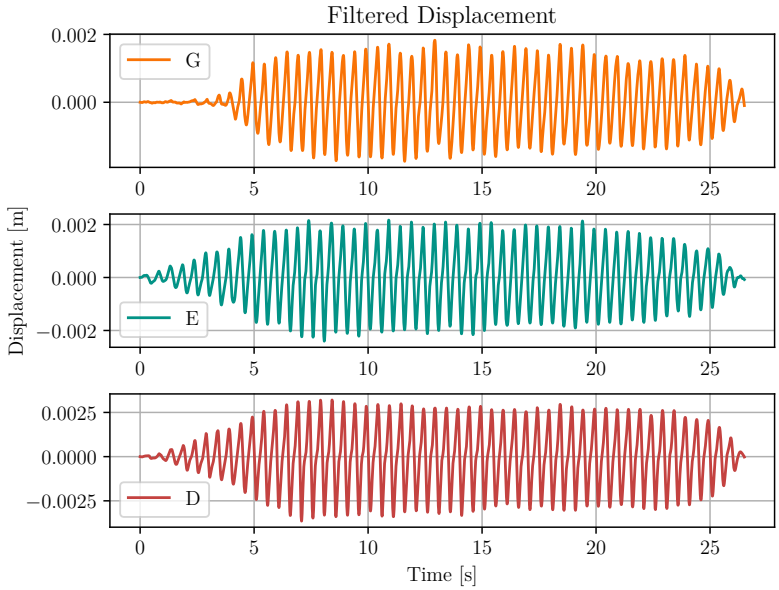


Figure B.47: Filtered Displacement from Pippi 3 vs Molde

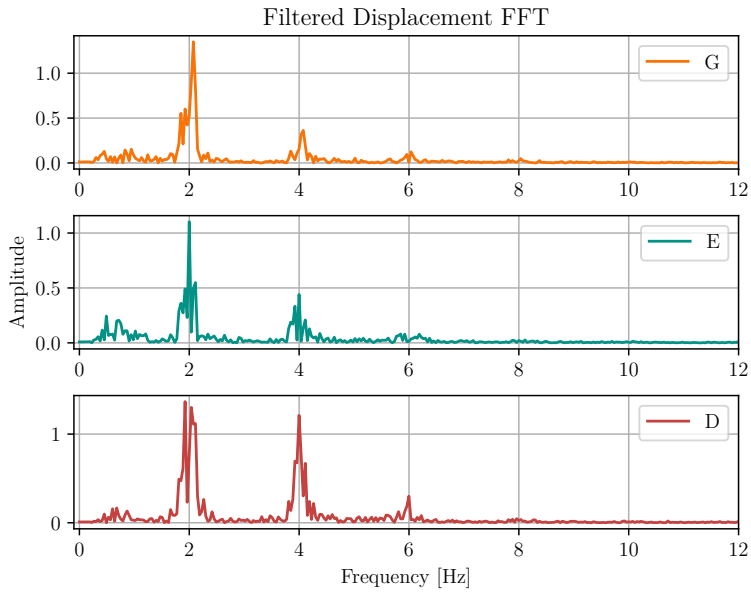


Figure B.48: FFT of Filtered Displacement from Pippi 3 vs Molde

## B.5 Ranheim

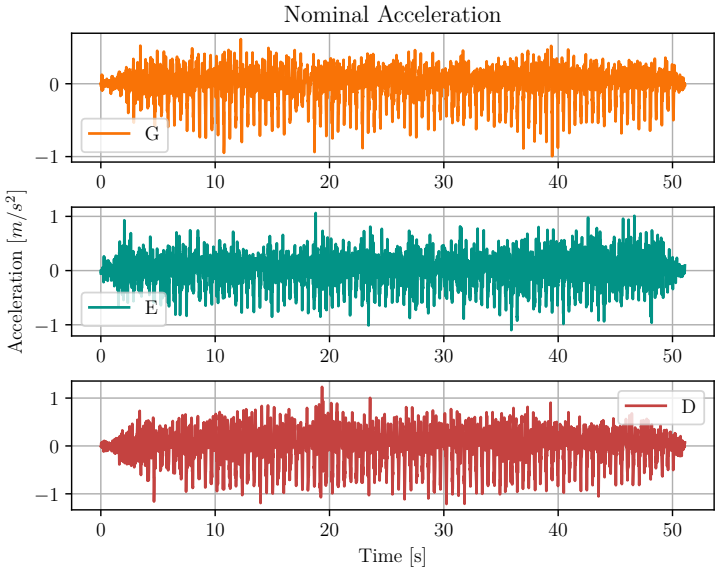


Figure B.49: Nominal Acceleration from Pippi vs Ranheim

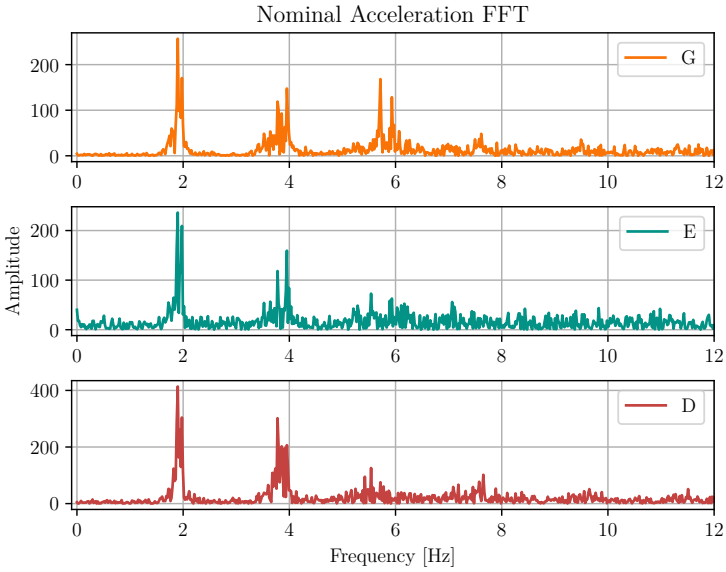


Figure B.50: FFT of Nominal Acceleration from Pippi vs Ranheim

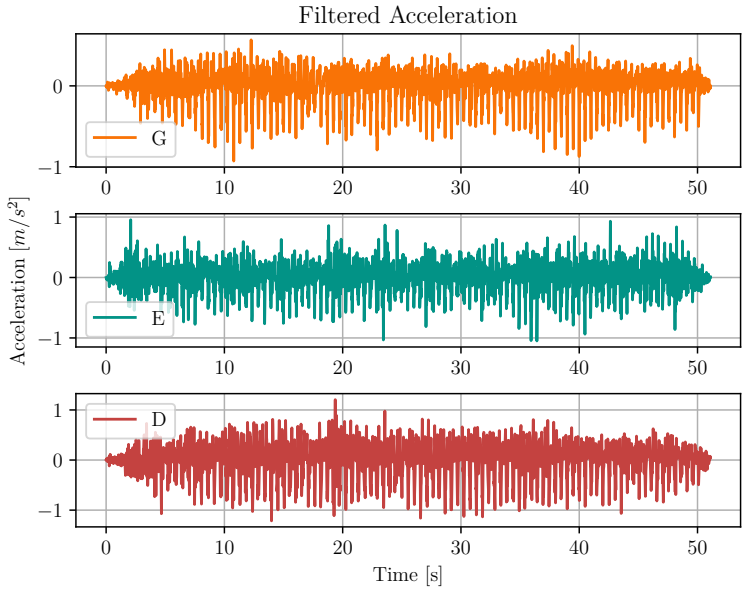


Figure B.51: Filtered Acceleration from Pippi vs Ranheim

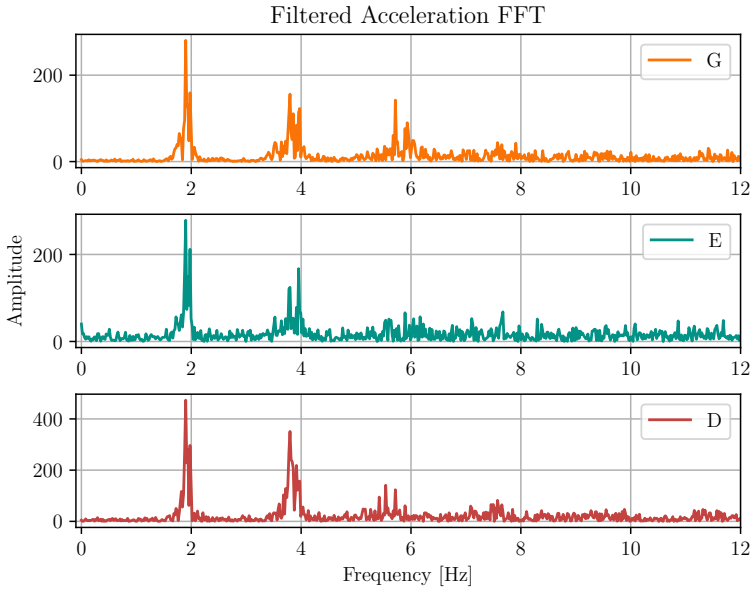


Figure B.52: FFT of Filtered Acceleration from Pippi vs Ranheim

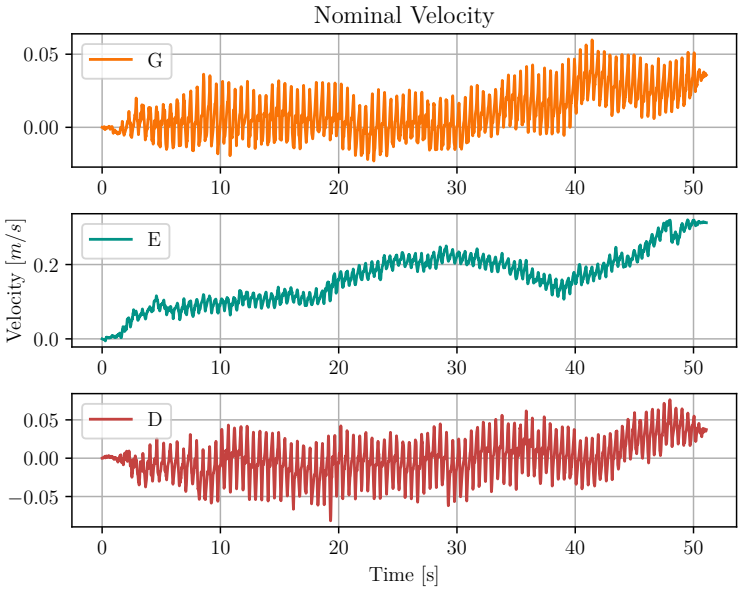


Figure B.53: Nominal Velocity from Pippi vs Ranheim

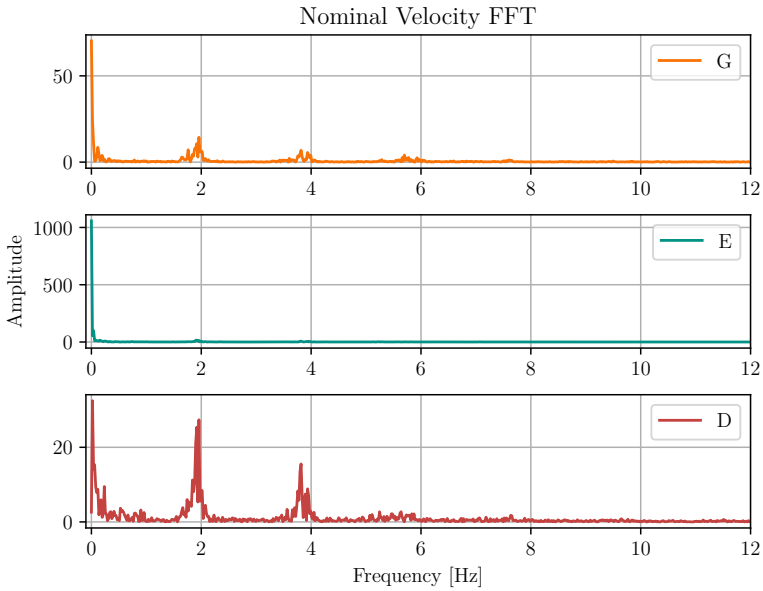


Figure B.54: FFT of Nominal Velocity from Pippi vs Ranheim

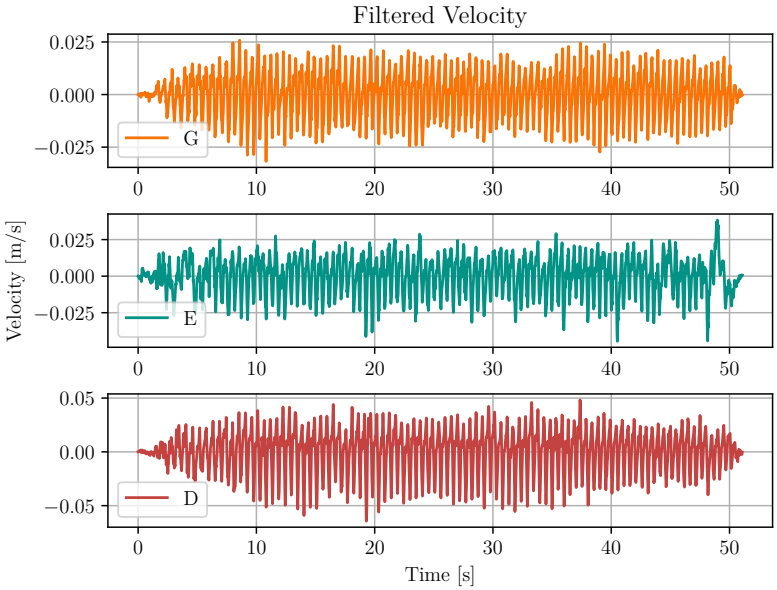


Figure B.55: Filtered Velocity from Pippi vs Ranheim

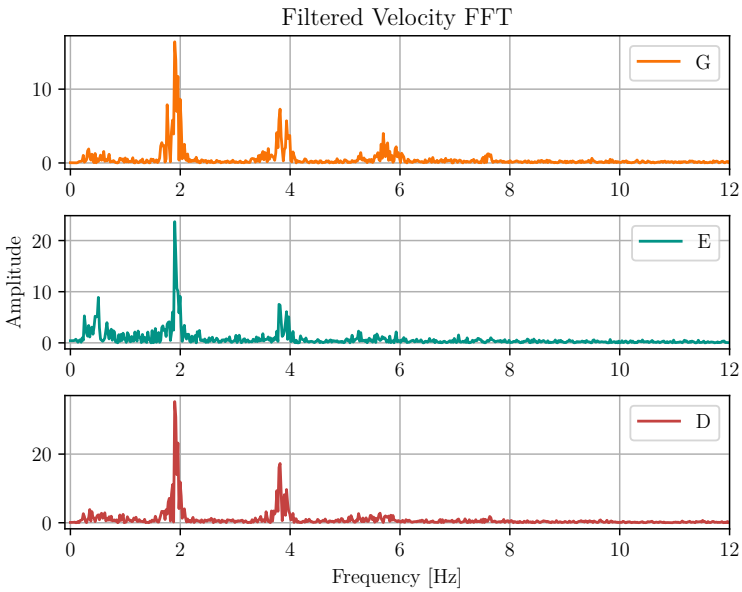


Figure B.56: FFT of Filtered Velocity from Pippi vs Ranheim

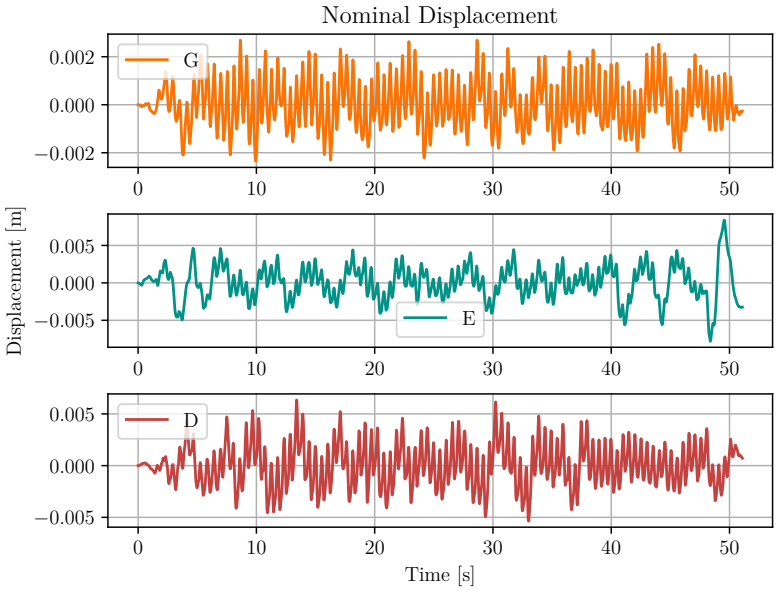


Figure B.57: Nominal Displacement from Pippi vs Ranheim

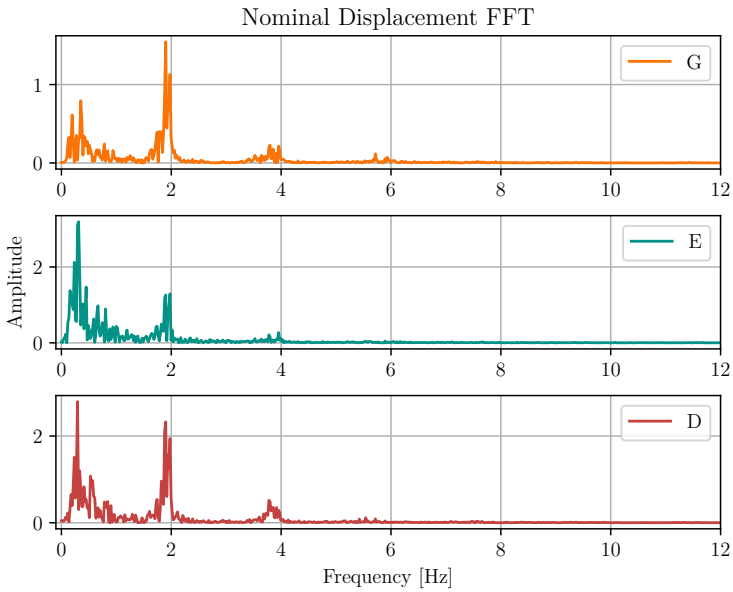


Figure B.58: FFT of Nominal Displacement from Pippi vs Ranheim

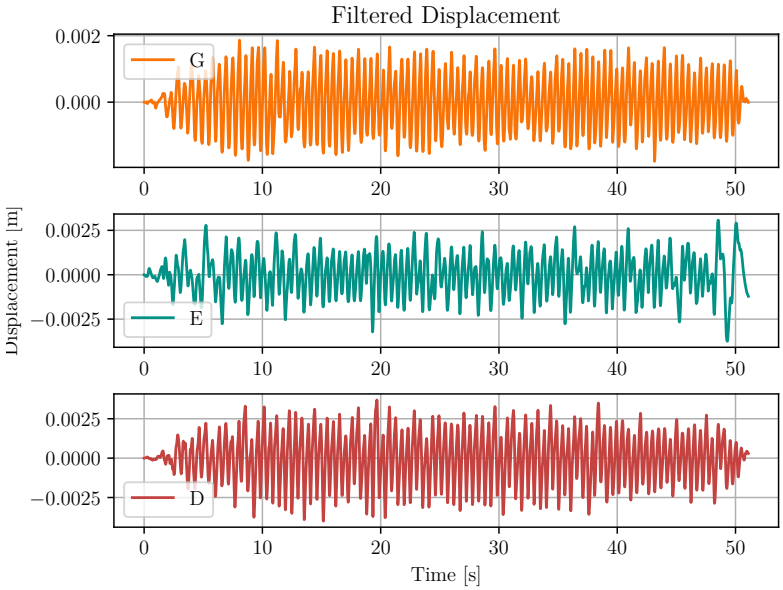


Figure B.59: Filtered Displacement from Pippi vs Ranheim

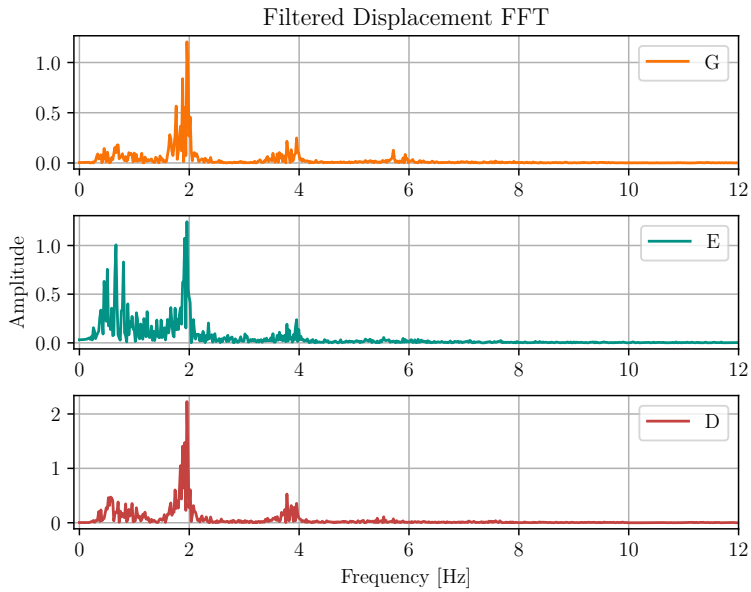


Figure B.60: FFT of Filtered Displacement from Pippi vs Ranheim

## B.6 Lillestrøm 1

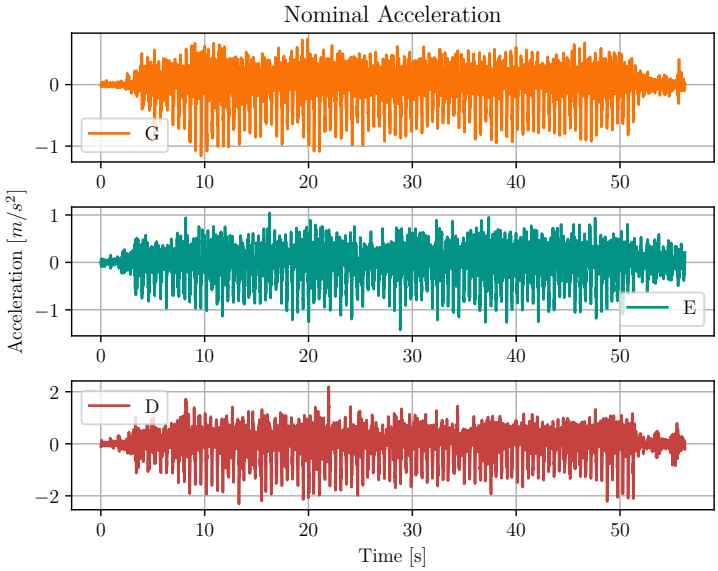


Figure B.61: Nominal Acceleration from Pippi 1 vs Lillestrom

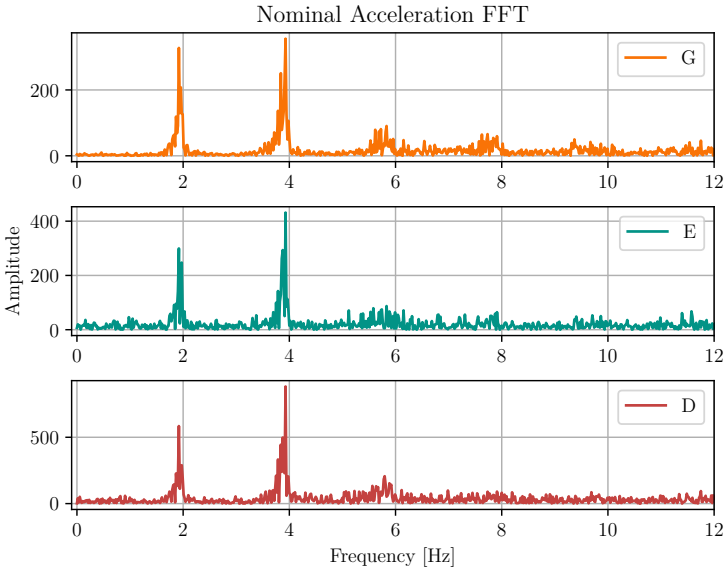


Figure B.62: FFT of Nominal Acceleration from Pippi 1 vs Lillestrom

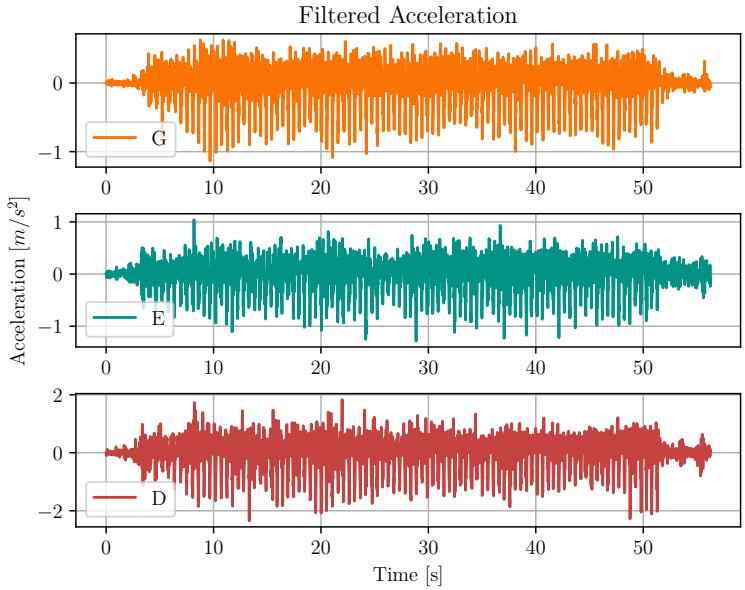


Figure B.63: Filtered Acceleration from Pippi 1 vs Lillestrom

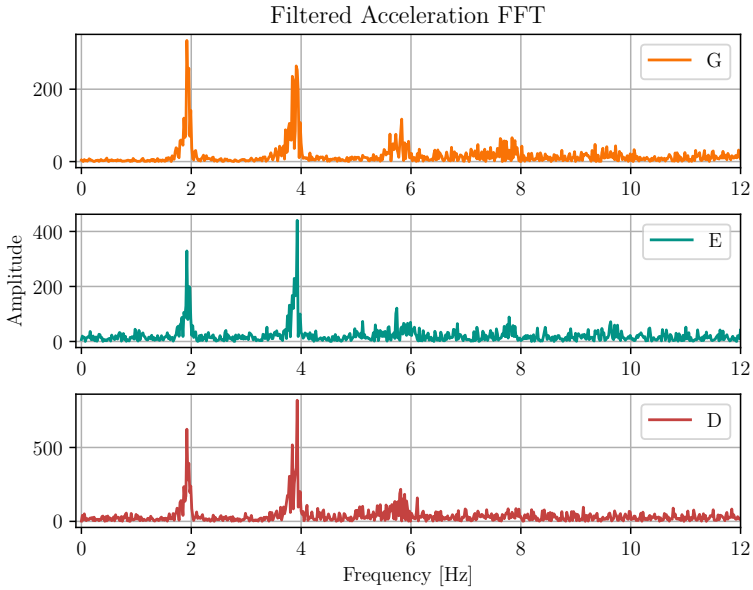


Figure B.64: FFT of Filtered Acceleration from Pippi 1 vs Lillestrom

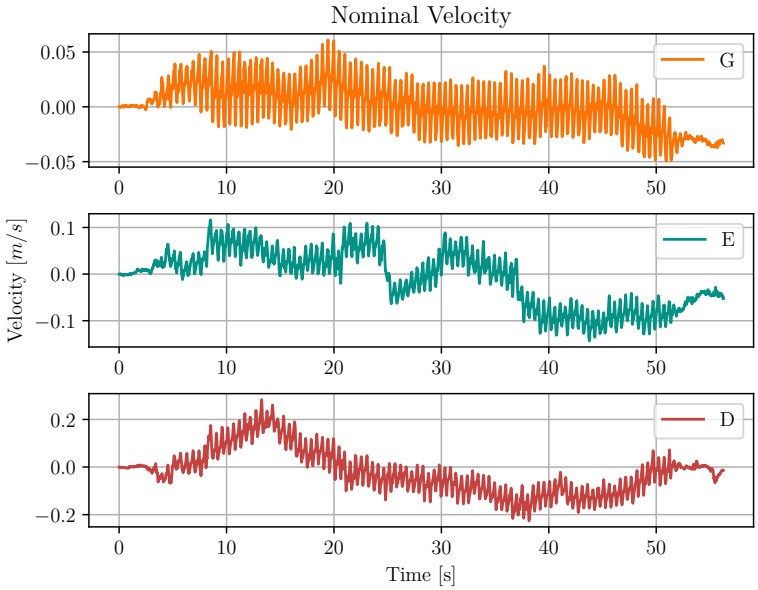


Figure B.65: Nominal Velocity from Pippi 1 vs Lillestrom

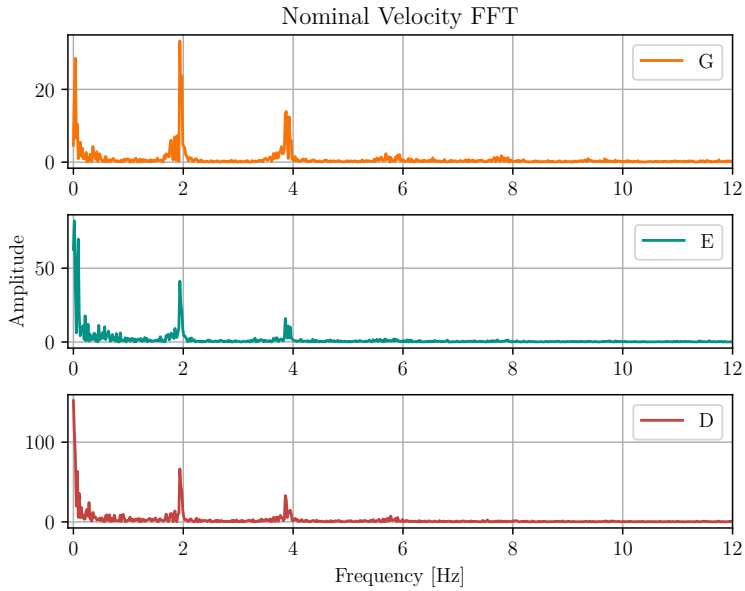


Figure B.66: FFT of Nominal Velocity from Pippi 1 vs Lillestrom

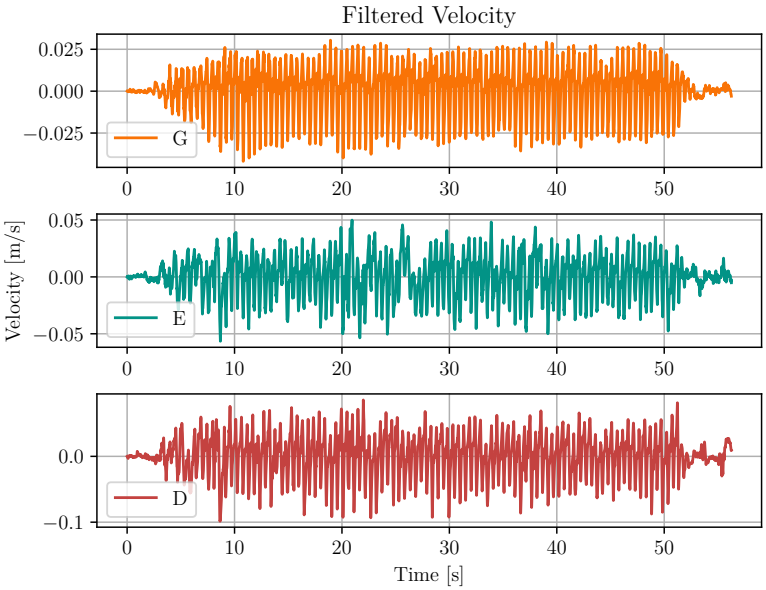


Figure B.67: Filtered Velocity from Pippi 1 vs Lillestrom

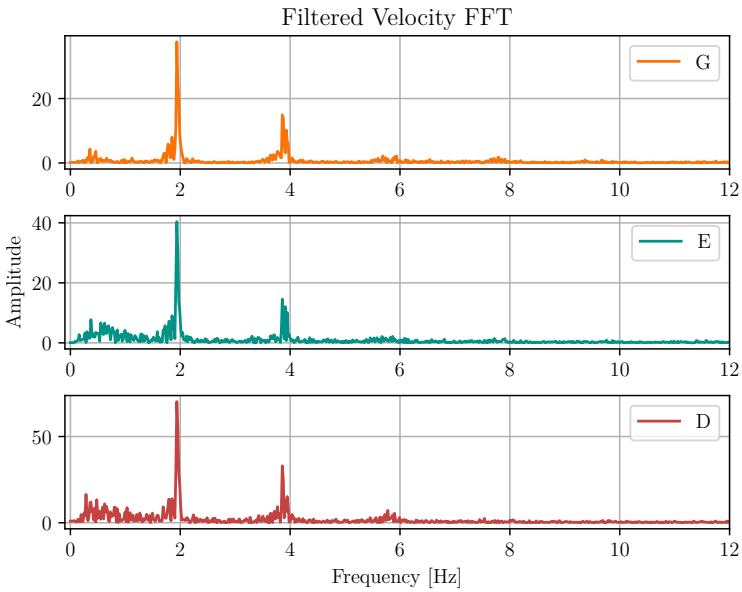


Figure B.68: FFT of Filtered Velocity from Pippi 1 vs Lillestrom

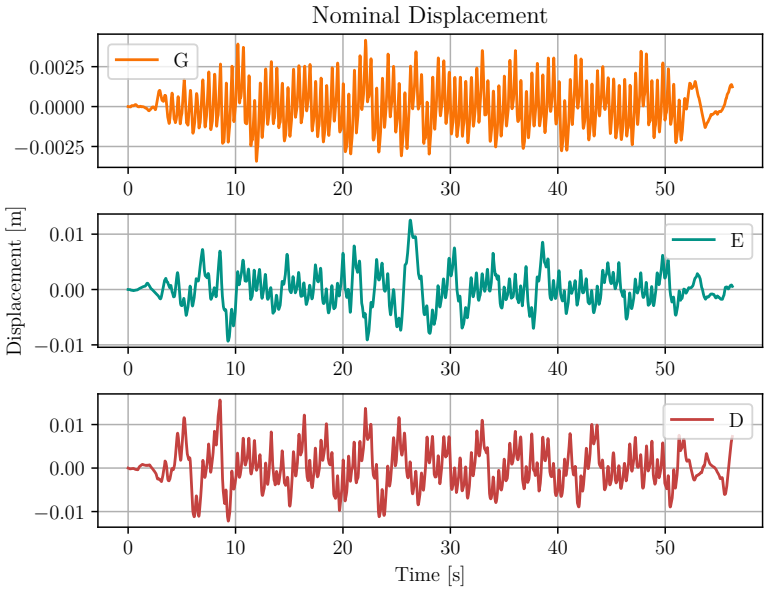


Figure B.69: Nominal Displacement from Pippi 1 vs Lillestrom

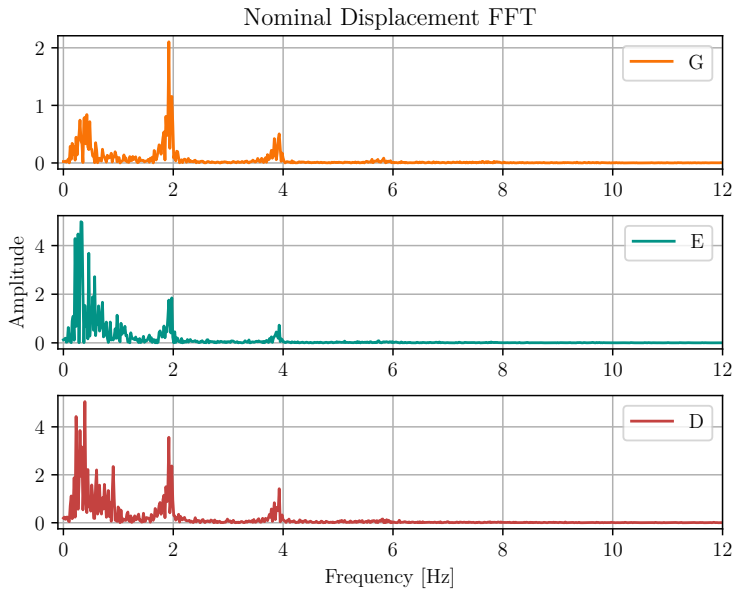


Figure B.70: FFT of Nominal Displacement from Pippi 1 vs Lillestrom

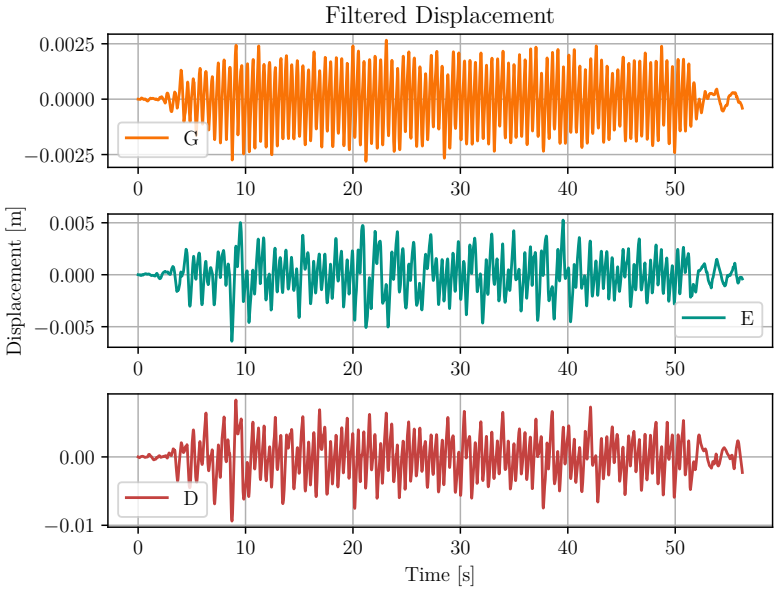


Figure B.71: Filtered Displacement from Pippi 1 vs Lillestrom

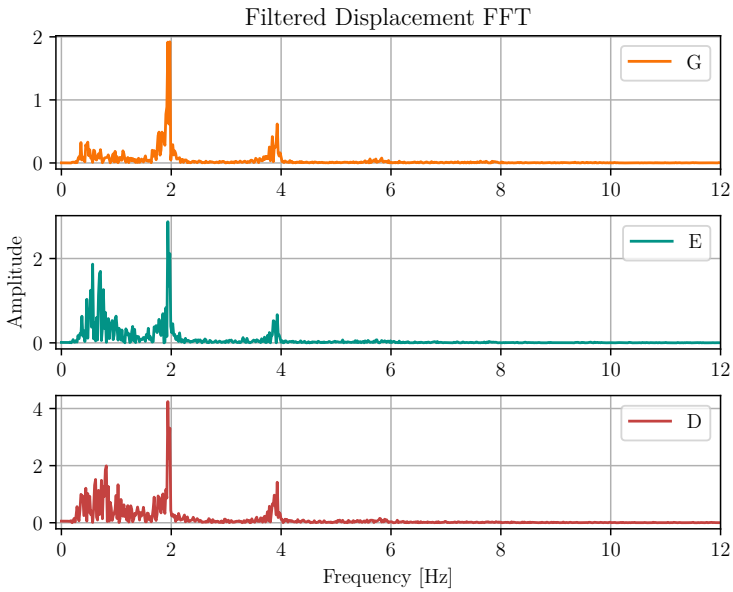


Figure B.72: FFT of Filtered Displacement from Pippi 1 vs Lillestrom

## B.7 Lillestrøm 2

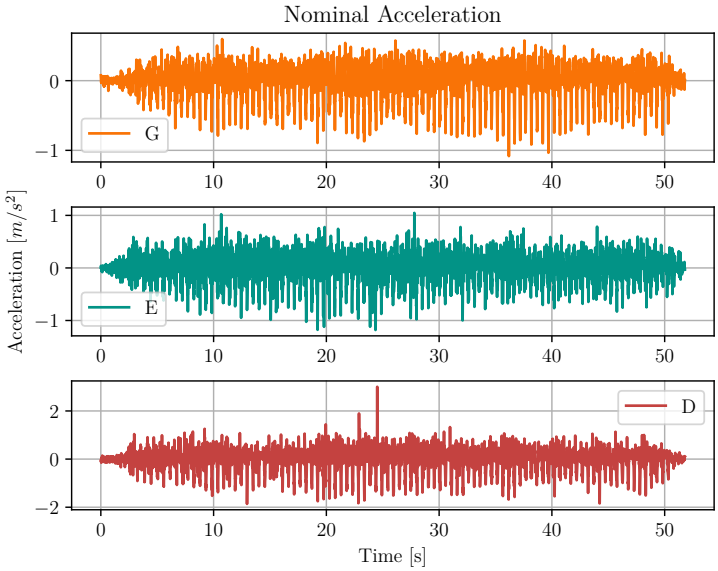


Figure B.73: Nominal Acceleration from Pippi 2 vs Lillestrom

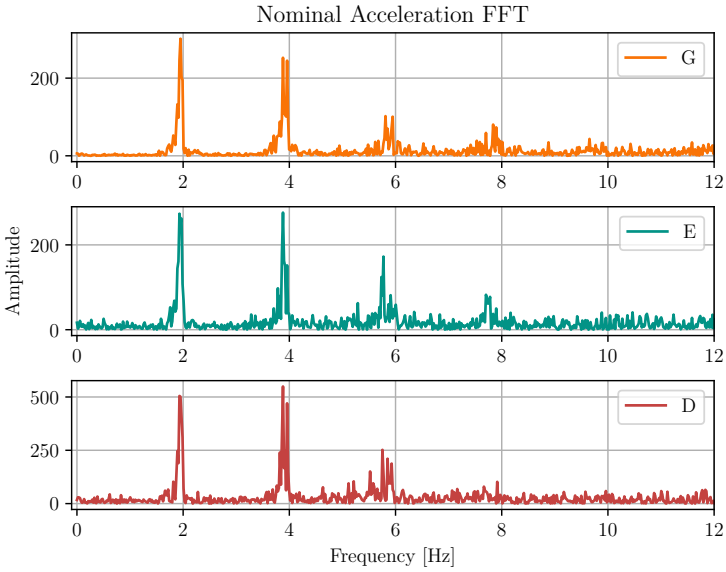


Figure B.74: FFT of Nominal Acceleration from Pippi 2 vs Lillestrom

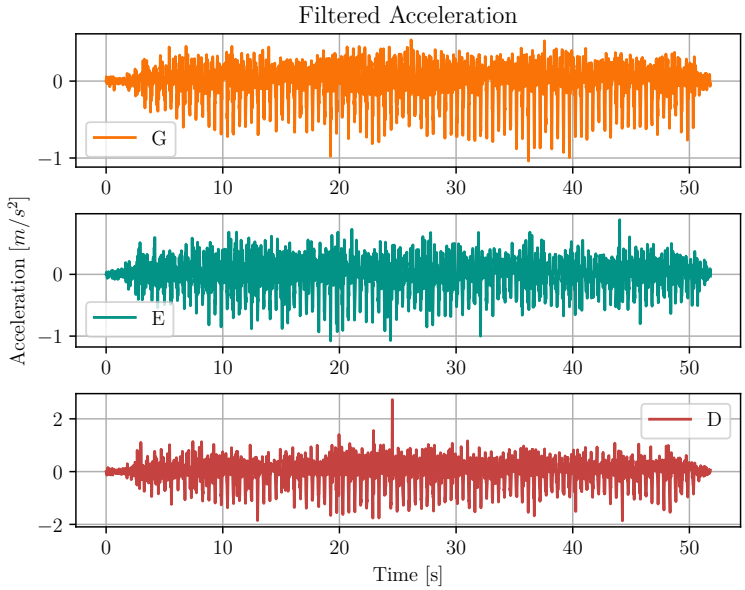


Figure B.75: Filtered Acceleration from Pippi 2 vs Lillestrom

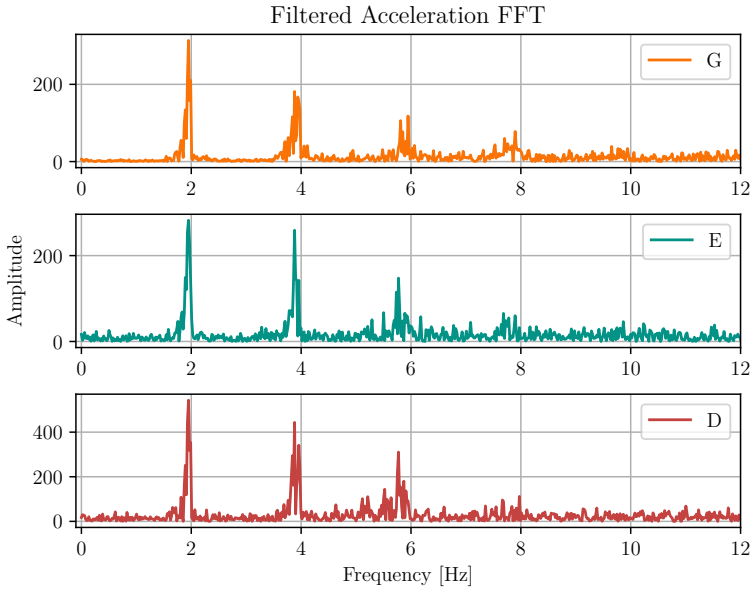


Figure B.76: FFT of Filtered Acceleration from Pippi 2 vs Lillestrom

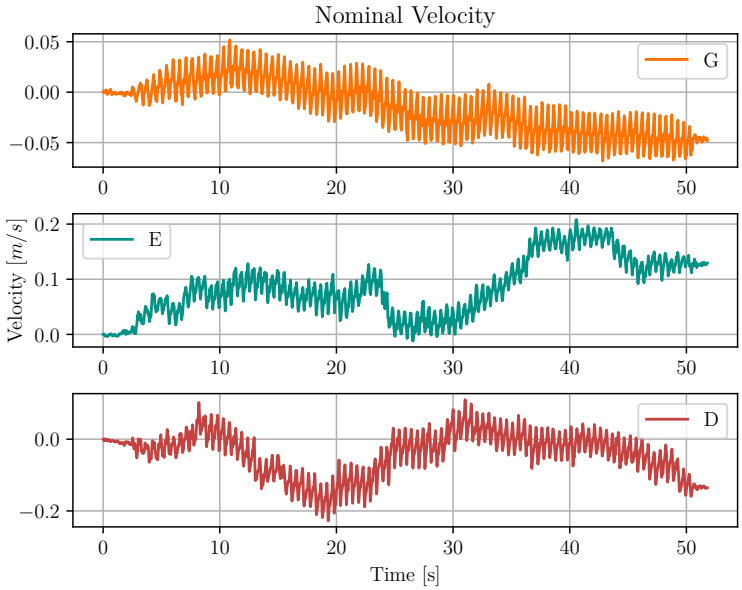


Figure B.77: Nominal Velocity from Pippi 2 vs Lillestrom

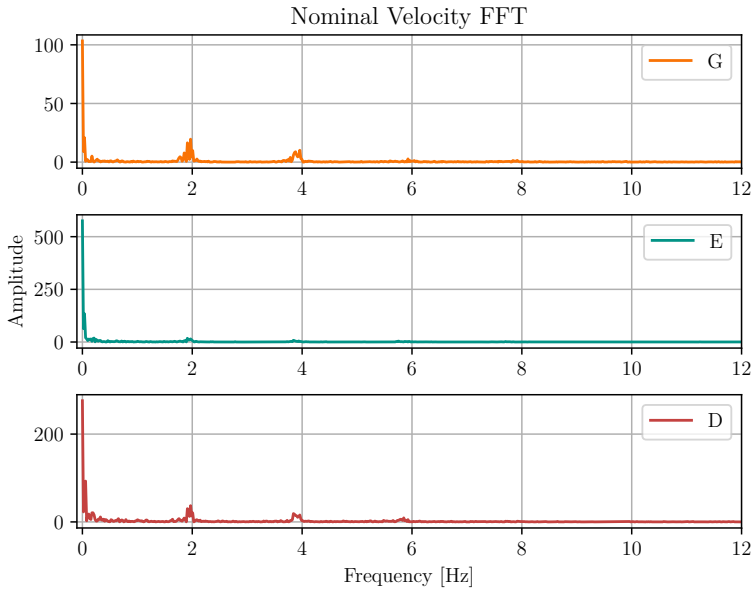


Figure B.78: FFT of Nominal Velocity from Pippi 2 vs Lillestrom

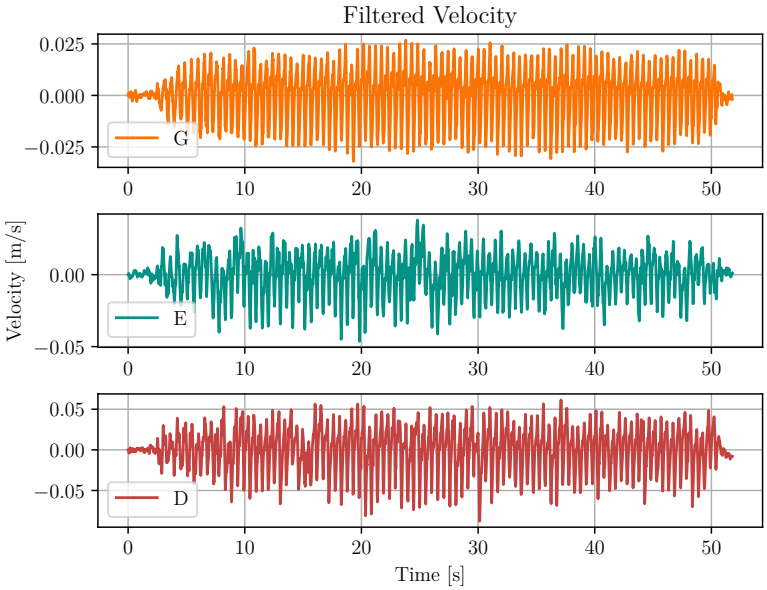


Figure B.79: Filtered Velocity from Pippi 2 vs Lillestrom

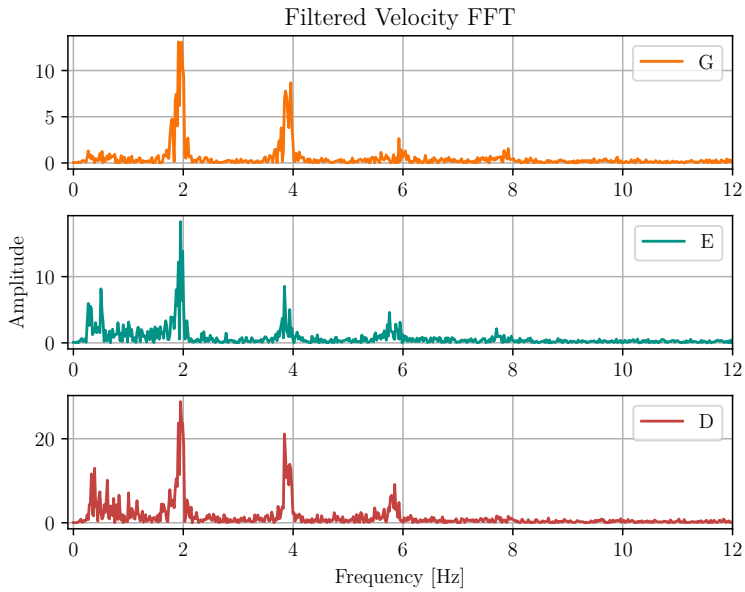


Figure B.80: FFT of Filtered Velocity from Pippi 2 vs Lillestrom

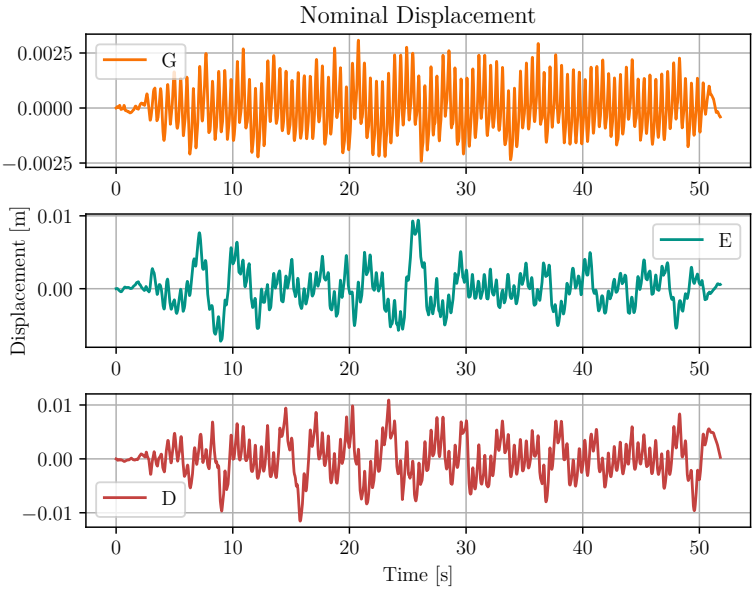


Figure B.81: Nominal Displacement from Pippi 2 vs Lillestrom

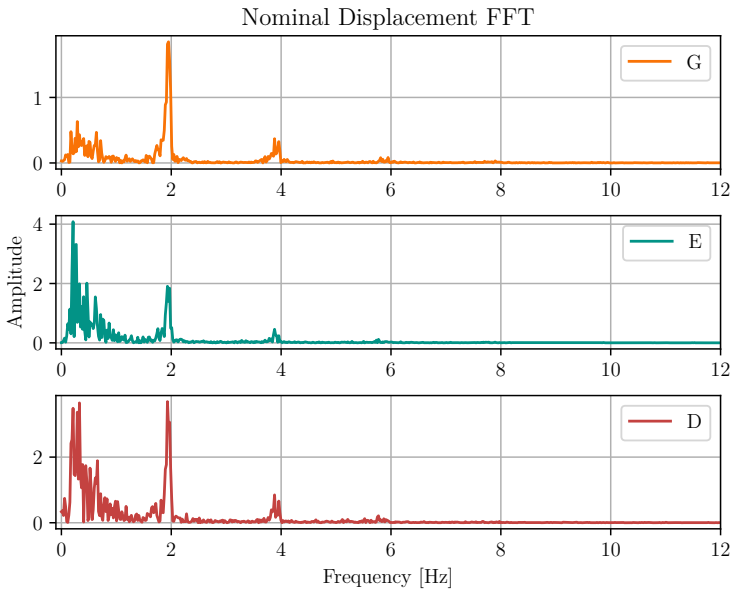


Figure B.82: FFT of Nominal Displacement from Pippi 2 vs Lillestrom

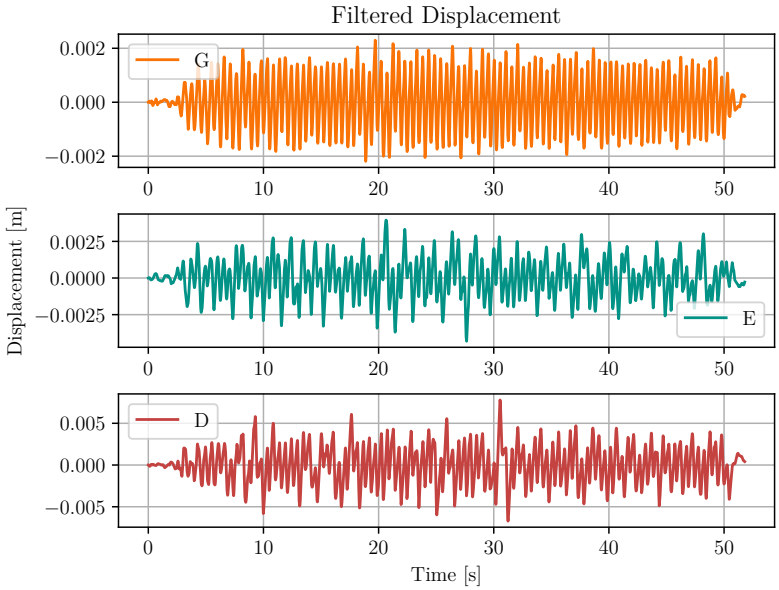


Figure B.83: Filtered Displacement from Pippi 2 vs Lillestrom

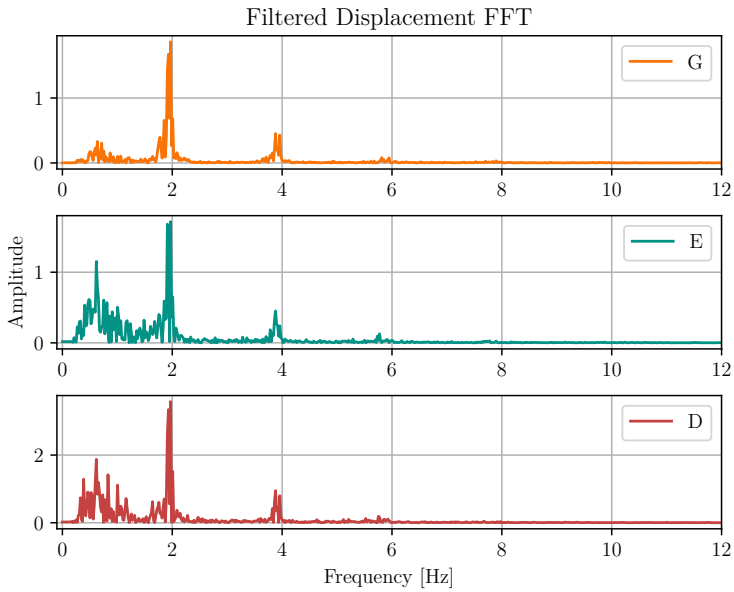


Figure B.84: FFT of Filtered Displacement from Pippi 2 vs Lillestrom

# Appendix C

# Reinertsen Reports

REINERTSEN
ENGINEERING

# SVINGEANALYSER AV TRIBUNEELEMENTER TRIBUNE C, LERKENDAL STADION

*Trondheim 24.01.2001*


Utførende

Anja Estensen

Anja Estensen

Kontroll

Tore Søreide

Tore Søreide

# Innholdsliste

## Innledning

Dokumentet inneholder svingeanalyser av tribuneelementer i tribune C på Lerkendal Stadion. De analyserte tribuneelementene omfatter sitteelementer samt 6 tribune-bjelker. Statiske beregninger av tribuneelementene er ivaretatt av Spenncon.

Tribuneelementene skal utformes slik at de får en egenfrekvens som gjør at en unngår merkbare svingninger av elementene. For å unngå merkbare svingninger er det satt et krav om en egenfrekvens på minimum 6 Hz, og helst over 7 Hz. Tribuneelementene analyseres for å kontrollere at de oppfyller kravet til egenfrekvensen.

Tegninger og beregningsgrunnlag er mottatt fra Spenncon.

## Beregninger

Sitteelementene er modellert og analysert i SOLVIA, vedlegg A.

Tribunebjelkene er modellert og analysert i StaadPro, vedlegg B-G. Bjelkemodellene som er benyttet i StaadPro-analysene er bygd opp av bjelkeelementer. Opplagerbetingelser samt bjelkegeometri i de ulike analysene er vist i vedlegg B-G.

Egenfrekvensanalysene er utført i bruksgrensetilstand. Tribuneelementene er påført egenlast med lastfaktor 1,0. Egenlasten til sitteelementene på øvre-, nedre-, og VIP-tribunen er beregnet i vedlegg H. I analysene er det i tillegg lagt til 2,5 kN/m for å ivareta egenvekten av seter og andre permanente innretninger. Bjelkenes egenvekt er selvgenerert i StaadPro.

I beregningene er det antatt urisset betongtversnitt, og følgelig er bjelkenes stivhet beregnet på grunnlag av hele bjelketverrsnittet.

Analysene er utført som en iterasjonsprosess, der de tribunebjelkene som ikke tilfredsstiller kravet til egenfrekvensen endres og forsterkes for å oppnå ønskelig egenfrekvens.

## Resultater

Tabell 1 viser egenfrekvensene for de analyserte tribuneelementene. Analysene er vist i vedlegg A-G. Tabellen viser at alle tribuneelementene har egenfrekvenser på over 6 Hz. For å oppnå dette ble geometrien til hovedtribunebjelken endret i forhold til opprinnelig geometri.

**Tabell 1. Egenfrekvens tribuneelementer.**

| Tribuneelement | Vedlegg | Egenfrekvens [Hz] |
|---|---|---|
| Sitteelement hovedtribune | *A* | *9,00* |
| Hovedtribunebjelke | *B* | *6,96* |
| Hovedtribunebjelke med utsparing | *C* | *7,06* |
| VIP – bjelke | *D* | *6,96* |
| Nedre tribuneplan, bjelke 1 | *E* | *7,95* |
| Nedre tribuneplan, bjelke 2 | *F* | *7,25* |
| Nedre tribuneplan, bjelke 3 | *G* | *6,23* |

Med sin opprinnelige geometri fikk hovedtribunebjelken en egenfrekvens på 3,5 Hz ved analyser i StaadPro. Bjelken ble også analysert i SOLVIA, noe som gav en egenfrekvens på 3,39 Hz. Følgelig er det bra samsvar mellom SOLVIA-, og StaadPro-analysene.

## Konklusjon

Dersom tribuneelementene blir utført slik som vedlegg A-G viser, vil kravet til egenfrekvensene bli tilfredsstilt, og følgelig vil en unngå merkbare svingninger av elementene.

Hovedtribunebjelken hadde i sin opprinnelige utforming en egenfrekvens på 3,39 Hz. Følgelig er bjelken endret og forsterket betraktelig for å oppnå en egenfrekvens på over 6 Hz. VIP-bjelken, bjelkene på nedre tribuneplan, samt sitteelementene, er det ikke funnet nødvendig å endre utforming på.

# Lerkendal Stadion
# Kontroll av svingninger

| REV. | DATO | BESKRIVELSE | Laget | Sjekket | Godkj. | | |
|---|---|---|---|---|---|---|---|
| | | | LEVERANDØR | | | SELSKAP | |
| 02 | 21.05.2009 | Til oppdragsgiver | VH | THS | THS | | |
| 01 | 27.04.2009 | Internkontroll | TB | THS | VH | | |

DOKUMENT TITTEL

Lerkendal Stadion, kontroll av svingninger

REINERTSEN ENGINEERING

DOKUMENT NUMMER

**2710184-01**

| Kontrakt Nr.: | KTR Nr.: | DFO | Prosjekt Nr. | Sekv.Nr. | Rev. |
|---|---|---|---|---|---|
| 2710184 | | | **2710184** | | **02** |

# INNHOLDSLISTE

SIDE

# 1 SAMMENDRAG


Etter henvendelse fra Rosenborg BallKlubb vedr vibrasjoner i øvre plan av tribune D har Reinertsen utført supplerende målinger og beregninger. Vibrasjonene har fremkommet ved at supporterklubben "Kjernen" er flyttet fra nedre nivå på tribune C til øvre nivå på tribune D hvor det tidligere var sitteplasser. Vibrasjonene henger sammen med utkragingen av øvre nivå over VIP-tribune, en utkragning på 3.5 m, og den nedbøyning man her får på tuppen.

Konklusjonen fra gjennomgangen som er foretatt er at nedbøyningene som er registrert er så små at de ikke utgjør noen sikkerhetsrisiko, dvs at påkjenningen i dragerne ligger godt under bruddkapasitet. Men målingene viser vibrasjoner som er klart merkbare, i størrelsesorden 16mm/s.

Anbefalingen er derfor at man ikke trenger sette i gang videre tiltak, dersom det ikke skulle komme henvendelser om at publikum føler ubehag.

Av tiltak man da kan vurdere er:

- Redusert dynamisk belastning. Ikke tilgang for Kjernen på ytterste rad.
- Avstaging av utkrager. Stålstag ned på VIP-tribune, skrått inn mot glassfasade. Rømningsvei i fm brann må da utredes. Tiltaket må prosjekteres.

Vårt firma står til rådighet for videre kontakt fremover.

# 2 INNLEDNING

Reinertsen (RE) ved Tore Søreide ble den 17.03.2009 kontaktet av banemester Arne Lorentsen i Rosenborg BallKlubb (RBK) vedr vibrasjoner i tribune D under kampen mot Vålerenga den 15.03.2009. Vibrasjonene, som kunne føles på øvre tribuneplan, oppstod i forbindelse med at supporterklubben Kjernen var flyttet fra nedre nivå på tribune C til øvre nivå på tribune D. Maksimalt omfatter dette ca 3000 personer som delvis under kampene utfører taktfast bevegelse. Så lenge tribunen var benyttet som ordinær sittetribune var det ikke rapportert noen merkbar bevegelse.

Etter avtale med Arne Lorentsen dro Tore Søreide og Viggo Henriksen fra RE opp på Lerkendal den 18.03.2009 for nærmere å få innsyn i det som var opplevd under kampen, se mail av 18.03.2009 i vedlegg A. I denne mailen er også redegjort for mulige årsaker til vibrasjonene, nemlig det å gå fra sittetribune til ståtribune med mye taktfast bevegelse blant supporterne. Ved å gå tilbake til de opprinnelige beregningene fra 24.01.2001, Vedlegg B, kunne Reinertsen forsikre at sikkerheten mhp konstruksjonens styrke var ivaretatt.

På møtet den 18.03.2009 ble det konkludert med at RE skulle få utført målinger for å bekrefte antagelser og resultater i de opprinnelige beregninger. RE kontaktet firma Multiconsult for vibrasjonsmålinger, som ble utført den 19.03.2009. RBK hadde ordnet med ca 15 mann fra Ranheim Fotball som hoppet taktfast på tribunen under målingen. Det ble gjort målinger fremme på tuppen av utkrager samt helt bak på tribunen, det siste fordi det var observert bevegelse i taket under kampen, lyskastere som vibrerte. Målingene viste vibrasjonsnivå i det følsomme området, maksimalt utslag i størrelse 2 mm på tuppen mellom to dragere, se vedlegg D. Vibrasjonshastighet lå på enkelte målinger i området maksimalt noe over 20 mm/s ved kraftig taktfast hopping. De 15 personene ble plassert helt på tuppen langs tribunegulvet. Det ble målt både over hoveddragere c/c 9.6 m og på tribunegulv midt mellom to hoveddragere. I ettertid har det vist seg at disse målinger med ca 15 personer hoppende på tuppen gav større vibrasjonshastighet enn det som er målt under kamp, sannsynligvis på grunn av mer koordinert og hardere hopping.

Arne Lorentsen og Tore Søreide ble enige om at TV-skjermer på VIP under øvre nivå skulle flyttes inn mot hoveddragere. De stod tidligere i midtfelt mellom dragerne, hvor nedbøyningene vil være maksimale, og det ble observert vibrasjoner i disse den 15.03.2009.

Parallelt med at nye målinger ble utført gikk RE mer grundig igjennom den opprinnelige dynamiske analyserapport fra 24.01.2001, vedlegg B, samt utførte nye beregninger, som gjengitt nedenfor. Det ble sett både på dragerne, tribuneelement mellom dragerne, og globalt for hele "bygget".

# 3 BEREGNINGER

Det er laget 2 modeller i elementmetode-programmet STAADPro. Den ene modellen er relativt enkel, der bare bjelken er modellert. Den andre modellen omfatter nesten hele Tribune D. Dette er gjort for å se om det er mulighet for innslag av globale moder, når en så stor dynamisk last påføres.

## 3.1 BJELKE MODELL

Dette er en 2D-modell, der kun bjelken og dens opplegg er modellert. Bjelken er modellert ved hjelp av relativt korte bjelkeelementer for å få massen mest mulig realistisk representert. Oppleggene er modellert som vist i figur 3.1.

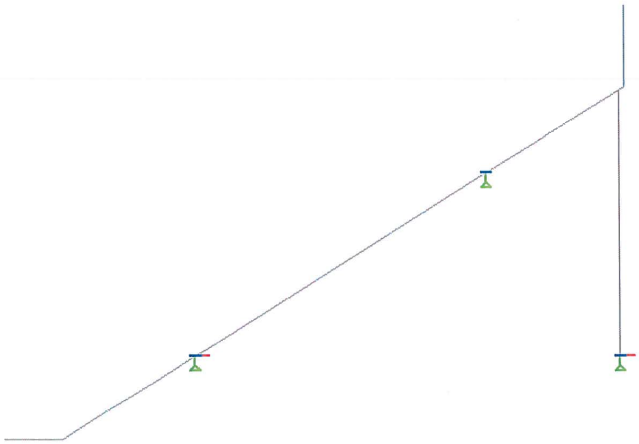

*Figur 3.1 Bjelke-modell.*

Massen er påført som last i begge retninger.

## 3.2 3D-MODELL

I denne modellen er alle bjelker og søyler modellert med bjelkeelementer med reelt tverrsnitt. Tribuneelementene er modellert som bjelkeelementer med et rektangulært tverrsnitt som skal gi riktig bøyestivhet og tverrsnittsareal. De vertikale skivene er skallelementer med samme tykkelse som i vikeligheten. Mens hulldekkene er representert ved skallelementer med tykkelse 150mm, for å gi en mest mulig riktig stivhet med tanke på skivekrefter.

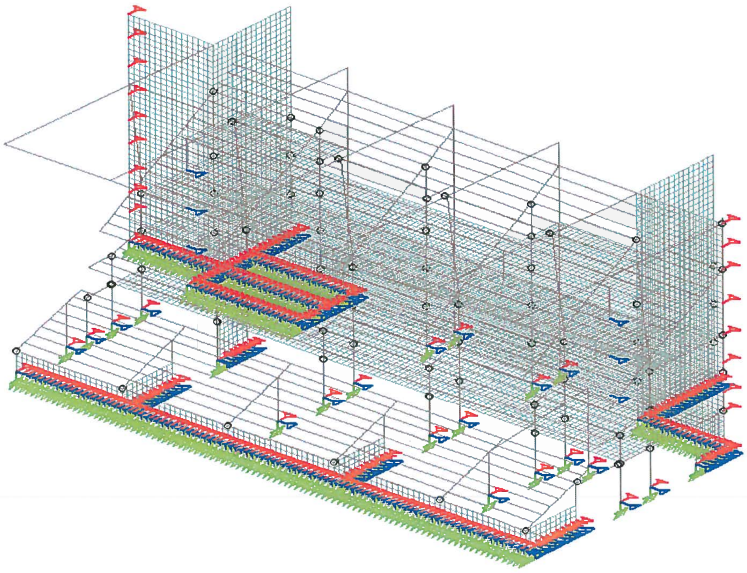

*Figur 3.2. 3D-modell.*

Massene av konstruksjonen er påført ved hjelp av selfweight-funksjonen i STAAD i alle 3 retninger. I tillegg er det lagt på en masse på tribuneelementene, som tilsvarer 2 personer a 75kg pr meter, altså 1,5kN/m.

# 4 MÅLINGER

Det er utført målinger ved 3 tilfeller:

1. **19.03.2009:** Måling på tomme tribuner hvor de eneste som var på tribunen var 15 mann som hoppet med full tyngde. Her ble det gjort målinger på tuppen av bjelken, og helt bak på tribunen. Vedlegg D.
2. **05.04.2009:** Måling på kamp, Rosenborg - Brann. Det ble utført målinger inne i puben til Kjernen før kamp. I løpet av kampen ble det foretatt en serie målinger nederst på den tribunen kjernen står på, mellom to bjelker, altså der utslaget er størst. Vedlegg E.
3. **19.04.2009:** Måling på kamp, Rosenborg – Odd Grenland. Det ble logget hele 1. Omgang, og største svingehastighet for hvert minutt ble lagret. Lokasjon for målingene var nederst på tribunen, men denne gangen like over en bjelke. Vedlegg F.

Under kampen mot Brann den 05.04.2009 var Viggo Henriksen, Tomas Brikselli og Tore Søreide fra RE tilstede og gjorde målinger under kampen, samt gikk rundt på øvre plan. Det ble gjort målinger både ute på øvre tribune og inne på dekke i 4. etasje, i puben. Her fikk RE også opplyst at under kampen den 15.03.2009 var det blitt hoppet inne på gulvelementene (hulldekke) av Kjernen, og at man da hadde følt vibrasjon. RE sine representanter kunne føle noe vibrasjon i tribunen under kampen, men mindre enn forventet.

Under kampen mot Molde den 16.05.2009 var Viggo Henriksen og Tore Søreide fra RE tilstede, da man kunne forvente mer aktivitet blant Kjernen denne dagen. Det ble bare gjort visuell registrering, og man hverken så eller merket noe mer bevegelse enn på de to foregående kamper hvor målinger ble utført.

# 5 RESULTATER

## 5.1 BEREGNINGER

### 5.1.1 Bjelke – modell

Analysen av kun bjelken gav en egenfrekvens på 5.7Hz for mode 1. Alle de andre modene har frekvens over 14Hz, og er dermed helt uinteressante. Men vi mener at en egenfrekvens på 5.7Hz også er høyt nok til å unngå å få betydelig dynamisk forsterkning.

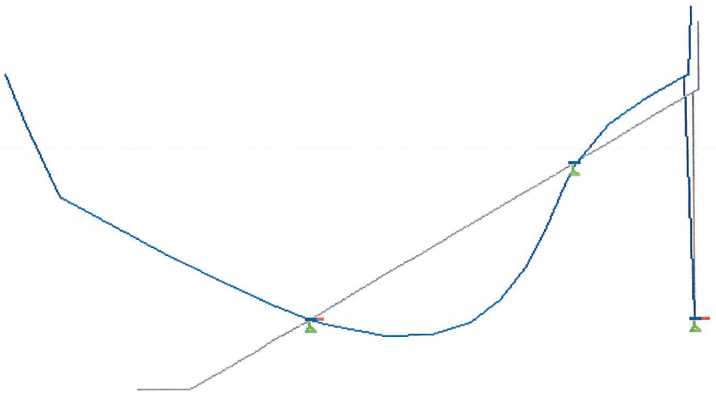

*Figur 5.1. Mode 1, bjelke - modell.*

Det fremgår av modeformen i figuren over at den dominerende lasteffekt vi være hopping på tuppen av utkrageren hvor nedbøyningen er størst.

### 5.1.2 3D – modell

I denne analysen får vi fram de 50 laveste modene for hele tribunen. Den laveste frekvensen er 1.4Hz, men denne moden gjelder kun taket. Den laveste moden som er av interesse for oss med tanke bevegelse av tribunen er mode 12, som er en global mode der hele bygget svinger horisontalt. Denne moden har egenfrekvens på 3.8Hz. Denne svingeretningen sammenfaller ikke med retningen på den dynamiske lasten som vil være hovedsakelig vertikal. Derfor mener vi at det ikke er noen fare for at denne moden aktiveres. Forklaring på denne mode kan være at tribunen ikke er sammenhengende ned til nedre nivå i midtpartiet, det er åpning på langs over kjelleretasje.

De modene som gjelder vertikalbevegelse av tuppen på bjelken ligger også i denne modellen over 5Hz. I vedlegg G vises alle de 50 laveste egenfrekvensene, og de mest interessante modene.

## 5.2 MÅLINGER

I vedlegg D vises resultater fra måling 19.03.2009.
I vedlegg E vises resultater fra måling 05.04.2009.
I vedlegg H vises resultater fra måling 19.04.2009.

Vi ser av målingene at vi får størst utslag og størst svingehastighet på måling 19.03.2009 med ca 15 personer i taktfast hopp. Dette kommer nok av at det i større grad ble hoppet i takt, og med større kraft under den første målingen, da det var bare 15 mann på tribunen.

Vi ser også at det er ingen av målingene som tyder på resonans i konstruksjonen. Høyeste målte hastighet under kamp er 17mm/s. Dette er nok en hastighet som kan føles ubehagelig for mange. Men vi ser både av observasjoner og målinger at utslagene er relativt små, i underkant av 2mm nedbøyning på tuppen, som er lite i forhold til en bruddsituasjon i konstruksjonen.

# VEDLEGG G

## 3D ANALYSER AV TRIBUNE

# Calculated Modal Frequencies & Mass Participations

| Mode | Frequency (Hz) | Period (seconds) | Participation X (%) | Participation Y (%) | Participation Z (%) |
|---|---|---|---|---|---|
| 1 | 1.442 | 0.694 | 0.003 | 0.000 | 2.012 |
| 2 | 2.018 | 0.496 | 0.003 | 0.000 | 0.634 |
| 3 | 2.600 | 0.385 | 1.203 | 0.000 | 0.518 |
| 4 | 2.727 | 0.367 | 0.016 | 0.000 | 3.108 |
| 5 | 2.825 | 0.354 | 3.000 | 0.000 | 0.009 |
| 6 | 3.078 | 0.325 | 2.385 | 0.001 | 0.169 |
| 7 | 3.283 | 0.305 | 0.185 | 0.000 | 3.775 |
| 8 | 3.313 | 0.302 | 0.143 | 0.451 | 0.006 |
| 9 | 3.447 | 0.290 | 0.012 | 0.010 | 0.000 |
| 10 | 3.523 | 0.284 | 7.809 | 0.031 | 0.230 |
| 11 | 3.678 | 0.272 | 0.068 | 0.217 | 0.000 |
| 12 | 3.758 | 0.266 | 32.126 | 0.175 | 0.031 |
| 13 | 3.815 | 0.262 | 0.151 | 0.002 | 6.332 |
| 14 | 3.865 | 0.259 | 0.005 | 0.000 | 0.000 |
| 15 | 4.277 | 0.234 | 0.000 | 0.021 | 0.000 |
| 16 | 4.638 | 0.216 | 0.001 | 1.594 | 0.002 |
| 17 | 4.651 | 0.215 | 0.003 | 3.028 | 0.001 |
| 18 | 4.679 | 0.214 | 0.000 | 0.032 | 0.000 |
| 19 | 4.753 | 0.210 | 0.000 | 0.099 | 0.001 |
| 20 | 4.794 | 0.209 | 0.000 | 0.015 | 0.005 |
| 21 | 4.804 | 0.208 | 0.004 | 0.019 | 0.394 |
| 22 | 4.846 | 0.206 | 0.001 | 0.450 | 0.013 |
| 23 | 4.882 | 0.205 | 0.014 | 6.852 | 0.003 |
| 24 | 4.916 | 0.203 | 0.000 | 0.023 | 0.003 |
| 25 | 4.981 | 0.201 | 0.009 | 0.120 | 0.002 |
| 26 | 5.011 | 0.200 | 0.001 | 1.379 | 0.001 |
| 27 | 5.045 | 0.198 | 0.000 | 0.042 | 0.195 |
| 28 | 5.056 | 0.198 | 0.003 | 1.279 | 0.035 |
| 29 | 5.063 | 0.198 | 0.000 | 0.001 | 0.000 |
| 30 | 5.087 | 0.197 | 0.004 | 1.170 | 0.029 |
| 31 | 5.201 | 0.192 | 0.062 | 0.043 | 1.377 |
| 32 | 5.242 | 0.191 | 0.005 | 2.556 | 0.022 |
| 33 | 5.317 | 0.188 | 0.036 | 0.013 | 4.289 |
| 34 | 5.679 | 0.176 | 10.954 | 0.581 | 0.099 |
| 35 | 5.831 | 0.172 | 0.004 | 0.024 | 0.000 |
| 36 | 6.050 | 0.165 | 1.127 | 0.081 | 5.669 |
| 37 | 6.067 | 0.165 | 0.011 | 0.000 | 0.059 |
| 38 | 6.137 | 0.163 | 0.000 | 0.000 | 0.000 |
| 39 | 6.225 | 0.161 | 0.000 | 0.003 | 0.009 |
| 40 | 6.264 | 0.160 | 0.014 | 0.006 | 0.000 |
| 41 | 6.275 | 0.159 | 0.001 | 0.001 | 0.003 |
| 42 | 6.306 | 0.159 | 0.000 | 0.248 | 0.196 |
| 43 | 6.327 | 0.158 | 0.000 | 0.003 | 0.001 |
| 44 | 6.342 | 0.158 | 0.000 | 0.005 | 0.004 |
| 45 | 6.366 | 0.157 | 0.009 | 0.007 | 0.002 |
| 46 | 6.391 | 0.156 | 0.058 | 0.008 | 0.002 |
| 47 | 6.412 | 0.156 | 0.010 | 0.001 | 0.016 |
| 48 | 6.459 | 0.155 | 0.000 | 0.000 | 0.197 |
| 49 | 6.483 | 0.154 | 0.000 | 0.000 | 0.001 |

## Calculated Modal Frequencies & Mass Participations Cont...

| Mode | Frequency (Hz) | Period (seconds) | Participation X (%) | Participation Y (%) | Participation Z (%) |
|---|---|---|---|---|---|
| 50 | 6.508 | 0.154 | 0.046 | 0.461 | 0.000 |

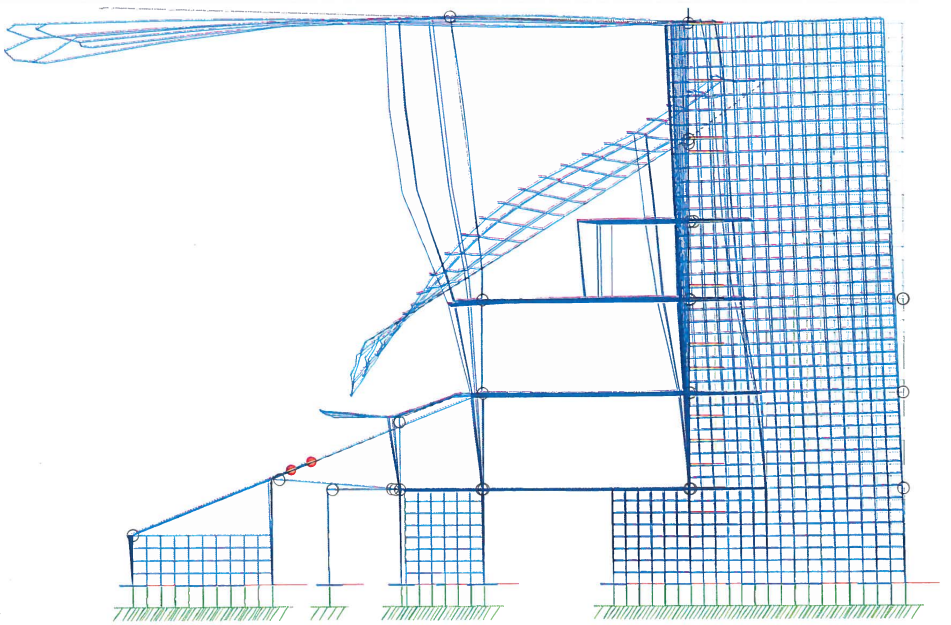


Load 1 : Mode Shape 12

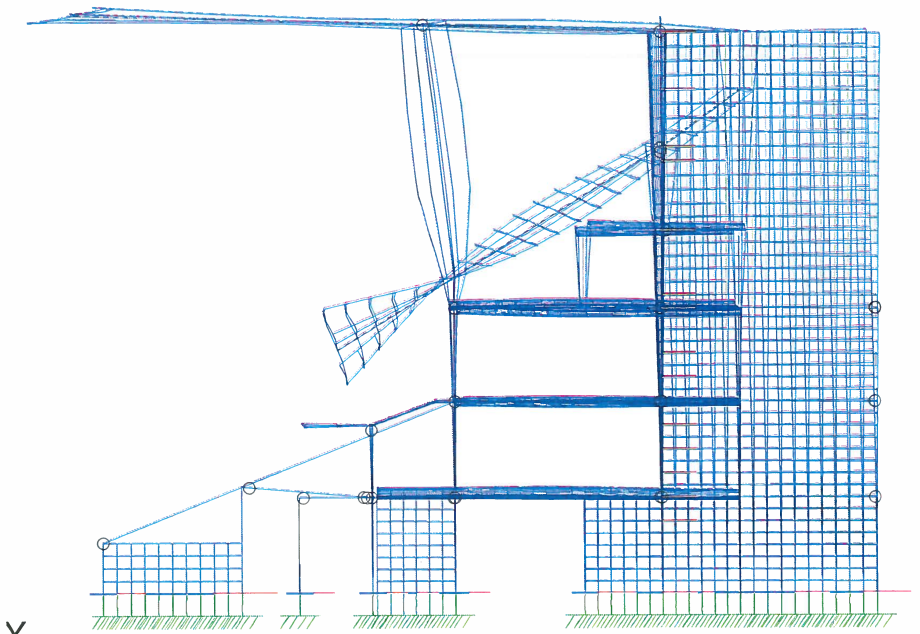


Load 1 : Mode Shape 31

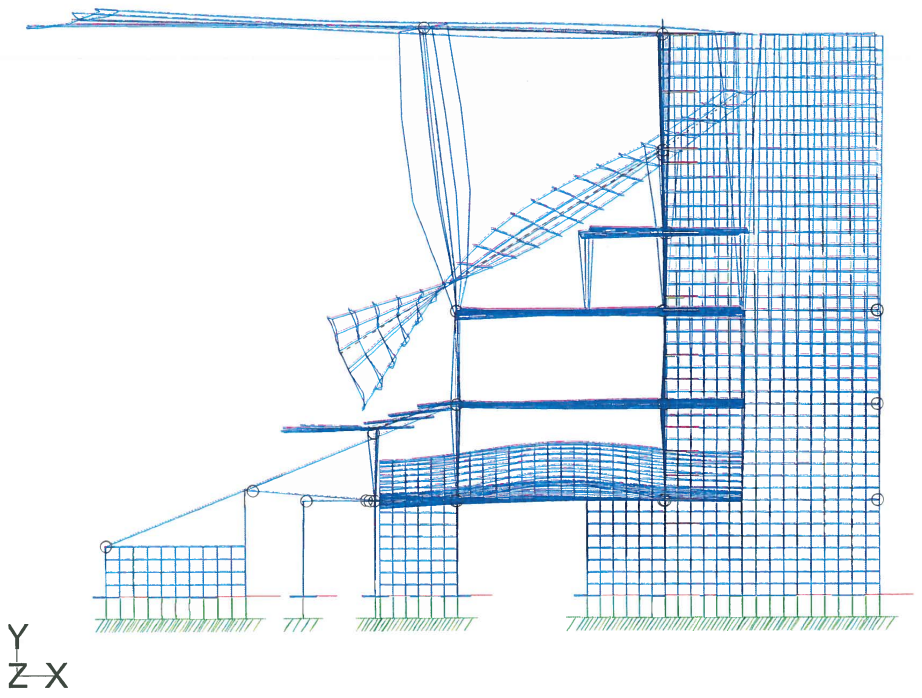


Load 1 : Mode Shape 33

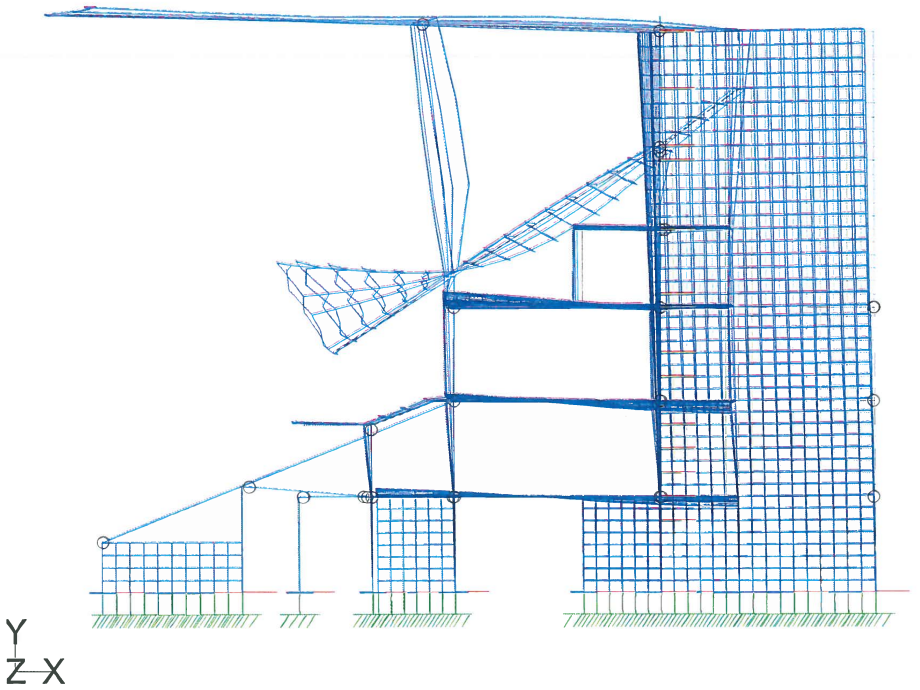


Load 1 : Mode Shape 34

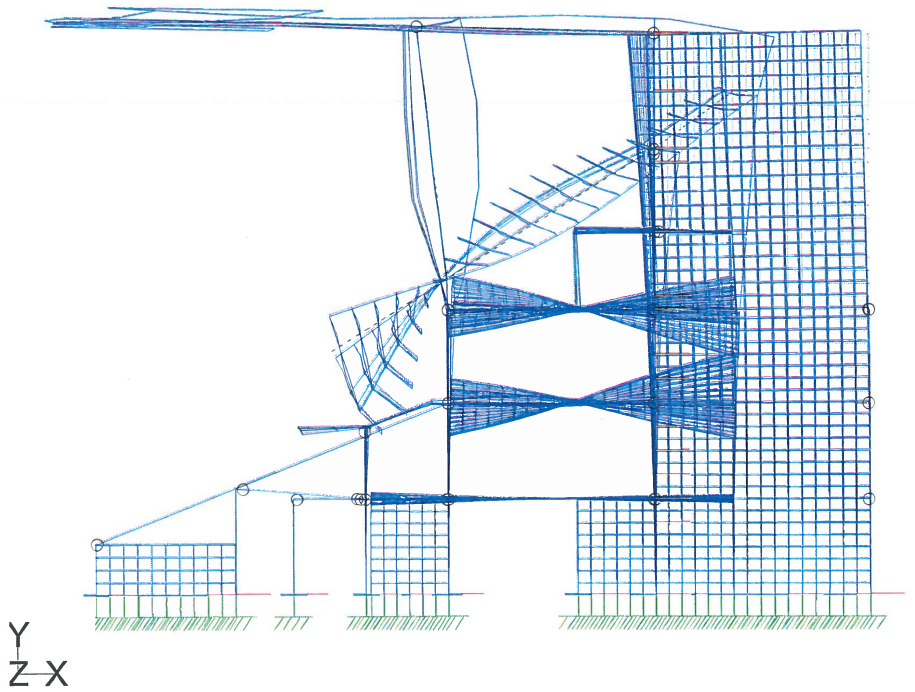


**Load 1 : Mode Shape 42**

# Appendix D

# Meshed Parts

The following appendix contains the different meshed parts of the model.

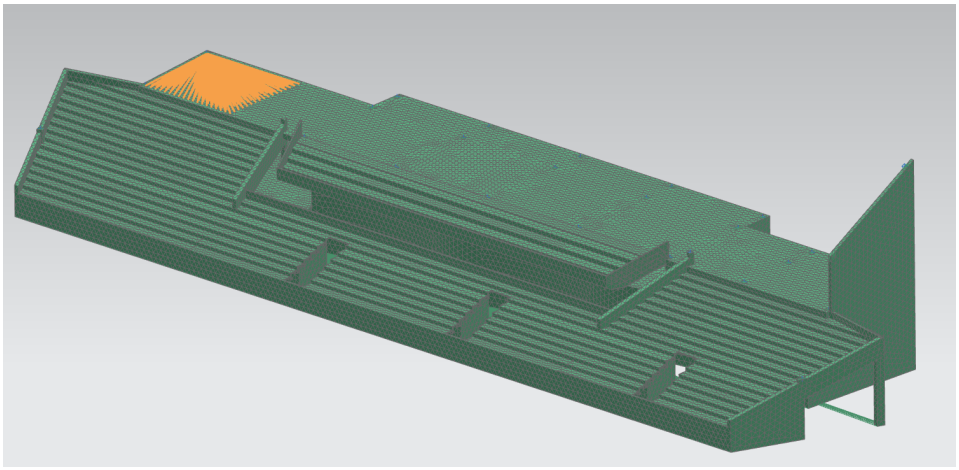

Figure D.1: Lower level

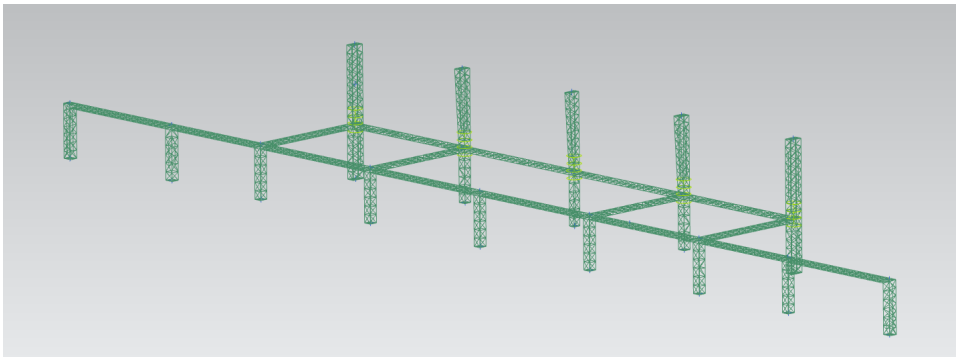

Figure D.2: Upper level frame

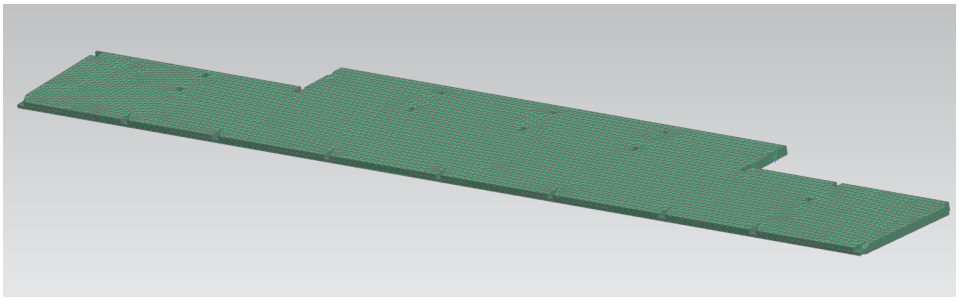

Figure D.3: Upper level floor

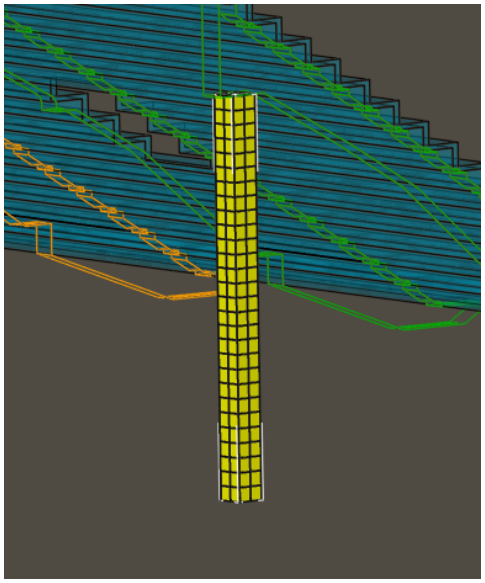

Figure D.4: Column A

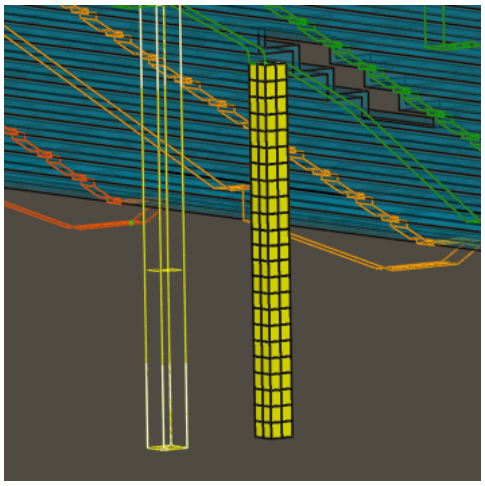

Figure D.5: Column B front

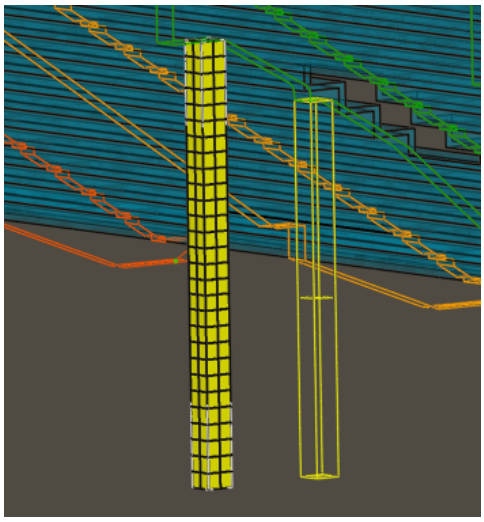

Figure D.6: Column B back

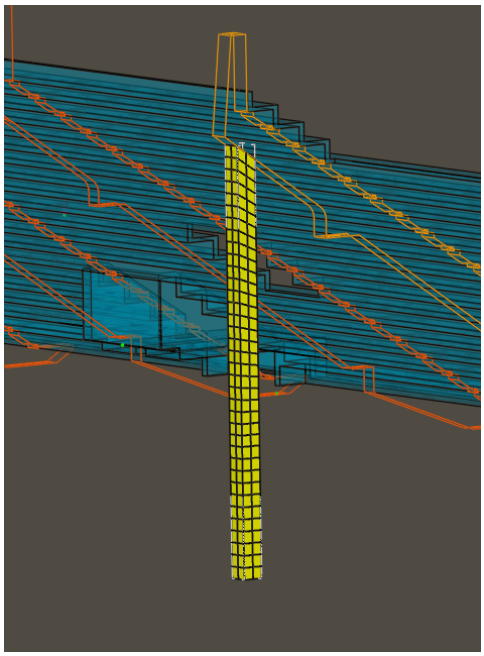

Figure D.7: Column C

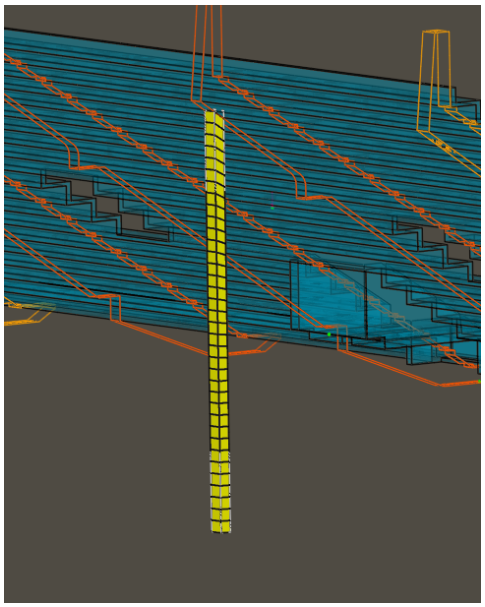

Figure D.8: Column D

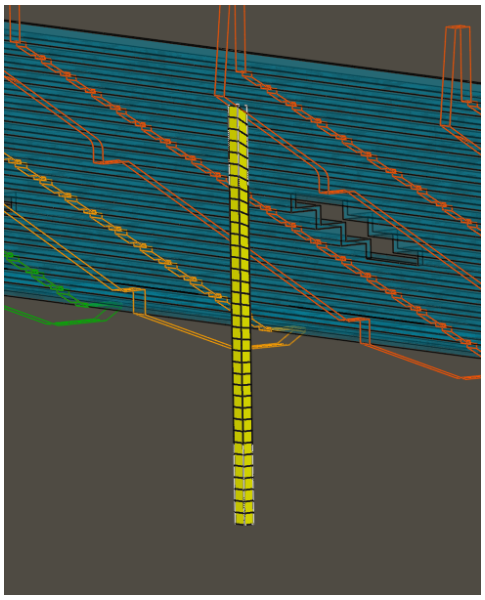

Figure D.9: Column E

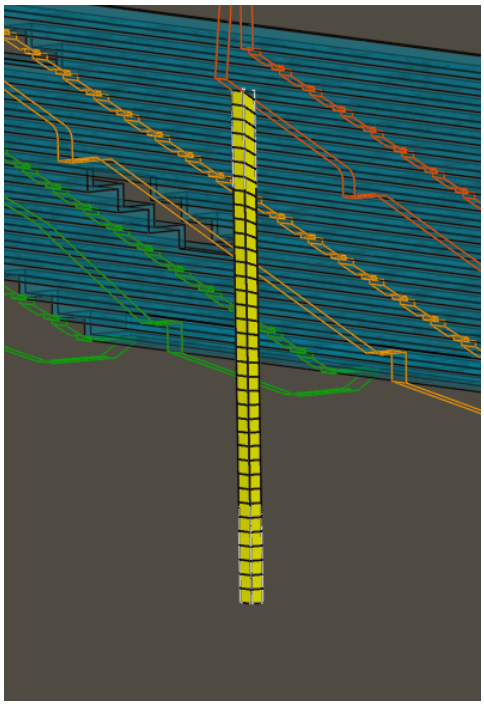

Figure D.10: Column G

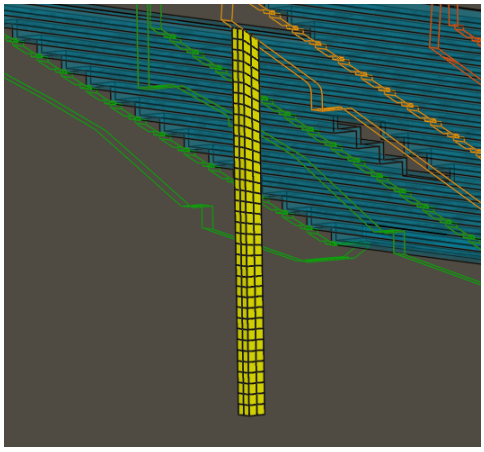

Figure D.11: Column H

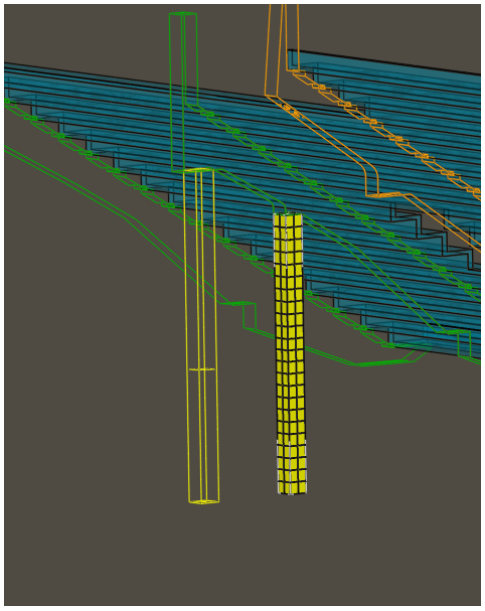

Figure D.12: Column J front

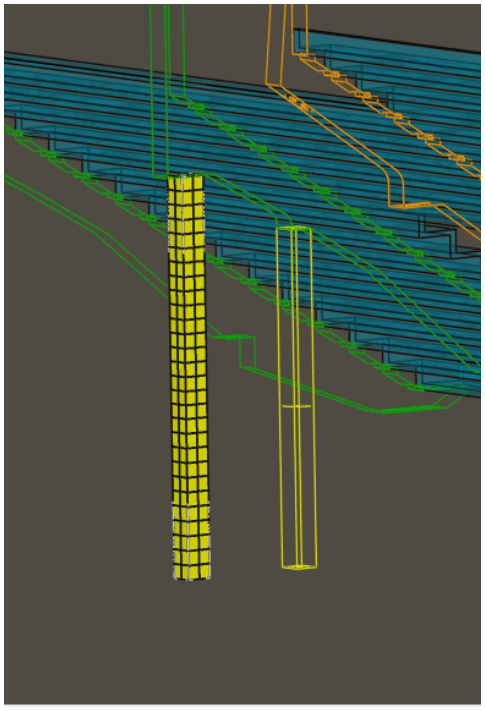

Figure D.13: Column J back

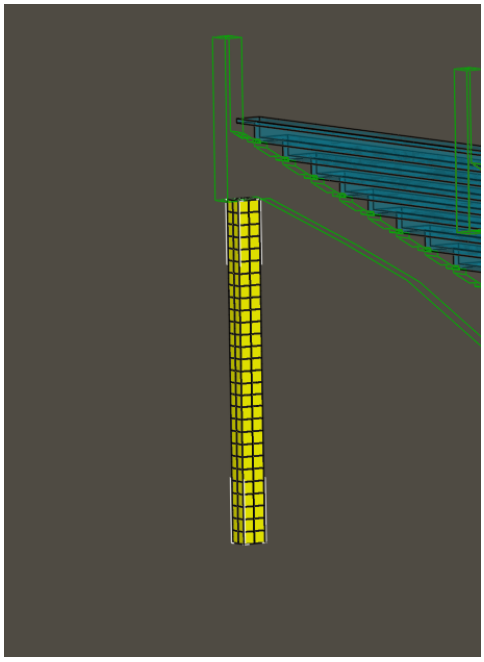

Figure D.14: Column K

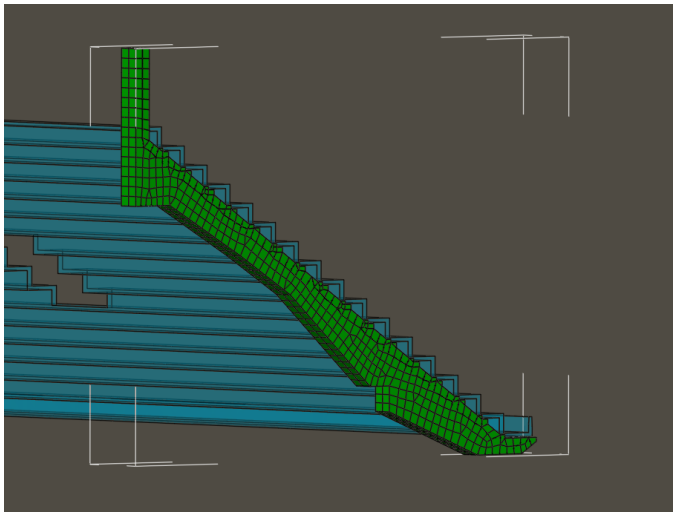

Figure D.15: Girder A

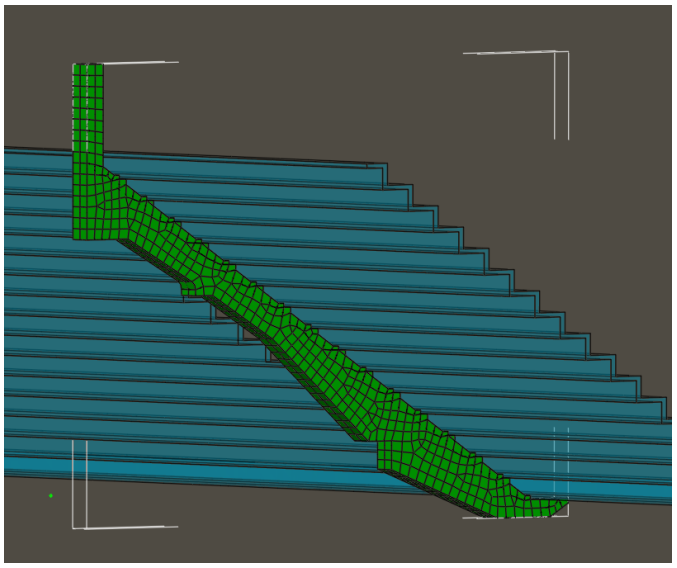

Figure D.16: Girder B

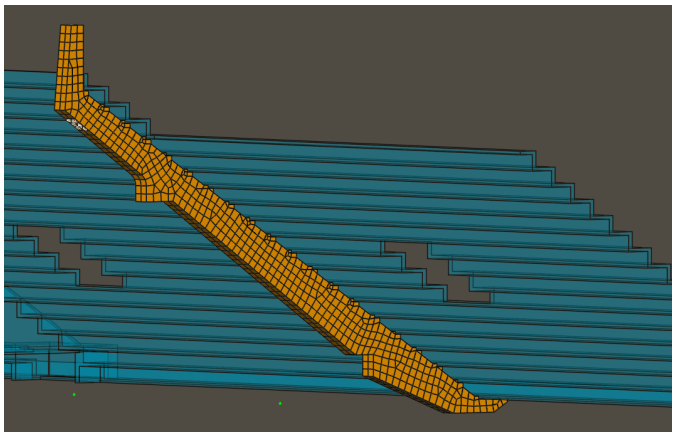

Figure D.17: Girder C

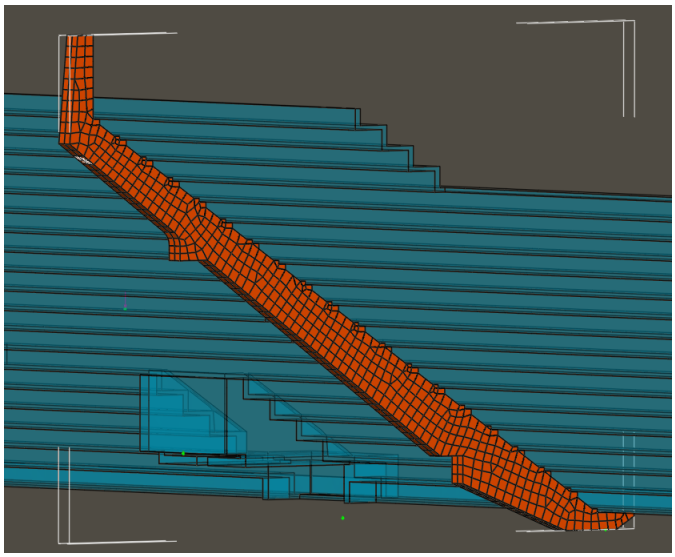

Figure D.18: Girder D

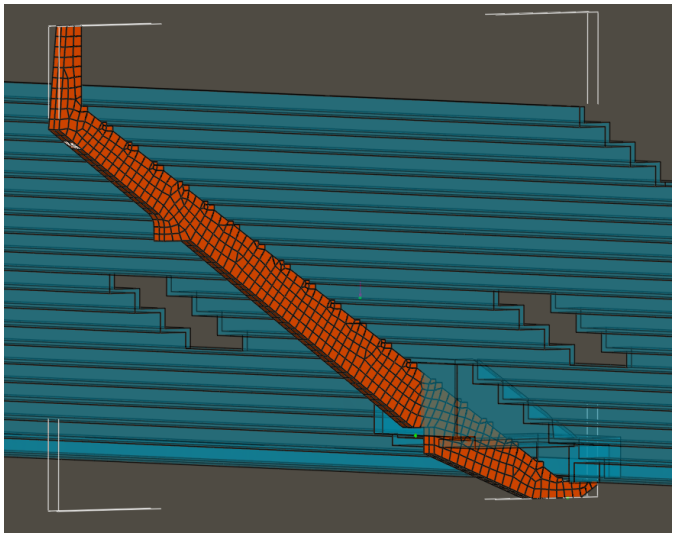

Figure D.19: Girder E

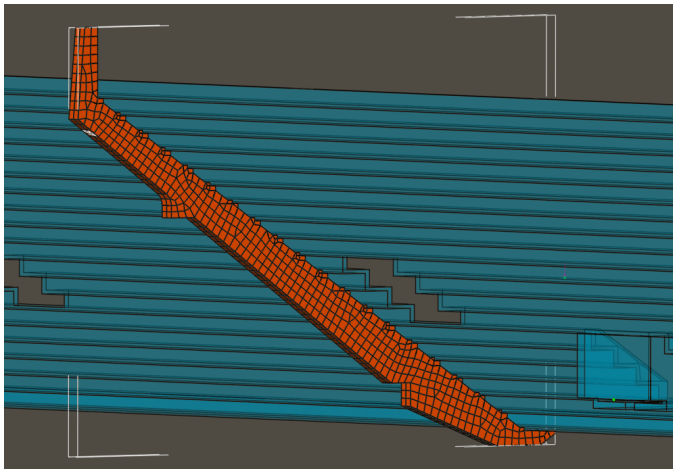

Figure D.20: Girder G

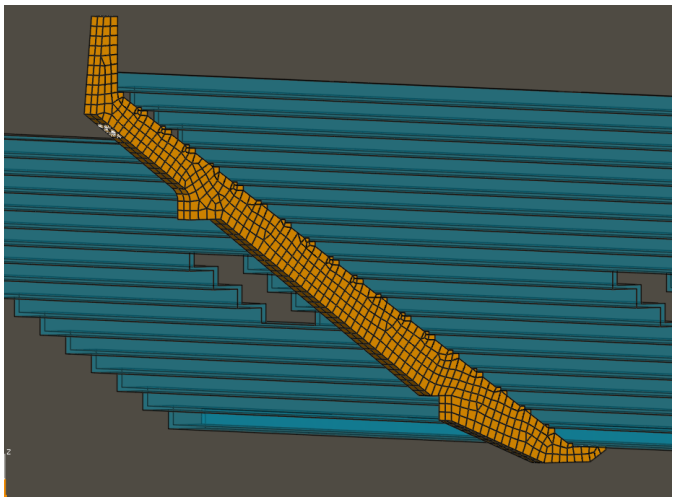

Figure D.21: Girder H

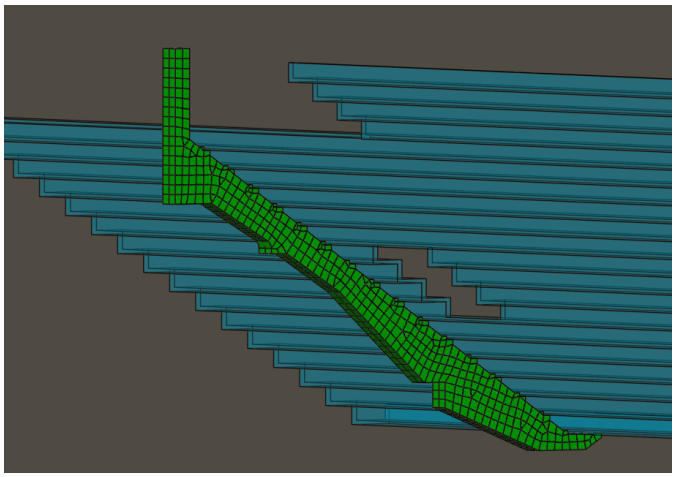

Figure D.22: Girder J

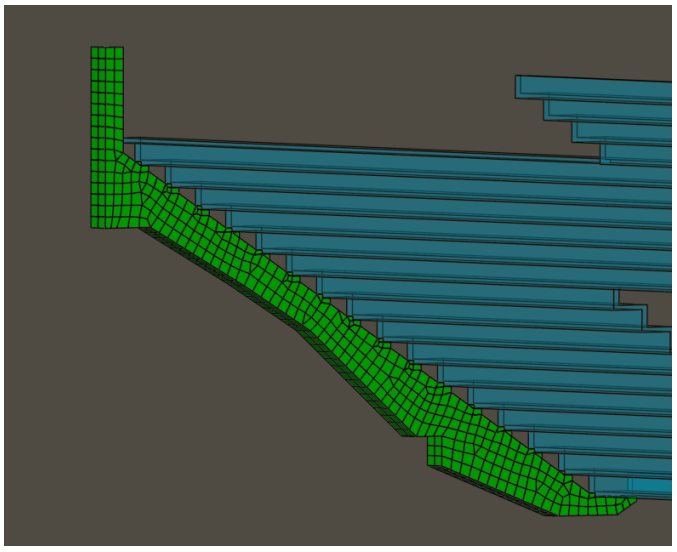

Figure D.23: Girder K

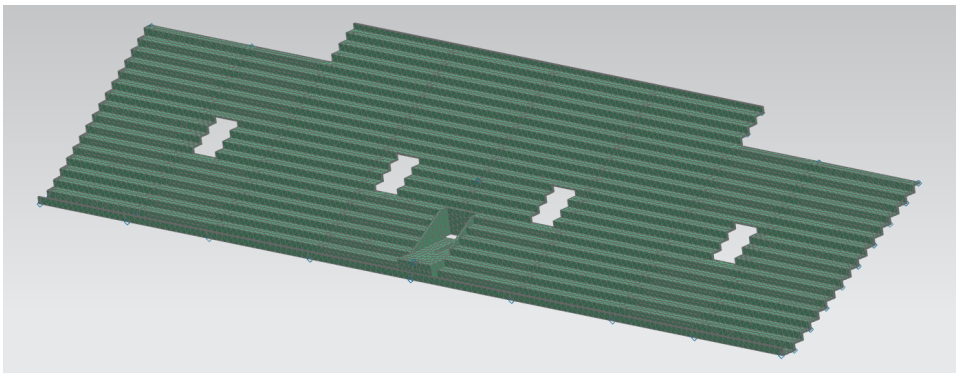

Figure D.24: Upper level seating element

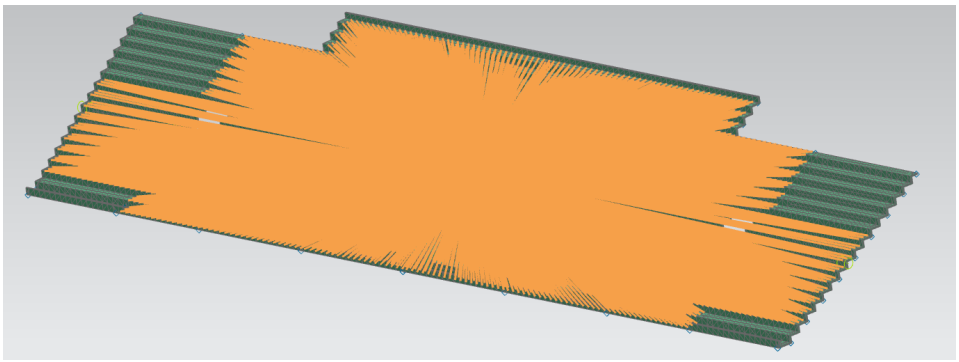

Figure D.25: Upper level seating element with RBE3 element representing supporters

# Appendix E

# Architectural schematics

The following appendix contains the schematics provided by the operations manager at Lerkendal Stadion. There are three schematics of the view from four sides of the grandstand. There are seven drawings of cuts seen from the south passing through the grandstand. There are five cuts giving the floor-plan at different levels of elevation.

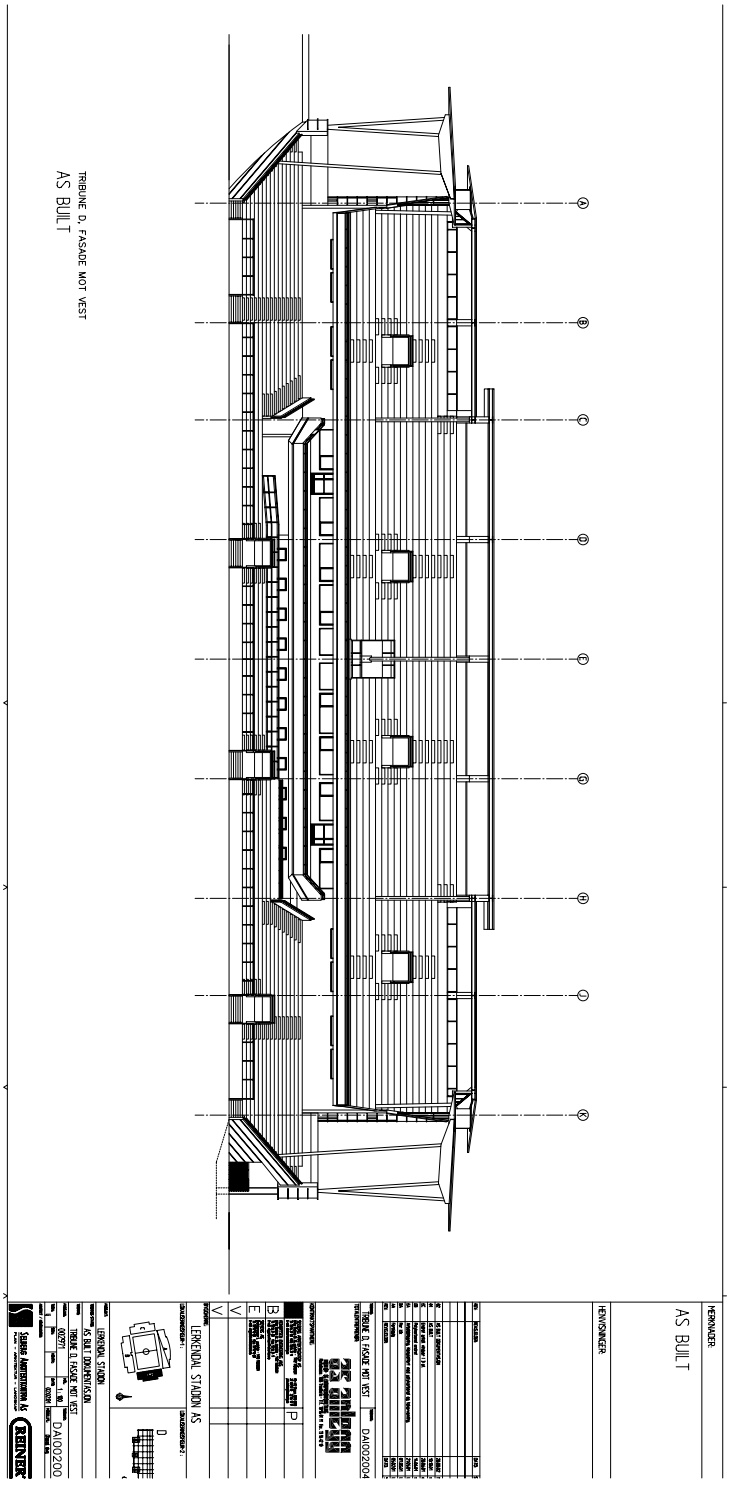


Figure E.1: West Facade

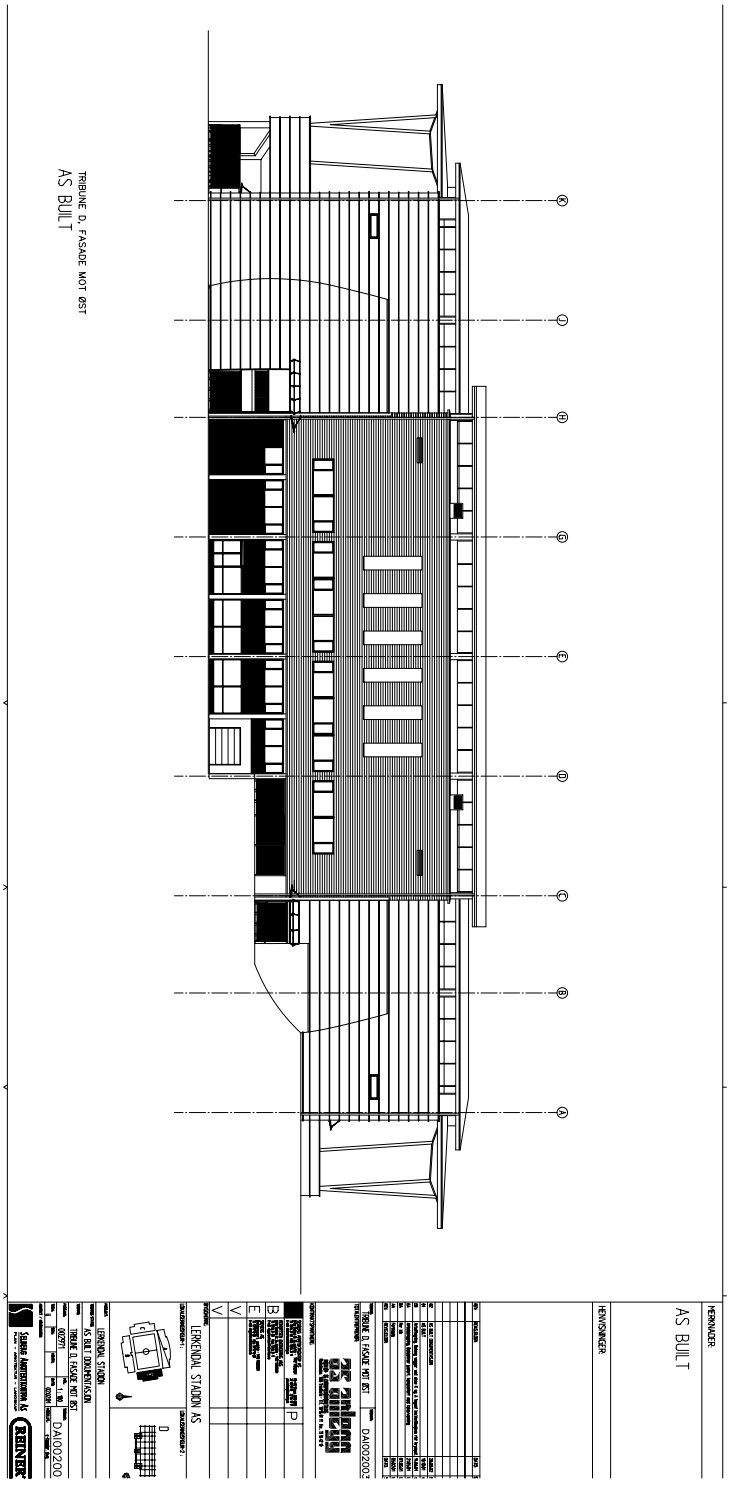


Figure E.2: East Facade

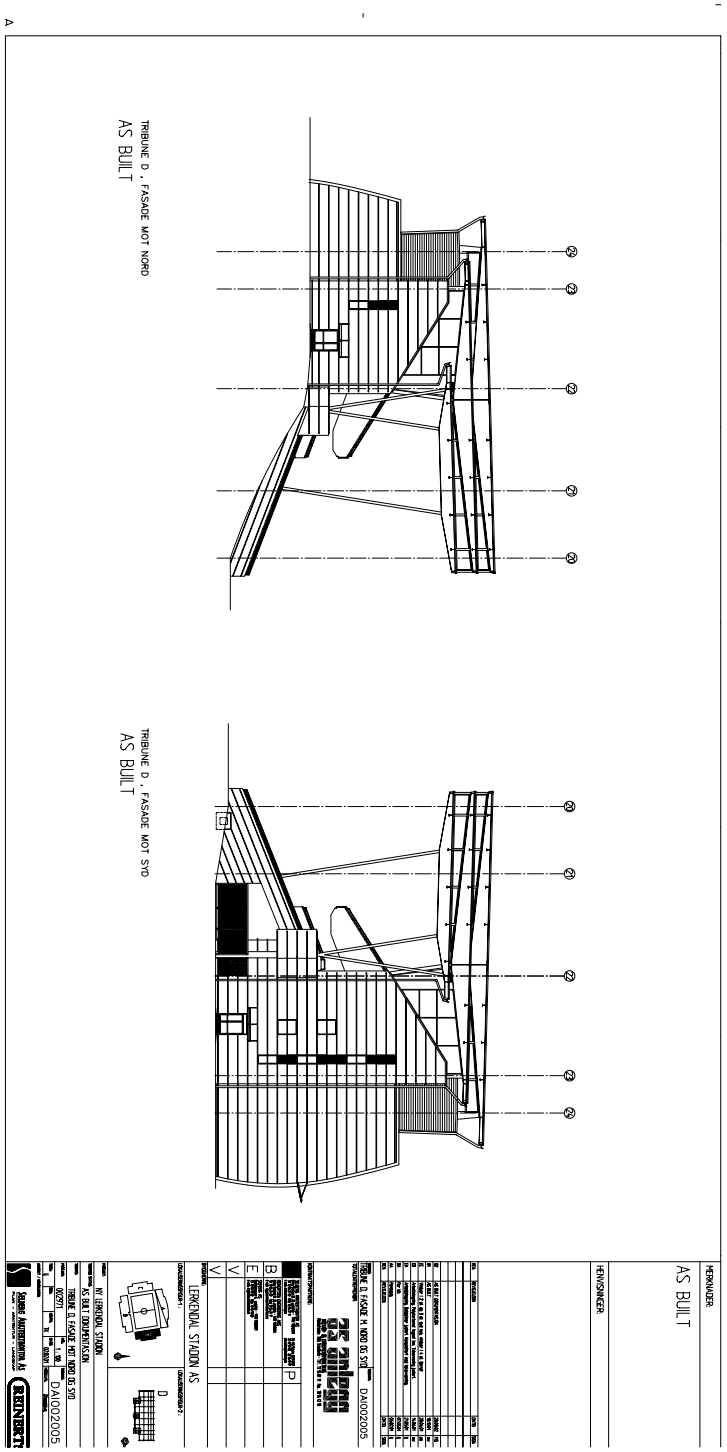


Figure E.3: North and South Facade

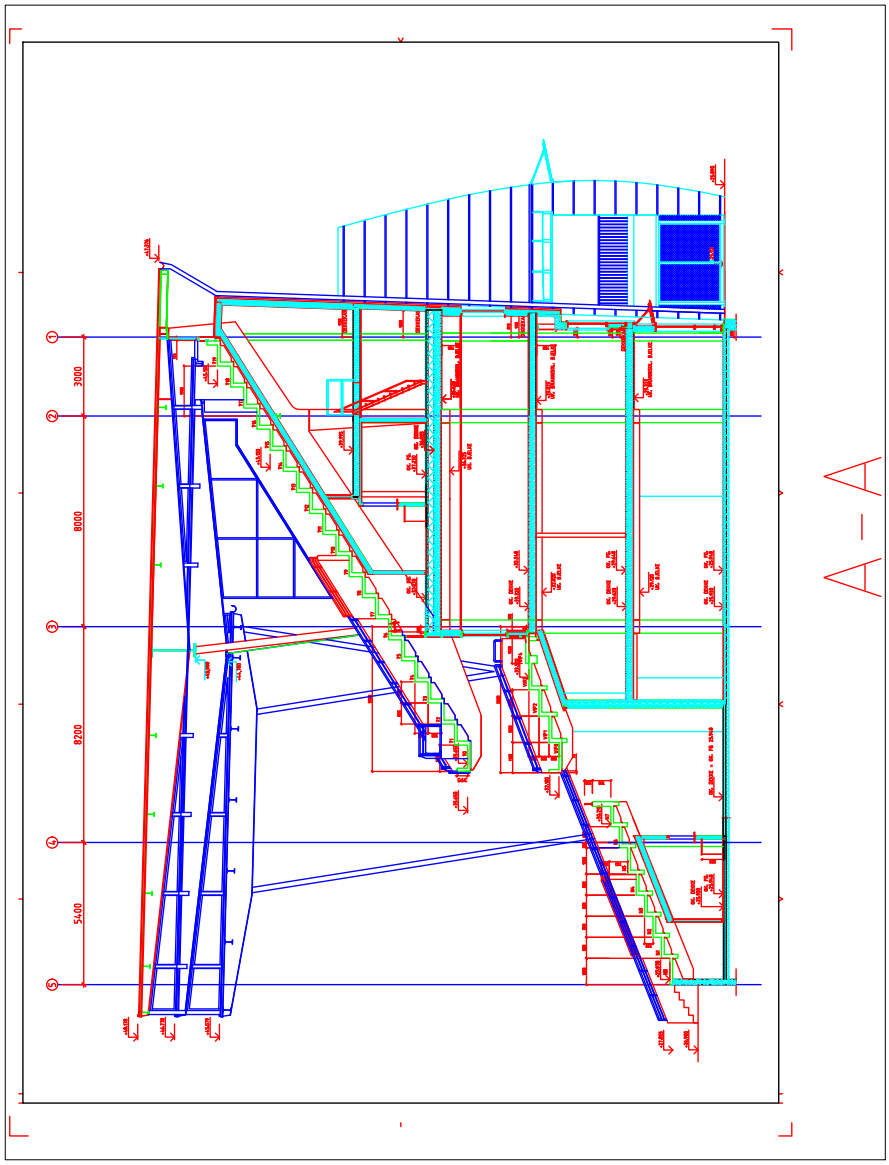


Figure E.4: Cut A

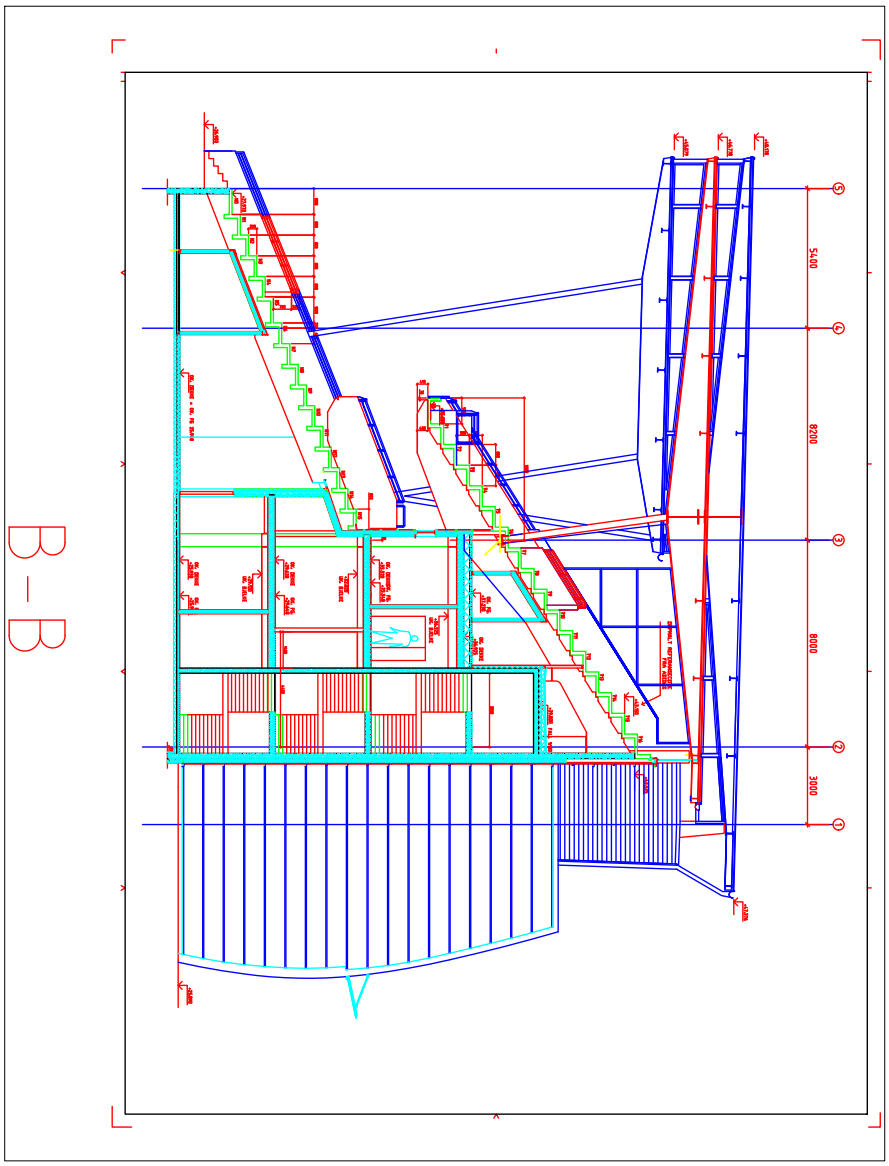


Figure E.5: Cut B

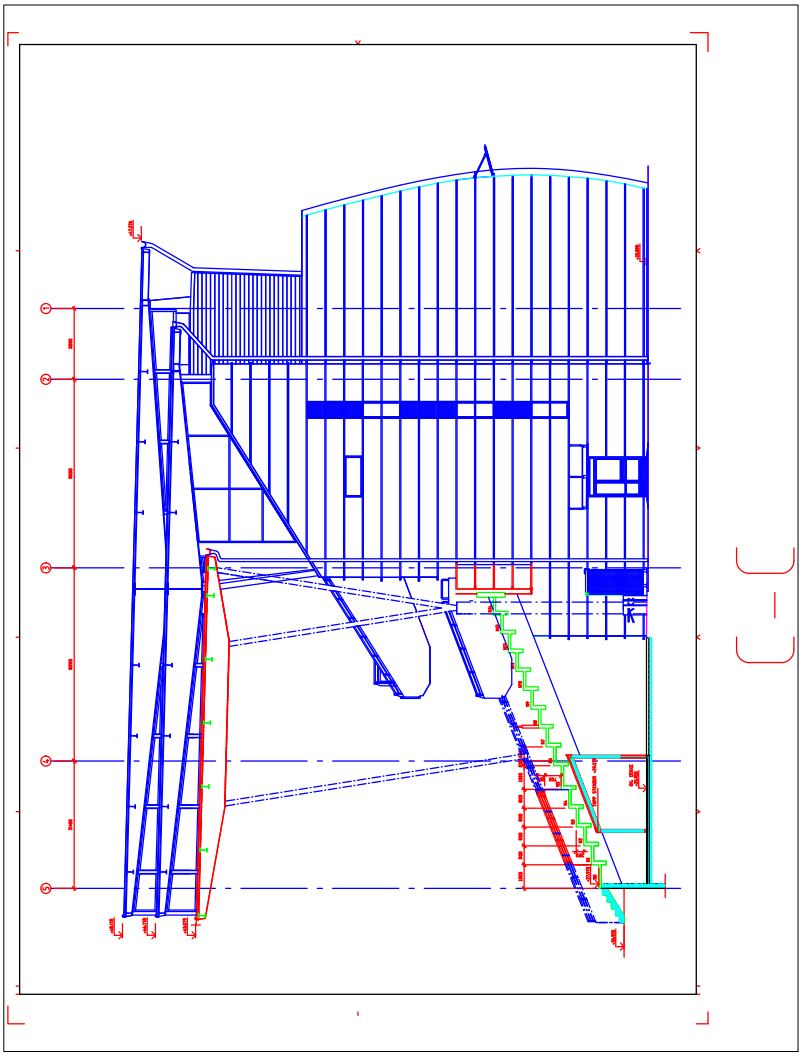


Figure E.6: Cut C

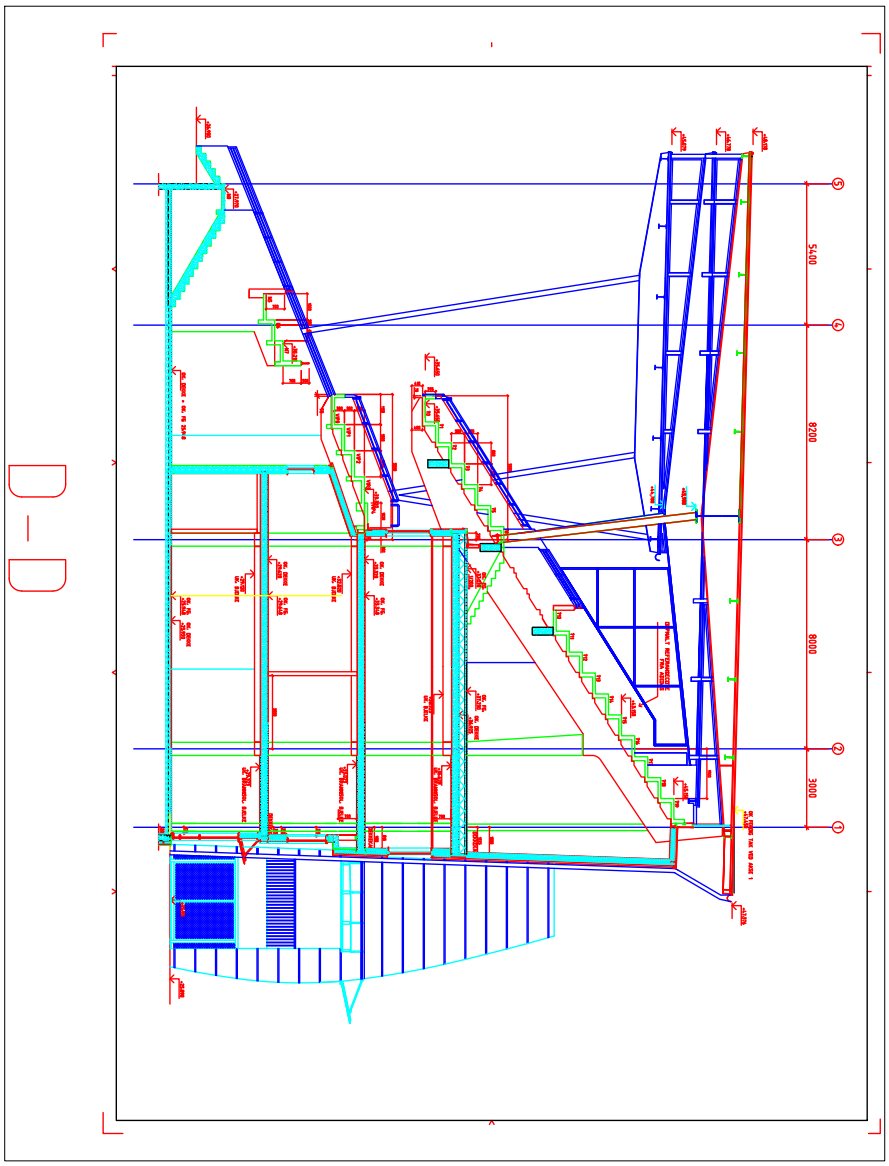


Figure E.7: Cut D

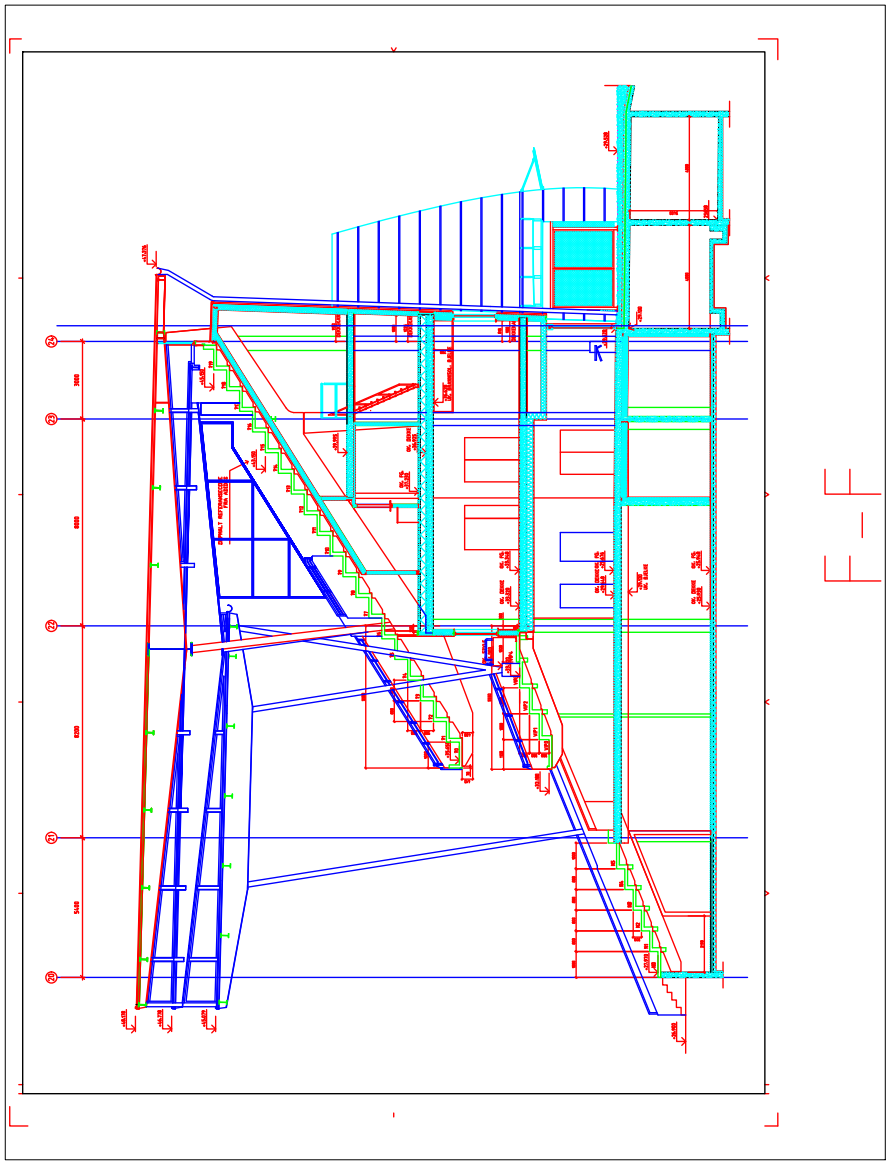


Figure E.8: Cut F

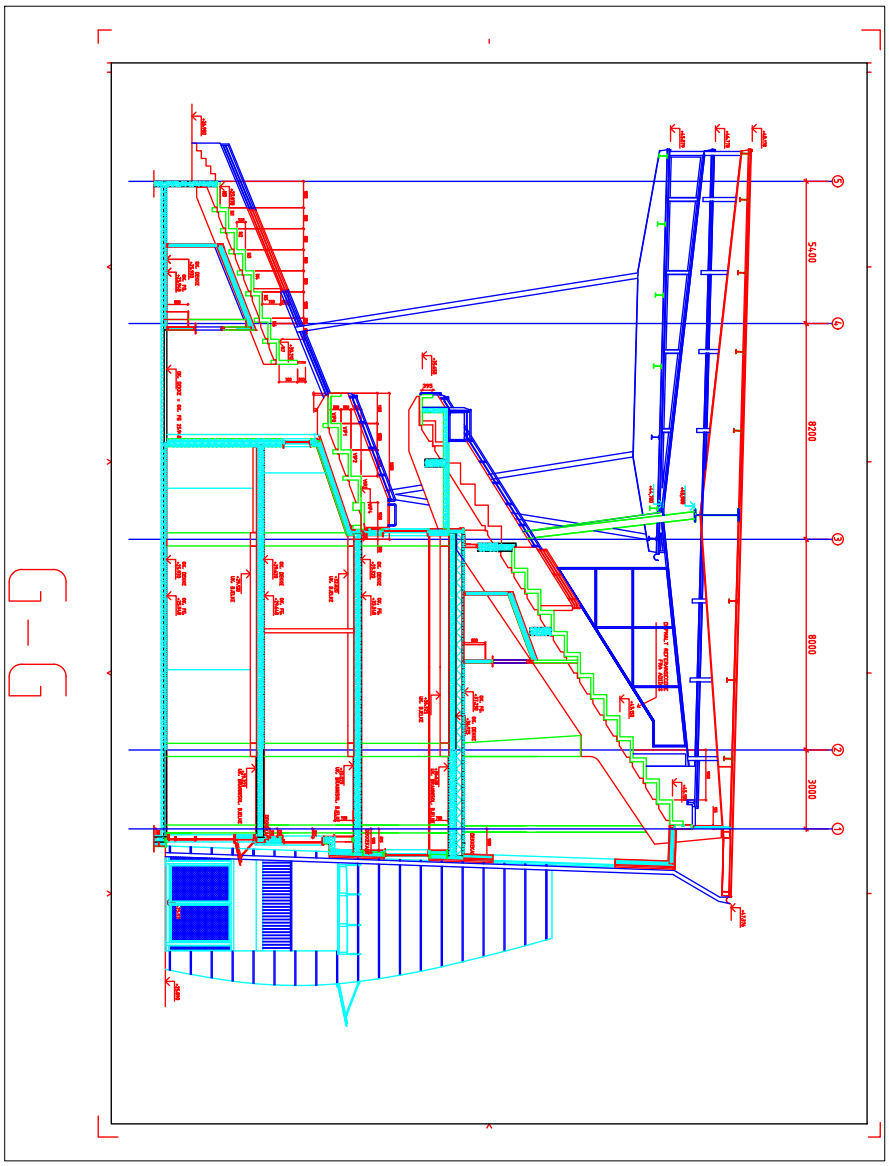


Figure E.9: Cut G

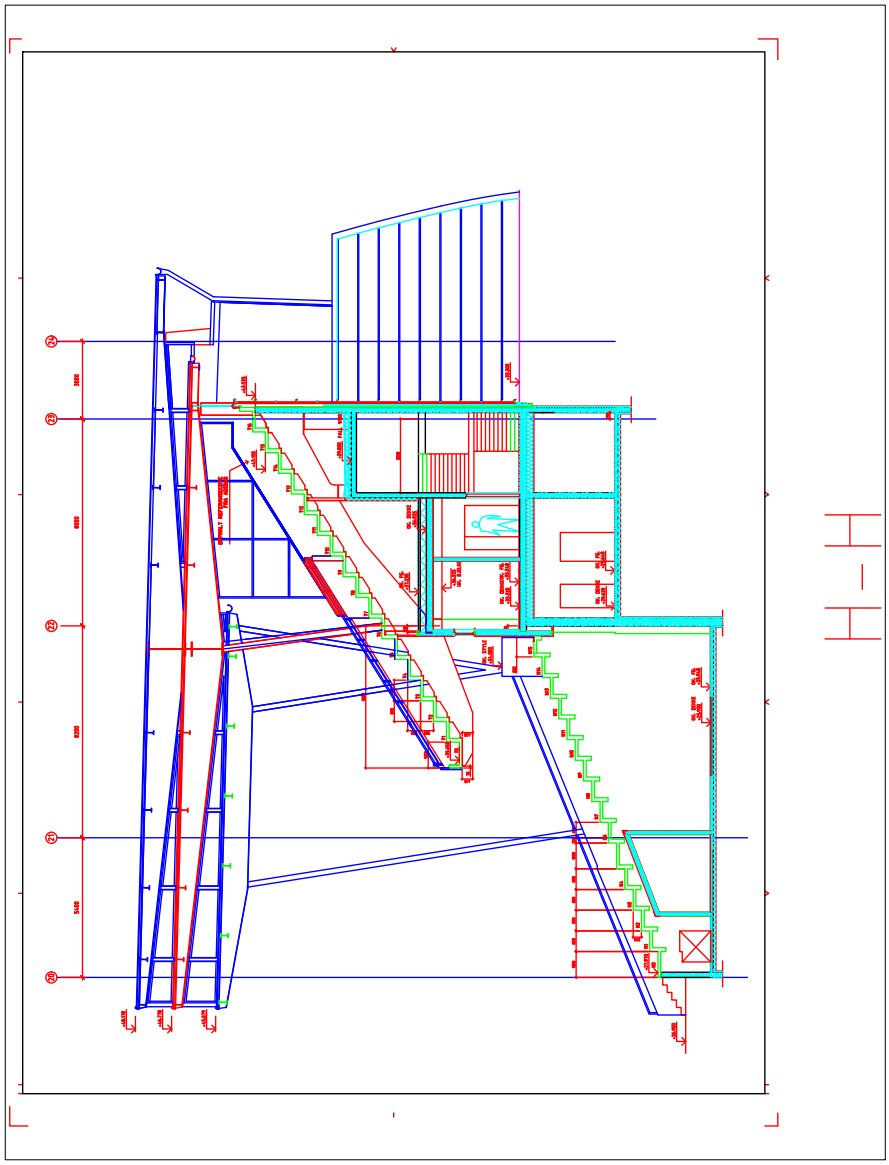


Figure E.10: Cut H

# Appendix F

# Scripts and Code

## F.1 biggestfall.py

Calculates the largest leap and fall for a given event.

```
import sys
sys.path.append("..")

import matplotlib.pyplot as plt
import integration_utils as intut
import numpy as np
from scipy import integrate
from scipy.signal import butter, lfilter, freqz

GRAVITY = 9.80665
accOrder = 6
order = 4
cutoffAcceleration = 30
cutoffVelocity = 0.30
cutoffDisplacement = 0.55
sampleRate = 128
start = 0.0
stop = 60
period = 1.0/sampleRate

accelerationFile = "pippi2.csv"
noiseFile = "stoy.csv"

def butter_lowpass(cutoff, fs, order=5):
  nyq = 0.5 * fs
  normal_cutoff = cutoff / nyq
```

```
  b, a = butter(order, normal_cutoff, btype='low', analog=False)
  return b, a

def butter_lowpass_filter(data, cutoff, fs, order=5):
  b, a = butter_lowpass(cutoff, fs, order=order)
  y = lfilter(b, a, data)
  return y

def butter_highpass(cutoff, fs, order=5):
  nyq = 0.5 * fs
  normal_cutoff = cutoff / nyq
  b, a = butter(order, normal_cutoff, btype='high', analog=False)
  return b, a

def butter_highpass_filter(data, cutoff, fs, order=5):
  b, a = butter_highpass(cutoff, fs, order=order)
  y = lfilter(b, a, data)
  return y

acceleration = intut.readThreeAccelerationFromFile(accelerationFile)
meanAcceleration = intut.threeMeanAccelerationFromFile(noiseFile)
print("meanAcceleration" + str(meanAcceleration))

numberOfSamples = len(acceleration[0])
numberOfSeconds = numberOfSamples/sampleRate
time = np.linspace(0, numberOfSeconds, numberOfSamples)

print("timeLength: " + str(len(time)) + "nSamples " + str(
                                    numberOfSeconds))

nominalAcceleration = []
filteredAcc = []
velocityFilteredAcc = []
velocityFiltered = []
displacementFilteredVel = []
displacementFiltered = []

for i in range(3):
  nom = []
  mean = meanAcceleration[i]
  for acc in acceleration[i]:
    nom.append((acc-mean)*GRAVITY)
  nominalAcceleration.append(nom)
  filteredAcc.append(butter_lowpass_filter(nominalAcceleration[i],
                                    cutoffAcceleration, sampleRate,
                                    accOrder))
```

```
  velocityFilteredAcc.append(integrate.cumtrapz(filteredAcc[i], time,
                                    initial=0))
  velocityFiltered.append(butter_highpass_filter(velocityFilteredAcc[i
                                    ], cutoffVelocity, sampleRate ,
                                    order))
  displacementFilteredVel.append(integrate.cumtrapz(velocityFiltered[i
                                    ], time, initial=0))
  displacementFiltered.append(butter_highpass_filter(
                                    displacementFilteredVel[i],
                                    cutoffDisplacement, sampleRate,
                                    order))

disp = displacementFiltered[2] # 0 for G, 1 for E, 2 for D
print(disp)
top = 0
bot = 0
nbots = 0
ntops = 0
biggestFall = 0
biggestLeap = 0
tops = []
bots = []

for i in range(len(disp)-5):
  if i > 0 and i < len((disp-5)):
    prev = np.mean(disp[(i-1):(i+1)])
    curr = np.mean(disp[(i+1):(i+3)])
    nex = np.mean(disp[(i+3):(i+5)])

    if curr > prev and curr > nex:
      top = curr
      ntops += 1
      tops.append(top)
    elif curr < prev and curr < nex:
      bot = curr
      nbots += 1
      bots.append(bot)
    if ntops == nbots:
      newFall = top - bot
      if newFall > biggestFall:
        biggestFall = newFall
        print("Biggest Fall: " + str(biggestFall) + " meters, time: "
                                    + str(i/128))
    if ntops == nbots-1: #change +- if no leaps are found
      newLeap = top - bot
      if newLeap > biggestLeap:
```

```
        biggestLeap = newLeap
print("Biggest Leap: " + str(biggestLeap) + " meters, time: " + str(i/
                                    128))
print(np.mean(tops))
print(np.var(disp))
plt.plot(time,displacementFiltered[2],color='xkcd:reddish', label='D')
plt.axhline(y=np.mean(tops), label="Mean Peak Values")
plt.axhline(y=np.mean(bots), label="Mean Valley Values")
plt.xlabel("Time [s]")
plt.legend()
plt.grid()
plt.subplots_adjust(hspace=0.35)
plt.show()
```

## F.2 aRMS

Calculates the $a_{\mathrm{RMS}}$ of a given signal with a specified sample range.

```
import integration_utils as intut
import numpy as np
from scipy import integrate
from scipy.signal import butter, lfilter, freqz

GRAVITY = 9.80665
accOrder = 6
order = 4
cutoffAcceleration = 30
sampleRate = 128.0
start = 12.75
stop = 13.75
length = stop-start
startSample = sampleRate*start
stopSample = stop*sampleRate
period = 1.0/sampleRate

accelerationFile = "pippi1"
file = accelerationFile+".csv"
noiseFile = "stoy.csv"

def butter_lowpass(cutoff, fs, order=5):
  nyq = 0.5 * fs
  normal_cutoff = cutoff / nyq
  b, a = butter(order, normal_cutoff, btype='low', analog=False)
  return b, a
```

```
def butter_lowpass_filter(data, cutoff, fs, order=5):
  b, a = butter_lowpass(cutoff, fs, order=order)
  y = lfilter(b, a, data)
  return y

def aRMS(a, T, sampleRate):
  aRMS = (1.0/(len(T)/sampleRate)*integrate.simps(a**4,T,dx=1/
                                    sampleRate))**0.5
  return aRMS

acceleration = intut.readThreeAccelerationFromFile(file)
meanAcceleration = intut.threeMeanAccelerationFromFile(noiseFile)

numberOfSamples = len(acceleration[0])
numberOfSeconds = numberOfSamples/sampleRate
time = np.linspace(0, numberOfSeconds, numberOfSamples)

nominalAcceleration = []
filteredAcc = []

for i in range(3):
  nom = []
  mean = meanAcceleration[i]
  for acc in acceleration[i]:
    nom.append((acc-mean)*GRAVITY)
    nominalAcceleration.append(nom)

filteredAcc.append(butter_lowpass_filter(nominalAcceleration[i],
                                    cutoffAcceleration, sampleRate,
                                    accOrder))
accD = filteredAcc[2]
a = accD[3200:4480] #specify samples for the 1s or 10 s range
T = time[:len(a)]
aRMS = aRMS(a, T, sampleRate)
```

## F.3 integration_utils.py

Library with utility functions used in other scripts.

```
from scipy import integrate
import matplotlib.pyplot as plt
import numpy as np
from scipy.signal import butter, lfilter, freqz

GRAVITY = 9.80665
accOrder = 6
order = 4
cutoffAcceleration = 30
cutoffVelocity = 0.30
cutoffDisplacement = 0.55

def butter_lowpass(cutoff, fs, order=5):
  nyq = 0.5 * fs
  normal_cutoff = cutoff / nyq
  b, a = butter(order, normal_cutoff, btype='low', analog=False)
  return b, a

def butter_lowpass_filter(data, cutoff, fs, order=5):
  b, a = butter_lowpass(cutoff, fs, order=order)
  y = lfilter(b, a, data)
  return y

def butter_highpass(cutoff, fs, order=5):
  nyq = 0.5 * fs
  normal_cutoff = cutoff / nyq
  b, a = butter(order, normal_cutoff, btype='high', analog=False)
  return b, a

def butter_highpass_filter(data, cutoff, fs, order=5):
  b, a = butter_highpass(cutoff, fs, order=order)
  y = lfilter(b, a, data)
  return y

# Input a noise file and returns an arithmetical mean acceleration
def meanAccelerationFromFile(noiseFile):
  with open(noiseFile) as of:
    dataNoise = of.readlines()
    i = -1
    accelerationNoise = []

    for line in dataNoise:
```

```
    i=i+1
    if i > 17:
    splitted = line.split(",")
    accelerationNoise.append(float(splitted[1]))

  #finds mean acceleration to remove before integration
  sumAcc = 0.0
  for acc in accelerationNoise:
    sumAcc = sumAcc + float(acc)

  meanAcc = sumAcc/len(accelerationNoise)

  return meanAcc

def threeMeanAccelerationFromFile(noiseFile):
  with open(noiseFile) as of:
    data = of.readlines()

    i = -1
    accelerationD = []
    accelerationE = []
    accelerationG = []
    timeStamp = []
    for line in data:
    # print(line)
    i = i + 1
    if i > 20 and i < len(data)-21:
      splitted = line.split(',')
      # print(splitted[1])
      timeSplit = splitted[0]
      timeStamp.append(timeSplit[9:])
      accSplitG = float(splitted[1])
      accSplitE = float(splitted[2])
      accSplitD = float(splitted[3])
      accelerationG.append(accSplitG)
      accelerationE.append(accSplitE)
      accelerationD.append(accSplitD)
  mean = [np.mean(accelerationG), np.mean(accelerationE), np.mean(
                                  accelerationD)]
  samplesStr = str(len(accelerationG))
  print("Read: " + noiseFile + " with " + samplesStr + " samples")
  return mean


def readAccelerationFromFile(accelerationFile, numberOfSamples):
  with open(accelerationFile) as of:
```

```
    data = of.readlines()
    i = -1
    acceleration = []
    timeStamp = []
    for line in data:
    i = i + 1
    if i > 17 and i < numberOfSamples+18:
    splitted = line.split(',')
    timeSplit = splitted[0]
    accSplit = splitted[1]
    timeStamp.append(timeSplit[9:])
    acceleration.append(float(accSplit))

  samplesStr = str(numberOfSamples)
  print("Read: " + accelerationFile + " with " + samplesStr + "
                                    samples")

  return acceleration, timeStamp

def readThreeAccelerationFromFile(accelerationFile):
  with open(accelerationFile) as of:
    data = of.readlines()

    i = -1
    accelerationG = []
    accelerationE = []
    accelerationD = []
    timeStamp = []
    for line in data:
    # print(line)
    i = i + 1
    if i > 20 and i < len(data)-21:
    splitted = line.split(',')
    # print(splitted[1])
    timeSplit = splitted[0]
    timeStamp.append(timeSplit[9:])
    accSplit5 = float(splitted[1])
    accSplit6 = float(splitted[2])
    accSplit7 = float(splitted[3])
    accelerationG.append(accSplit5)
    accelerationE.append(accSplit6)
    accelerationD.append(accSplit7)
  acceleration = [accelerationG, accelerationE, accelerationD]
  samplesStr = str(len(accelerationG))
  print("Read: " + accelerationFile +  " with " + samplesStr + "
                                    samples")
```

```
  return acceleration

def getDisplacementFromAcceleration(rawAcceleration,meanAcceleration,
                                    time,sampleRate):
  nominalAcc = []
  print
  for acc in rawAcceleration:
    print(acc)
    nominalAcc.append((float(acc) - meanAcceleration)*GRAVITY)
    print(nominalAcc)
  filteredAcc = butter_lowpass_filter(nominalAcc, cutoffAcceleration,
                                    sampleRate, accOrder)
  # velocity = integrate.cumtrapz(nominalAcc, time, initial=0)
  velocityFilteredAcc = integrate.cumtrapz(filteredAcc, time, initial=
                                    0)
  velocityFiltered = butter_highpass_filter(velocityFilteredAcc,
                                    cutoffVelocity, sampleRate , order)
  # displacement = integrate.cumtrapz(velocity,time, initial=0)
  displacementFilteredVel = integrate.cumtrapz(velocityFiltered,time,
                                    initial=0)
  displacementFiltered = butter_highpass_filter(
                                    displacementFilteredVel,
                                    cutoffDisplacement, sampleRate,
                                    order)

  return displacementFiltered
```